

Analytical solution of the cylindrical torsion problem for the relaxed micromorphic continuum and other generalized continua (including full derivations)

Gianluca Rizzi,¹ Gerafl Hütter,² Hassam Khan,³ Ionel Dumitrel Ghiba,⁴

Angela Madeo¹ and Patrizio Neff⁵

April 26, 2021

Abstract

We solve the St. Venant torsion problem for an infinite cylindrical rod whose behaviour is described by a family of isotropic generalized continua, including the relaxed micromorphic and classical micromorphic model. The results can be used to determine the material parameters of these models. Special attention is given to the possible nonphysical stiffness singularity for a vanishing rod diameter, since slender specimens are in general described as stiffer.

Keywords: generalized continua, torsion, torsional stiffness, characteristic length, size-effect, micromorphic continuum, Cosserat continuum, couple stress model, gradient elasticity, micropolar, relaxed micromorphic model, micro-stretch model, micro-strain model, micro-void model, bounded stiffness.

1 Introduction

In this paper we continue our endeavour to find analytical solutions to simple boundary value problems for families of generalized continua [3, 60, 61]. The focus is on non-homogeneous solutions that on one side activate the additional deformations modes offered by generalized continua (curvature terms) and which may be used, on the other side, in calibrating the additional (many) material parameters. The renewed interest in models of generalized continua comes in part from the fact that for small specimens one may observe size-effects, not accounted for by linear Cauchy elasticity. On the other hand, the description of man-made architecture materials/meta-materials need generalized continua to capture frequency band-gaps in the dynamic range, a prominent example being given by the relaxed micromorphic model [1, 2, 40, 59, 62].

Here, we consider the static St. Venant torsion problem. Since we aim at identifying material parameters, let us first review what can be said for isotropic linear elasticity.

1.1 Material parameters in linear elasticity vs. generalized continua

The determination of the two constitutive material parameters in isotropic linear elasticity can be achieved in several different ways. For example the Young's modulus and Poisson's ratio

$$E_{\text{macro}} = \frac{9\kappa_{\text{macro}} \mu_{\text{macro}}}{3\kappa_{\text{macro}} + \mu_{\text{macro}}}, \quad \nu_{\text{macro}} = \frac{3\kappa_{\text{macro}} - 2\mu_{\text{macro}}}{2(3\kappa_{\text{macro}} + \mu_{\text{macro}})}, \quad (1)$$

$$\lambda_{\text{macro}} = \frac{3\kappa_{\text{macro}} - 2\mu_{\text{macro}}}{3}, \quad \kappa_{\text{macro}} = \frac{2\mu_{\text{macro}} + 3\lambda_{\text{macro}}}{3}, \quad (2)$$

can be uniquely determined from a *homogeneous* macroscopic tension-compression test. Moreover, the shear modulus μ_{macro} and the Young's modulus E_{macro} can also be identified from the *inhomogeneous* torsion and bending test, respectively. Indeed, the classical torsional stiffness (per unit length) of a circular rod is given by

$$T_{\text{macro}} = \mu_{\text{macro}} I_p = \mu_{\text{macro}} \frac{\pi R^4}{2}, \quad (3)$$

¹corresponding author, GEOMAS, INSA-Lyon, Université de Lyon, 20 avenue Albert Einstein, 69621, Villeurbanne cedex, France, gianluca.rizzi@insa-lyon.fr

²Institute of Mechanics and Fluid Dynamics, Technische Universität Bergakademie Freiberg, Lampadiusstr. 4, 09596 Freiberg, Germany

³Fakultät für Mathematik, Universität Duisburg-Essen, Thea-Leymann-Straße 9, 45127 Essen, Germany

⁴Department of Mathematics, Alexandru Ioan Cuza University of Iași, Blvd. Carol I, no. 11, 700506 Iași, Romania; and Octav Mayer Institute of Mathematics of the Romanian Academy, Iași Branch, 700505 Iași

⁵Head of Chair for Nonlinear Analysis and Modelling, Fakultät für Mathematik, Universität Duisburg-Essen, Thea-Leymann-Straße 9, 45127 Essen, Germany

and the bending stiffness (per unit length and per unit thickness) in cylindrical bending [61] is equivalent to

$$D_{\text{macro}} = \frac{h^3}{12} \frac{E_{\text{macro}}}{(1 - \nu_{\text{macro}}^2)} = \frac{h^3}{12} \frac{4\mu_{\text{macro}}(3\kappa_{\text{macro}} + \mu_{\text{macro}})}{3\kappa_{\text{macro}} + 4\mu_{\text{macro}}}. \quad (4)$$

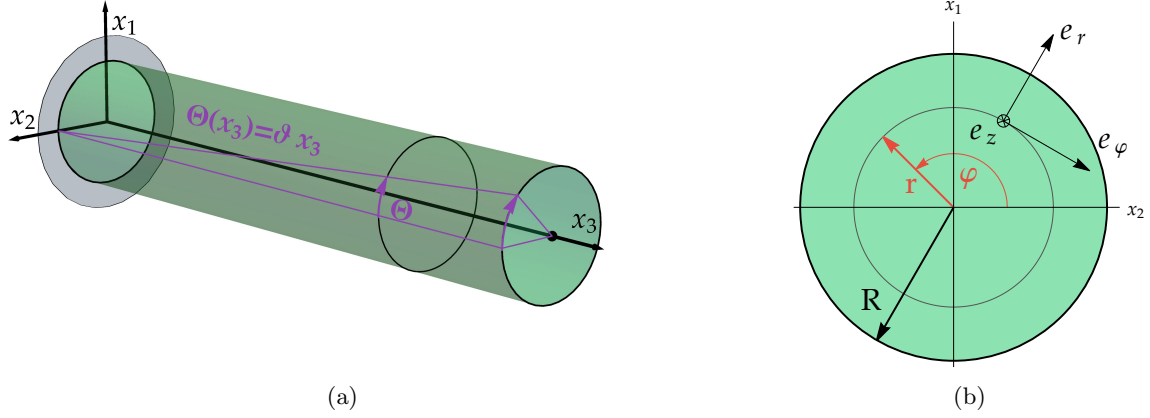


Figure 1: Geometry of the torsion problem: according to the St.Venant principle, we do not consider how the resultant end torque is applied. Furthermore, we assume that each cross-section (orthogonal to x_3) rotates as a rigid body with a constant rate of twist $\frac{\partial \Theta}{\partial x_3} = \vartheta$. Since there is no warping, every cross-section remains in the same plane before and after the deformation. Note that the final solution for linear elasticity satisfies this ansatz only to within first order in the rate of twist ϑ , see Fig. 2.

A third independent identification can be achieved with dynamic measurements, determining the shear wave speed (c_s) and the pressure wave speed (c_p)

$$c_s = \sqrt{\frac{\mu_{\text{macro}}}{\rho}}, \quad c_p = \sqrt{\frac{2\mu_{\text{macro}} + \lambda_{\text{macro}}}{\rho}}. \quad (5)$$

In reality, all these three methods may lead to slightly different values when used to fit real experiments due to the experimental set up. Nevertheless, they all are useful in complementing the identification procedure. We note that all mentioned tests convey a precise physical meaning to the appearing material parameters and this greatly helps in the mechanical application of linear elasticity to real world structures.

The situation is much more involved when trying to determine material parameters for generalized continua. Even when restricting the attention to linear and isotropic response, the number of additional parameters increase significantly and it is also not clear a priori what the physical meaning of the additional parameters really is. Lakes [34, 35] has prominently investigated the fitting procedure for isotropic Cosserat solids. In the linear isotropic Cosserat model (Section 6) there appear already six independent parameters and a series of experiments with differently sized materials allows to determine the Cosserat constants. A decisive tool for that purpose is the analytical solution for torsion and bending, which is already available in the literature [33, 39, 61]. The Cosserat model allows to describe size-effects in the sense that more slender specimen have an increased apparent stiffness' in bending and torsion. However, it is observed that the Cosserat model does have an unphysical stiffness singularity in bending [61] for a zero slenderness limit, the same appears in general in torsion (Section 6) but can be avoided upon setting to zero some curvature parameters (Sec 6.1). The mentioned stiffness singularity is not only an academic issue, but it concerns the stable identification of the material parameters [53]. Yet, in the Cosserat theory, the Young's modulus E_{macro} and the Poisson's ratio ν_{macro} can still be determined in a size-independent manner with a homogeneous tension-compression test. In question are the so-called Cosserat couple modulus $\mu_c \geq 0$ and the three curvature parameters.

A first extension of the Cosserat model is the so-called micro-stretch model, which allows for infinitesimal rotation and volume stretch as independent kinematic fields. For the micro-stretch model we show that the additional kinematic degree of freedom is not activated in the torsion problem.

Another extension of the Cosserat model is given by the recently introduced relaxed micromorphic model [44, 47, 67] (Section 4). In its static isotropic version it features only 8 independent material parameters comparing favourably to the large number of constitutive parameters in the classical micromorphic model. While the kinematics of the relaxed micromorphic model coincides with the classical micromorphic model

(9 additional degrees of freedom: stretch, shrink, shear, rotations) the curvature term is a direct extension of the Cosserat curvature written in terms of $\text{Curl } \mathbf{P}$. An important advantage of the model compared to the Cosserat model is that there is no stiffness singularity in whatsoever situation and four of the eight constants (μ_{macro} , λ_{macro} , μ_e , and λ_e) can be determined ab initio from size-independent homogeneous tests [46]. There remains to fit three curvature parameters and the Cosserat couple modulus $\mu_c \geq 0$ (which in some situations may be chosen to be zero since the model remains well-posed) [6, 36, 37, 38, 56].

Another advantage of the isotropic relaxed micromorphic model is given by the fact that it can replace the isotropic Cosserat model in a straightforward manner without additional costs. Indeed, the Cosserat curvature parameters can be taken as such as well as the Cosserat couple modulus μ_c . The only new parameter set is μ_{micro} , λ_{micro} , an estimate of which can be inferred from the small-scale response [46]. Regularity and continuous dependence results for the relaxed micromorphic model have been obtained in [15, 20, 47, 57] and first FEM-implementations in $H(\text{Curl})$ -space are presented in [46].

Next, the micro-strain model [13] is in a sense complementary to the Cosserat model: it assumes an additional strain like symmetric field S as extra degree of freedom. Here, we recover a simplified micro-strain model without mixed terms and a choice for the curvature parameters, see also [66] who considers a degenerate micro-strain model in disguise. We recover the analytical solution given by Hütter [24] for the micro-strain torsion problem. It turns out that for bending [61], simple shear [60] and torsion (Section 10) the micro-strain solution does not show a stiffness singularity either. However, this is not a general feature of the micro-strain model, but only related to the restricted kinematic possibilities: bending and torsion activate prominently rotations, but these are “filtered out” in the micro-strain model. Therefore, bounded stiffness in bending and torsion should come as no surprise. Next, we combine the Cosserat and the micro-strain ansatz in a novel ad-hoc model whose response is nevertheless governed by the Cosserat kinematics.

Lastly, we have the full micromorphic model [12, 42]. The kinematics is augmented with a non-symmetric micro-distortion tensor \mathbf{P} (as for the relaxed micromorphic model, too) but the curvature energy depends on the full gradient $D\mathbf{P}$ of the micro-distortion. For simplicity and for comparison, we consider a subclass without mixed terms and simplified curvature expression. In general, the bending and torsion responses show a stiffness singularity, which can be avoided in torsion by a very special ansatz for the curvature energy. However, nonphysical stiffness singularities cannot, in general, be avoided. Our investigation is complemented by considering the strain-gradient models and its couple-stress subclass. The reason for the singular stiffening behaviour in the other generalized continuum models (except the relaxed micromorphic one) can be connected to their *non-redundant* formulation of the curvature measure [63].

An alternative method to study the deformation of (finite) elastic cylinders is the semi-inverse method introduced by Ieşan in [26, 27], see also [18]. This method was also successfully used to study the deformation of elastic cylinders with microstructures, see [7, 16, 17] and the book [28], in which many of Ieşan’s results were unified. Regarding the semi-inverse method, all the results obtained in the classical micromorphic theory and all its subclasses (Cosserat, micro-stretch, micro-voids) are obtained by assuming that the internal energy is positive definite in terms of $D\mathbf{P}$. To the contrary, in the framework of the relaxed micromorphic model, the present results are valid also for internal energies which are not positive definite in terms of $D\mathbf{P}$, but rather in terms of $\text{Curl } \mathbf{P}$. We recall that an internal energy which is positive definite in terms of $\text{Curl } \mathbf{P}$ is only semi-positive definite in terms of $D\mathbf{P}$.

The paper is now structured as follows. After fixing our notation in Section 1.2 we shortly dwell on the formulation of the torsion problem in adapted variables, making it clear that we *do not* revert to express stresses and moments in cylindrical coordinate but we always use a Cartesian expression written in suitable variables. To set the stage we recall the linear isotropic torsion problem, which will then be suitably generalized.

1.2 Notation

For vectors $\mathbf{a}, \mathbf{b} \in \mathbb{R}^n$, we define the scalar product $\langle \mathbf{a}, \mathbf{b} \rangle := \sum_{i=1}^n a_i b_i \in \mathbb{R}$, the euclidean norm $\|\mathbf{a}\|^2 := \langle \mathbf{a}, \mathbf{a} \rangle$ and the dyadic product $\mathbf{a} \otimes \mathbf{b} := (a_i b_j)_{i,j=1,\dots,n} \in \mathbb{R}^{n \times n}$. In the same way, for tensors $\mathbf{P}, \mathbf{Q} \in \mathbb{R}^{n \times n}$, we define the scalar product $\langle \mathbf{P}, \mathbf{Q} \rangle := \sum_{i,j=1}^n P_{ij} Q_{ij} \in \mathbb{R}$ and the Frobenius-norm $\|\mathbf{P}\|^2 := \langle \mathbf{P}, \mathbf{P} \rangle$. Moreover, $\mathbf{P}^T := (P_{ji})_{i,j=1,\dots,n}$ denotes the transposition of the matrix $\mathbf{P} = (P_{ij})_{i,j=1,\dots,n}$, which decomposes orthogonally into the skew-symmetric part $\text{skew } \mathbf{P} := \frac{1}{2}(\mathbf{P} - \mathbf{P}^T)$ and the symmetric part $\text{sym } \mathbf{P} := \frac{1}{2}(\mathbf{P} + \mathbf{P}^T)$. The identity matrix is denoted by $\mathbf{1}$, so that the trace of a matrix \mathbf{P} is given by $\text{tr } \mathbf{P} := \langle \mathbf{P}, \mathbf{1} \rangle$, while the deviatoric component of a matrix is given by $\text{dev } \mathbf{P} := \mathbf{P} - \frac{\text{tr}(\mathbf{P})}{3} \mathbf{1}$. Given this, the orthogonal decomposition possible for a matrix is $\mathbf{P} = \text{dev sym } \mathbf{P} + \text{skew } \mathbf{P} + \frac{\text{tr}(\mathbf{P})}{3} \mathbf{1}$. The Lie-Algebra of skew-symmetric matrices is denoted by $\mathfrak{so}(3) := \{\mathbf{A} \in \mathbb{R}^{3 \times 3} \mid \mathbf{A}^T = -\mathbf{A}\}$, while the vector space of symmetric matrices

$\text{Sym}(3) := \{\mathbf{S} \in \mathbb{R}^{3 \times 3} \mid \mathbf{S}^T = \mathbf{S}\}$. Using the one-to-one map $\text{axl} : \mathfrak{so}(3) \rightarrow \mathbb{R}^3$ we have

$$\mathbf{A} \mathbf{b} = \text{axl}(\mathbf{A}) \times \mathbf{b} \quad \forall \mathbf{A} \in \mathfrak{so}(3), \quad \mathbf{b} \in \mathbb{R}^3. \quad (6)$$

where \times denotes the cross product in \mathbb{R}^3 . The inverse of axl is denoted by $\text{Anti} : \mathbb{R}^3 \rightarrow \mathfrak{so}(3)$. The Jacobian matrix $\mathbf{D}\mathbf{u}$ and the curl for a vector field \mathbf{u} are defined as

$$\mathbf{D}\mathbf{u} = \begin{pmatrix} u_{1,1} & u_{1,2} & u_{1,3} \\ u_{2,1} & u_{2,2} & u_{2,3} \\ u_{3,1} & u_{3,2} & u_{3,3} \end{pmatrix}, \quad \text{curl } \mathbf{u} = \nabla \times \mathbf{u} = \begin{pmatrix} u_{3,2} - u_{2,3} \\ u_{1,3} - u_{3,1} \\ u_{2,1} - u_{1,2} \end{pmatrix}. \quad (7)$$

We also introduce the Curl and the Div operators of the 3×3 matrix field \mathbf{P} as

$$\text{Curl } \mathbf{P} = \begin{pmatrix} (\text{curl}(P_{11}, P_{12}, P_{13}))^T \\ (\text{curl}(P_{21}, P_{22}, P_{23}))^T \\ (\text{curl}(P_{31}, P_{32}, P_{33}))^T \end{pmatrix}^T, \quad \text{Div } \mathbf{P} = \begin{pmatrix} \text{div}(P_{11}, P_{12}, P_{13}) \\ \text{div}(P_{21}, P_{22}, P_{23}) \\ \text{div}(P_{31}, P_{32}, P_{33}) \end{pmatrix}^T. \quad (8)$$

The cross product between a second order tensor and a vector is also needed and is defined row-wise as follow

$$\mathbf{m} \times \mathbf{b} = \begin{pmatrix} \mathbf{b} \times (m_{11}, m_{12}, m_{13})^T \\ \mathbf{b} \times (m_{21}, m_{22}, m_{23})^T \\ \mathbf{b} \times (m_{31}, m_{32}, m_{33})^T \end{pmatrix}^T = \mathbf{m} \cdot \boldsymbol{\epsilon} \cdot \mathbf{b} = m_{ik} \epsilon_{kjh} b_h, \quad (9)$$

where $\mathbf{m} \in \mathbb{R}^{3 \times 3}$, $\mathbf{b} \in \mathbb{R}^3$, and $\boldsymbol{\epsilon}$ is the Levi-Civita tensor. The two indices contraction $:$ is intended as

$$\mathbf{B} : \nabla \mathbf{m} = B_{ip} m_{ijk,p} = N_{jk}, \quad \mathbf{B} : \mathbf{m} = B_{ij} m_{ijk} = b_k, \quad (10)$$

where \mathbf{B} and \mathbf{N} are second order tensors, \mathbf{m} is a third order tensor, and \mathbf{b} is a vector.

1.3 Cartesian variables expressed through cylindrical variables

To address the torsional problem in its natural environment but with the comfort of the classical Cartesian coordinate system, we introduce the cylindrical set of coordinates which allows us to express the classic Cartesian orthogonal set of coordinates $\mathbf{x} = \{x_1, x_2, x_3\}$ through a more suitable set of variables $\mathbf{r} = \{r, \varphi, z\}$, without switching completely to a cylindrical coordinate system, i.e., without expressing all the quantities (strains, stresses etc.) in the basis corresponding to the cylindrical coordinates

$$\mathbf{e}_r = \begin{pmatrix} \cos \varphi \\ \sin \varphi \\ 0 \end{pmatrix}, \quad \mathbf{e}_\varphi = \begin{pmatrix} -\sin \varphi \\ \cos \varphi \\ 0 \end{pmatrix}, \quad \mathbf{e}_z = \begin{pmatrix} 0 \\ 0 \\ 1 \end{pmatrix}. \quad (11)$$

The relations for the coordinates are

$$x_1 = r \cos \varphi, \quad x_2 = r \sin \varphi, \quad x_3 = z, \quad (12)$$

while the relations between the first and the second derivative of a generic vector field \mathbf{f} are

$$\frac{\partial f_i(r, \varphi, z)}{\partial r_j} = \frac{\partial f_i(r, \varphi, z)}{\partial x_k} \frac{\partial x_k}{\partial r_j}, \quad \frac{\partial^2 f_i(r, \varphi, z)}{\partial r_j \partial r_k} = \frac{\partial^2 f_i(r, \varphi, z)}{\partial x_m \partial x_n} \frac{\partial x_m}{\partial r_j} \frac{\partial x_n}{\partial r_k} + \frac{\partial f_i(r, \varphi, z)}{\partial x_m} \frac{\partial^2 x_m}{\partial r_j \partial r_k}. \quad (13)$$

The quantities we want to obtain are $\frac{\partial f_i(r, \varphi, z)}{\partial x_k}$ and $\frac{\partial^2 f_i(r, \varphi, z)}{\partial x_m \partial x_n}$, which are obtainable thanks to (13) (see Appendix A for full calculations).

It is emphasized again that **we will not represent the torsional problem in cylindrical coordinates** (namely all the differential operators, the equilibrium equation, and the kinematic fields), but we will use the classical Cartesian coordinates $\{x_1, x_2, x_3\}$ parameterized in cylindrical variables $\{r, \varphi, z\}$.

1.4 Structure of the higher-order ansatz

The ansatz for the displacement field for the cylindrical torsion problem, regardless of the treated model, is always given by

$$\mathbf{u}(r, \varphi, z) = \boldsymbol{\vartheta} \begin{pmatrix} -x_2(r, \varphi) x_3(z) \\ x_1(r, \varphi) x_3(z) \\ 0 \end{pmatrix}. \quad (14)$$

Here, ϑ is the rate of twist per unit length. It is highlighted that the displacement field has the third component equal to zero since we are studying a cylindrical rod, whose cross-section is not subjected to warping. The most general ansatz for the micro-distortion tensor, which will be used for the full and the relaxed micromorphic model, is

$$\mathbf{P}(r, \varphi, z) = \vartheta \begin{pmatrix} 0 & -x_3(z) & -g_2(r) x_2(r, \varphi) \\ x_3(z) & 0 & g_2(r) x_1(r, \varphi) \\ g_1(r) x_2(r, \varphi) & -g_1(r) x_1(r, \varphi) & 0 \end{pmatrix}, \quad (15)$$

where $g_1, g_2 : [0, \infty) \rightarrow \mathbb{R}$. Starting from the form (15) of the ansatz for \mathbf{P} , it is possible to obtain the ansatz for the micro-stretch model ($\mathbf{A} = \text{skew } \mathbf{P}$ and $\omega \mathbf{1} = \text{tr}(\mathbf{P}) \mathbf{1}$), the Cosserat model ($\mathbf{A} = \text{skew } \mathbf{P}$), the micro-void model ($\omega \mathbf{1} = \text{tr}(\mathbf{P}) \mathbf{1}$), and the micro-strain model ($\mathbf{S} = \text{sym } \mathbf{P}$), by taking the skew-symmetric part, the trace of \mathbf{P} , or the symmetric part depending on what is needed. Here are reported the symmetric part, the skew-symmetric part and the trace of \mathbf{P}

$$\mathbf{S}(r, \varphi, z) = \text{sym } \mathbf{P}(r, \varphi, z) = \frac{\vartheta}{2} \begin{pmatrix} 0 & 0 & g_m(r) x_2(r, \varphi) \\ 0 & 0 & -g_m(r) x_1(r, \varphi) \\ g_m(r) x_2(r, \varphi) & -g_m(r) x_1(r, \varphi) & 0 \end{pmatrix}, \quad (16)$$

$$\mathbf{A}(r, \varphi, z) = \text{skew } \mathbf{P}(r, \varphi, z) = \frac{\vartheta}{2} \begin{pmatrix} 0 & -2x_3(z) & -g_p(r) x_2(r, \varphi) \\ 2x_3(z) & 0 & g_p(r) x_1(r, \varphi) \\ g_p(r) x_2(r, \varphi) & -g_p(r) x_1(r, \varphi) & 0 \end{pmatrix}, \quad (17)$$

where $g_p(r) = g_1(r) + g_2(r)$, $g_m(r) = g_1(r) - g_2(r)$, and ω is not reported since the ansatz (15) has a zero trace.

It is highlighted that each section remains “rigid” is not really correct, since the deformation of a cylinder section due to the displacement field (14) (which is a linear approximation of a rigid rotation) looks like

$$\mathbf{x} + \mathbf{u}(\mathbf{x}) = \begin{pmatrix} x_1 \\ x_2 \\ 0 \end{pmatrix} + \begin{pmatrix} 0 & -\vartheta x_3 & 0 \\ \vartheta x_3 & 0 & 0 \\ 0 & 0 & 0 \end{pmatrix} \begin{pmatrix} x_1 \\ x_2 \\ 0 \end{pmatrix} = \begin{pmatrix} x_1 - x_2 x_3 \vartheta \\ x_2 + x_1 x_3 \vartheta \\ 0 \end{pmatrix}. \quad (18)$$

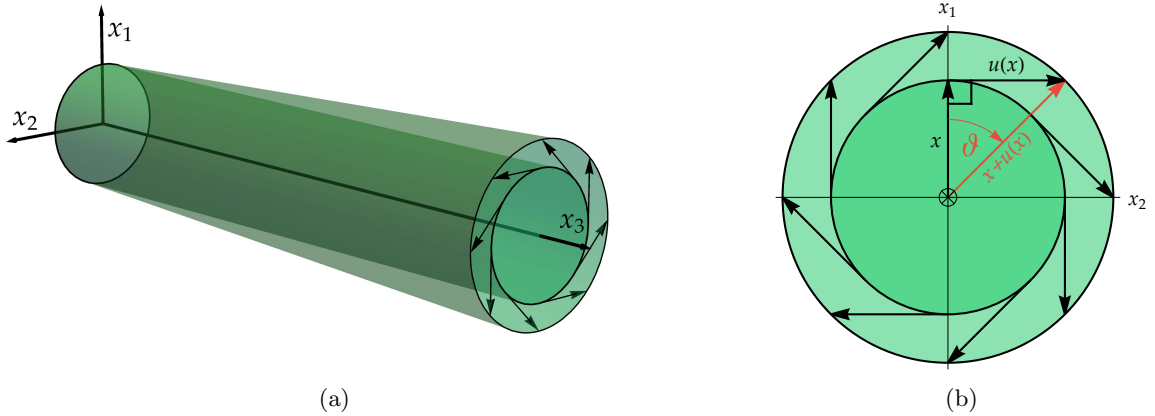


Figure 2: In the linear approximation, sections of the cylindrical rod are not only rotated, but also expanded radially for non zero rate of twist ϑ . With (b) we see that the change of radius $\delta R = \frac{R}{\cos \vartheta} - R = \frac{1 - \cos \vartheta}{\cos \vartheta} R = \left(\frac{\vartheta^2}{2} + \frac{5}{24} \vartheta^4 + \text{h.o.t.} \right) R$, being of second order in ϑ . Thus, the linear kinematics is correct to within first order in ϑ , as is well-known.

Of course this radial expansion does not contribute energetically under the small displacement hypothesis, and this can be seen from (23), in which it is clear that the symmetric strain tensor $\varepsilon = \text{sym } \mathbf{D}\mathbf{u}$ does not depend on $x_3 \equiv z$.

2 Overview of some generalized continuum models and their interconnections

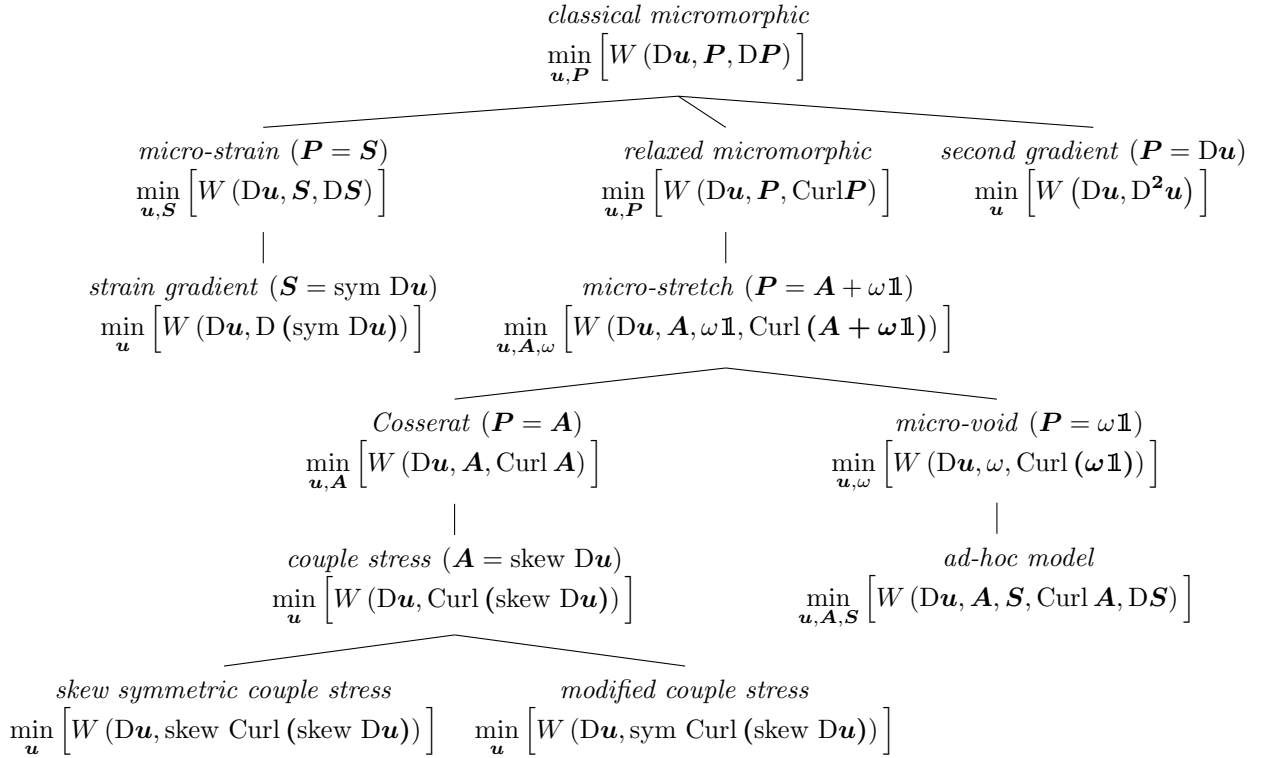
Considering the following notations for the involved quantities:

$$\begin{aligned}
 \mathbf{u} : \Omega \subset \mathbb{R}^3 &\rightarrow \mathbb{R}^3, & \text{displacement,} \\
 \mathbf{P} : \Omega \subset \mathbb{R}^3 &\rightarrow \mathbb{R}^{3 \times 3}, & \text{micro-distortion,} \\
 \mathbf{A} : \Omega \subset \mathbb{R}^3 &\rightarrow \mathfrak{so}(3), & \text{micro-rotation,} \\
 \mathbf{S} : \Omega \subset \mathbb{R}^3 &\rightarrow \text{Sym}(3), & \text{micro-strain,} \\
 \omega : \Omega \subset \mathbb{R}^3 &\rightarrow \mathbb{R}, & \text{micro-dilatation}
 \end{aligned}$$

and the orthogonal decomposition

$$\mathbf{P} = \text{dev sym } \mathbf{P} + \text{skew } \mathbf{P} + \frac{1}{3} \text{tr}(\mathbf{P}) \mathbf{1} = \text{dev } \mathbf{S} + \mathbf{A} + \omega \mathbf{1} \quad (19)$$

we give the following genealogy tree of the generalized continuum models:



The strain gradient theory and second gradient theory are equivalent [3, 42], and contain additionally the couple stress theory as a special case. Using the Curl as primary differential operator for the curvature terms allows a neat unification of concepts.

3 Torsional problem for the isotropic Cauchy continuum

In order to set up a comparison with the models we will present in the next sections, we start by presenting the solution of the classical cylindrical torsional problem. The strain energy for a linear elastic isotropic Cauchy continuum is

$$W(\mathbf{Du}) = \mu_{\text{macro}} \|\text{sym } \mathbf{Du}\|^2 + \frac{\lambda_{\text{macro}}}{2} \text{tr}^2(\mathbf{Du}), \quad (20)$$

where λ_{macro} and μ_{macro} are the macroscopic Lamé constants.

In terms of the symmetric Cauchy stress tensor $\boldsymbol{\sigma} = 2\mu_{\text{macro}} \text{sym } \mathbf{Du} + \lambda_{\text{macro}} \text{tr}(\mathbf{Du}) \mathbf{1}$, where $\boldsymbol{\varepsilon} = \text{sym } \mathbf{Du}$ denotes the classical symmetric strain tensor, the equilibrium equation (in the absence of body forces) and the Neumann lateral boundary conditions (at the free surface) are

$$\text{Div } \boldsymbol{\sigma} = \mathbf{0}, \quad \mathbf{t}(r=R) = \boldsymbol{\sigma}(r=R) \cdot \mathbf{e}_r = \mathbf{0}. \quad (21)$$

Our aim is to study a **state of uniform torsion** ϑ for an infinitely extended cylindrical rod. According to the cylindrical reference system shown in Fig. 1, the ansatz for the displacement is

$$\mathbf{u}(x_1, x_2, x_3) = \mathbf{u}(r, \varphi, z) = \vartheta \begin{pmatrix} -x_2(r, \varphi) x_3(z) \\ x_1(r, \varphi) x_3(z) \\ 0 \end{pmatrix} = \vartheta \begin{pmatrix} -z r \sin \varphi \\ z r \cos \varphi \\ 0 \end{pmatrix}, \quad (22)$$

where ϑ is the angle of twist per unit length. It is underlined that the third component of the displacement is chosen equal to zero since the cross-section is circular and therefore no warping is expected. The gradient of the displacement and its symmetric part are (the gradient is always taken with respect to the Cartesian coordinate system and then rewritten in the variables $\{r, \varphi, z\}$)

$$\mathbf{D}\mathbf{u} = \vartheta \begin{pmatrix} 0 & -z & -r \sin \varphi \\ z & 0 & r \cos \varphi \\ 0 & 0 & 0 \end{pmatrix}, \quad \boldsymbol{\varepsilon} = \text{sym } \mathbf{D}\mathbf{u} = \frac{\vartheta}{2} \begin{pmatrix} 0 & 0 & -r \sin \varphi \\ 0 & 0 & r \cos \varphi \\ -r \sin \varphi & r \cos \varphi & 0 \end{pmatrix}. \quad (23)$$

Substituting the ansatz (23) in the equilibrium equation (21), it is easy to verify that they are identically satisfied.

In order to help the geometric interpretation of the torque, see Fig. 3, we present its expression in Cartesian coordinates along with its representation in the cylindrical variables

$$M_C(\vartheta) := \iint_{\Gamma} \left[\overbrace{\left\langle \underbrace{\boldsymbol{\sigma} \mathbf{e}_3}_{\text{traction}}, \begin{pmatrix} -x_2 \\ x_1 \\ 0 \end{pmatrix} \right\rangle}_{\text{length of lever arm}} \frac{1}{\sqrt{x_1^2 + x_2^2}} \right] dx_1 dx_2 \quad (24)$$

$$= \iint_{\Gamma} [x_1 \sigma_{23} - x_2 \sigma_{13}] dx_1 dx_2 = \int_0^{2\pi} \int_0^R [\langle \boldsymbol{\sigma} \mathbf{e}_z, \mathbf{e}_\varphi \rangle r] r dr d\varphi, \quad (25)$$

where $\mathbf{e}_3 = \mathbf{e}_z = (0, 0, 1)$ is the unit vector aligned with the mid-axis of the cylindrical rod.

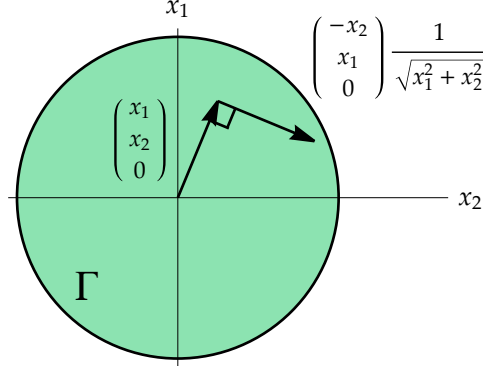


Figure 3: Calculation of the classical torque.

The torque (or moment of torsion) about the x_3 -axis and energy (per unit length dx_3) expressions are

$$M_C(\vartheta) := \int_0^{2\pi} \int_0^R [\langle \boldsymbol{\sigma} \mathbf{e}_z, \mathbf{e}_\varphi \rangle r] r dr d\varphi = \mu_{\text{macro}} \frac{\pi R^4}{2} \vartheta = \mu_{\text{macro}} I_p \vartheta = T_{\text{macro}} \vartheta, \quad (26)$$

$$W_{\text{tot}}(\vartheta) := \int_0^{2\pi} \int_0^R W(\mathbf{D}\mathbf{u}) r dr d\varphi = \frac{1}{2} \mu_{\text{macro}} \frac{\pi R^4}{2} \vartheta^2 = \frac{1}{2} \mu_{\text{macro}} I_p \vartheta^2 = \frac{1}{2} T_{\text{macro}} \vartheta^2,$$

where μ_{macro} is the macroscopic shear modulus, $I_p = \frac{\pi R^4}{2}$ is the polar moment of inertia, and $T_{\text{macro}} = \mu_{\text{macro}} I_p$ is the torsional stiffness. It is also highlighted that

$$\frac{d}{d\vartheta} W_{\text{tot}}(\vartheta) = M_C(\vartheta) = T_{\text{macro}} \vartheta, \quad \frac{d^2}{d\vartheta^2} W_{\text{tot}}(\vartheta) = T_{\text{macro}}. \quad (27)$$

Here and in the remainder of this work, the elastic coefficients $\mu_i, \lambda_i, \kappa_i$ are expressed in [MPa], the coefficients a_i are dimensionless, the characteristic lengths L_c and the radius R in meter [m], the rate of twist ϑ in [1/m].

4 Torsional problem for the isotropic relaxed micromorphic model

The relaxed micromorphic model, contrary to all the other proposals for generalized continua in the literature, lives on two well-defined and separated scales, each describing linear elastic response: the classical *macroscopic response* (characteristic length $L_c \rightarrow 0$, available for experiments with large specimens) is described as usual by

$$E_{\text{macro}} = \frac{9\kappa_{\text{macro}} \mu_{\text{macro}}}{3\kappa_{\text{macro}} + \mu_{\text{macro}}}, \quad \nu_{\text{macro}} = \frac{3\kappa_{\text{macro}} - 2\mu_{\text{macro}}}{2(3\kappa_{\text{macro}} + \mu_{\text{macro}})}, \quad (28)$$

$$\lambda_{\text{macro}} = \frac{3\kappa_{\text{macro}} - 2\mu_{\text{macro}}}{3}, \quad \kappa_{\text{macro}} = \frac{2\mu_{\text{macro}} + 3\lambda_{\text{macro}}}{3}. \quad (29)$$

The macroscopic parameters can be uniquely determined from a *homogeneous* macroscopic tension-compression test. However, the shear modulus μ_{macro} and the Young's modulus E_{macro} can also be identified from the *inhomogeneous* torsion and bending test, respectively. Indeed, the classical torsional stiffness of a circular rod is given by

$$T_{\text{macro}} = \mu_{\text{macro}} I_p = \mu_{\text{macro}} \frac{\pi R^4}{2}. \quad (30)$$

The *microscopic scale* (appearing for $L_c \rightarrow \infty$), representing a *surrogate stiffness* connected to the smallest meaningful scale of the material is described by the parameters

$$E_{\text{micro}} = \frac{9\kappa_{\text{micro}} \mu_{\text{micro}}}{3\kappa_{\text{micro}} + \mu_{\text{micro}}}, \quad \nu_{\text{micro}} = \frac{3\kappa_{\text{micro}} - 2\mu_{\text{micro}}}{2(3\kappa_{\text{micro}} + \mu_{\text{micro}})}, \quad (31)$$

$$\lambda_{\text{micro}} = \frac{3\kappa_{\text{micro}} - 2\mu_{\text{micro}}}{3}, \quad \kappa_{\text{micro}} = \frac{2\mu_{\text{micro}} + 3\lambda_{\text{micro}}}{3}, \quad (32)$$

The macroscopic parameters μ_{macro} and λ_{macro} do not directly intervene in the formulation of the relaxed micromorphic model (34), but the connection is necessarily given by the *Reuss-like homogenization formula* [58]

$$\begin{aligned} \mu_{\text{macro}} &= \frac{\mu_e \mu_{\text{micro}}}{\mu_e + \mu_{\text{micro}}} \iff \mu_e = \frac{\mu_{\text{macro}} \mu_{\text{micro}}}{\mu_{\text{micro}} - \mu_{\text{macro}}}, \\ \kappa_{\text{macro}} &= \frac{\kappa_e \kappa_{\text{micro}}}{\kappa_e + \kappa_{\text{micro}}} \iff \kappa_e = \frac{\kappa_{\text{macro}} \kappa_{\text{micro}}}{\kappa_{\text{micro}} - \kappa_{\text{macro}}}. \end{aligned} \quad (33)$$

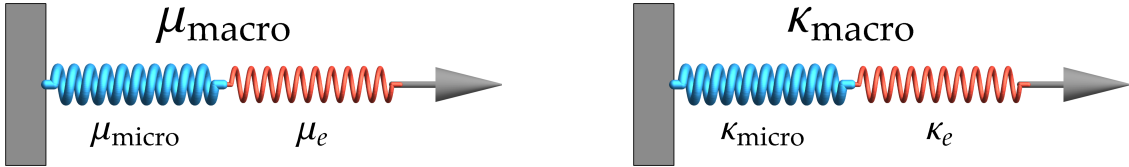


Figure 4: Macro and micro-scale stiffness governed by two springs in series. If $\mu_{\text{micro}} \rightarrow \infty$, this implies that $\mu_{\text{macro}} = \mu_e$. In all suitable cases for our family of considered generalized continua (depending on the kinematics), we use the same/similar lower order energy expression (the energy without curvature).

Note that the Cosserat couple modulus $\mu_c \geq 0$ is not appearing in the homogenization formulas (33). As a consequence, both parameter sets (29)-(33) can be identified independently of the scale consideration (being particularly careful with the techniques for the micro-parameters identification) and they uniquely determine the meso-scale parameter set μ_e, λ_e appearing in (33)₂.

The general expression of the strain energy for the isotropic relaxed micromorphic continuum is

$$\begin{aligned} W(\mathbf{Du}, \mathbf{P}, \text{Curl } \mathbf{P}) &= \mu_e \|\text{sym}(\mathbf{Du} - \mathbf{P})\|^2 + \frac{\lambda_e}{2} \text{tr}^2(\mathbf{Du} - \mathbf{P}) + \mu_c \|\text{skew}(\mathbf{Du} - \mathbf{P})\|^2 \\ &+ \mu_{\text{micro}} \|\text{sym } \mathbf{P}\|^2 + \frac{\lambda_{\text{micro}}}{2} \text{tr}^2(\mathbf{P}) \\ &+ \frac{\mu L_c^2}{2} \left(a_1 \|\text{dev sym Curl } \mathbf{P}\|^2 + a_2 \|\text{skew Curl } \mathbf{P}\|^2 + \frac{a_3}{3} \text{tr}^2(\text{Curl } \mathbf{P}) \right), \end{aligned} \quad (34)$$

where (μ_e, λ_e) , $(\mu_{\text{micro}}, \lambda_{\text{micro}})$, μ_c , $L_c > 0$, and (a_1, a_2, a_3) are the parameters related to the meso-scale, the parameters related to the micro-scale, the Cosserat couple modulus, the characteristic length, and the three general isotropic curvature parameters, respectively. This energy expression represents the most general

isotropic form possible for the relaxed micromorphic model. It is important to underline that, given the subsequent ansatz (38), it holds that $\text{skew Curl } \mathbf{P} = 0$. This reduces immediately the number of curvature parameters appearing in the torsion solution. In the absence of body forces, the equilibrium equations are then

$$\begin{aligned} \text{Div} \left[\overbrace{2\mu_e \text{sym}(\mathbf{Du} - \mathbf{P}) + \lambda_e \text{tr}(\mathbf{Du} - \mathbf{P}) \mathbb{1} + 2\mu_c \text{skew}(\mathbf{Du} - \mathbf{P})}^{\tilde{\sigma} :=} \right] &= \mathbf{0}, \\ \tilde{\sigma} - 2\mu_{\text{micro}} \text{sym } \mathbf{P} - \lambda_{\text{micro}} \text{tr}(\mathbf{P}) \mathbb{1} - \mu L_c^2 \text{Curl} \left(a_1 \text{dev sym Curl } \mathbf{P} + \frac{a_3}{3} \text{tr}(\text{Curl } \mathbf{P}) \mathbb{1} \right) &= \mathbf{0}. \end{aligned} \quad (35)$$

The boundary conditions at the lateral free surface are

$$\begin{aligned} \tilde{\mathbf{t}}(r=R) &= \tilde{\boldsymbol{\sigma}}(r) \cdot \mathbf{e}_r = \mathbf{0}_{\mathbb{R}^3}, & (\text{traction free}), \\ \boldsymbol{\eta}(r=R) &= \mathbf{m}(r) \cdot \boldsymbol{\epsilon} \cdot \mathbf{e}_r = \mathbf{m}(r) \times \mathbf{e}_r = \mathbf{0}_{\mathbb{R}^{3 \times 3}}, & (\text{moment free}), \end{aligned} \quad (36)$$

where

$$\mathbf{m} = \mu L_c^2 \left(a_1 \text{dev sym Curl } \mathbf{P} + \frac{a_3}{3} \text{tr}(\text{Curl } \mathbf{P}) \mathbb{1} \right) \quad (37)$$

is a generalized non-symmetric second order moment tensor, the (non-symmetric) force-stress tensor $\tilde{\boldsymbol{\sigma}}$ is given in (35), \mathbf{e}_r is the radial unit vector, and $\boldsymbol{\epsilon}$ is the Levi-Civita tensor. The vector $\tilde{\mathbf{t}}(r) \in \mathbb{R}^3$ is the generalised traction and the tensor $\boldsymbol{\eta}(r) \in \mathbb{R}^{3 \times 3}$ is called the generalized double traction tensor. According to the cylindrical reference system shown in Fig. 1, the ansatz for the displacement and for the micro-distortion \mathbf{P} is

$$\begin{aligned} \mathbf{u}(x_1, x_2, x_3) &= \mathbf{u}(r, \varphi, z) = \boldsymbol{\vartheta} \begin{pmatrix} -x_2(r, \varphi) x_3(z) \\ x_1(r, \varphi) x_3(z) \\ 0 \end{pmatrix}, \\ \mathbf{P}(x_1, x_2, x_3) &= \mathbf{P}(r, \varphi, z) = \boldsymbol{\vartheta} \begin{pmatrix} 0 & -x_3(z) & -g_2(r) x_2(r, \varphi) \\ x_3(z) & 0 & g_2(r) x_1(r, \varphi) \\ g_1(r) x_2(r, \varphi) & -g_1(r) x_1(r, \varphi) & 0 \end{pmatrix}, \end{aligned} \quad (38)$$

where $x_1(r, \varphi) = r \cos \varphi$, $x_2(r, \varphi) = r \sin \varphi$, and $x_3(z) = z$. The Cartesian \mathbf{Du} and the Cartesian $\text{Curl } \mathbf{P}$ expressed in the cylindrical variables (r, φ, z) are

$$\begin{aligned} \mathbf{Du}(r, \varphi, z) &= \boldsymbol{\vartheta} \begin{pmatrix} 0 & -z & -r \sin \varphi \\ z & 0 & r \cos \varphi \\ 0 & 0 & 0 \end{pmatrix}, \\ \text{Curl } \mathbf{P}(r, \varphi, z) &= \boldsymbol{\vartheta} \begin{pmatrix} 1 - g_2(r) - r g_2'(r) \sin^2 \varphi & r g_2'(r) \sin \varphi \cos \varphi & 0 \\ r g_2'(r) \sin \varphi \cos \varphi & 1 - g_2(r) - r g_2'(r) \cos^2 \varphi & 0 \\ 0 & 0 & -(2g_1(r) + r g_1'(r)) \end{pmatrix}. \end{aligned} \quad (39)$$

It can be remarked that $\text{Curl } \mathbf{P}$ is symmetric.

Inserting the ansatz (38)-(39) in (35), the 12 equilibrium equations are reduced to the following 4 ordinary differential equilibrium equations

$$\begin{aligned} \frac{1}{3} \boldsymbol{\vartheta} \sin \varphi \left(r \left(\mu L_c^2 ((a_1 - a_3) g_1''(r) - (2a_1 + a_3) g_2''(r)) + 3\mu_c (g_1(r) + g_2(r) - 1) \right. \right. \\ \left. \left. - 3(\mu_e + \mu_{\text{micro}}) (g_1(r) - g_2(r)) - 3\mu_e \right) + 3\mu L_c^2 ((a_1 - a_3) g_1'(r) - (2a_1 + a_3) g_2'(r)) \right) &= 0, \\ \frac{1}{3} \boldsymbol{\vartheta} \cos \varphi \left(r \left(\mu L_c^2 ((a_3 - a_1) g_1''(r) + (2a_1 + a_3) g_2''(r)) - 3\mu_c (g_1(r) + g_2(r) - 1) \right. \right. \\ \left. \left. + 3(\mu_e + \mu_{\text{micro}}) (g_1(r) - g_2(r)) + 3\mu_e \right) + 3\mu L_c^2 ((a_3 - a_1) g_1'(r) + (2a_1 + a_3) g_2'(r)) \right) &= 0, \\ \frac{1}{3} \boldsymbol{\vartheta} \sin \varphi \left(r \left(\mu L_c^2 ((2a_1 + a_3) g_1''(r) + (a_3 - a_1) g_2''(r)) - 3(\mu_c (g_1(r) + g_2(r) - 1) \right. \right. \\ \left. \left. + (\mu_e + \mu_{\text{micro}}) (g_1(r) - g_2(r))) - 3\mu_e \right) + 3\mu L_c^2 ((2a_1 + a_3) g_1'(r) + (a_3 - a_1) g_2'(r)) \right) &= 0, \\ \frac{1}{3} \boldsymbol{\vartheta} \cos \varphi \left(r \left(\mu L_c^2 ((a_1 - a_3) g_2''(r) - (2a_1 + a_3) g_1''(r)) + 3(\mu_c (g_1(r) + g_2(r) - 1) \right. \right. \\ \left. \left. + (\mu_e + \mu_{\text{micro}}) (g_1(r) - g_2(r))) + 3\mu_e \right) + 3\mu L_c^2 ((a_1 - a_3) g_2'(r) - (2a_1 + a_3) g_1'(r)) \right) &= 0. \end{aligned} \quad (40)$$

It is important to underline that $(35)_1$ is identically satisfied, and that from the entire set of four equilibrium equations (40) only two are not redundant since $(40)_1 = \tan \varphi (40)_2$ and $(40)_3 = \tan \varphi (40)_4$.

It is also pointed out that the two remaining linearly independent equations $(40)_{1,3}$ can be uncoupled and are of the Bessel ODE type (see Appendix B). Indeed, if we *take their sum and difference*, while being careful of substituting $g_p(r) = g_1(r) + g_2(r)$ and $g_m(r) = g_1(r) - g_2(r)$ along with their derivatives, we deduce

$$\begin{aligned} \vartheta \sin \varphi \left(a_1 \mu L_c^2 (3 g'_m(r) + r g''_m(r)) - 2 r \mu_e (g_m(r) + 1) - 2 r g_m(r) \mu_{\text{micro}} \right) &= 0, \\ \frac{1}{3} \vartheta \sin \varphi \left(6 r \mu_c (g_p(r) - 1) - \mu L_c^2 (a_1 + 2 a_3) (3 g'_p(r) + r g''_p(r)) \right) &= 0. \end{aligned} \quad (41)$$

Since $g_1(r) := \frac{g_p(r) + g_m(r)}{2}$ and $g_2(r) := \frac{g_p(r) - g_m(r)}{2}$, the solution in terms of $g_1(r)$ and $g_2(r)$ of (41) is

$$\begin{aligned} g_1(r) &= \frac{1}{2} \left(1 - \frac{i A_1 I_1 \left(\frac{r f_2}{L_c} \right) - A_2 Y_1 \left(-i \frac{r f_2}{L_c} \right) + i B_1 I_1 \left(\frac{r f_1}{L_c} \right) - B_2 Y_1 \left(-i \frac{r f_1}{L_c} \right)}{r} - \frac{\mu_e}{\mu_e + \mu_{\text{micro}}} \right), \\ g_2(r) &= \frac{1}{2} \left(1 + \frac{i A_1 I_1 \left(\frac{r f_2}{L_c} \right) - A_2 Y_1 \left(-i \frac{r f_2}{L_c} \right) - i B_1 I_1 \left(\frac{r f_1}{L_c} \right) + B_2 Y_1 \left(-i \frac{r f_1}{L_c} \right)}{r} + \frac{\mu_e}{\mu_e + \mu_{\text{micro}}} \right), \\ f_1 &:= \sqrt{\frac{6 \mu_c}{(a_1 + 2 a_3) \mu}}, \quad f_2 := \sqrt{\frac{2(\mu_e + \mu_{\text{micro}})}{a_1 \mu}}, \end{aligned} \quad (42)$$

where $I_n(\cdot)$ is the *modified Bessel function of the first kind*, $Y_n(\cdot)$ is the *Bessel function of the second kind* (see appendix B for the formal definitions), and A_1, B_1, A_2, B_2 are integration constants.

The values of A_1, B_1 are determined from the boundary conditions (36), while, due to the divergent behaviour of the Bessel function of the second kind at $r = 0$, we have to set $A_2 = 0$ and $B_2 = 0$ in order to have a continuous solution. The fulfilment of the boundary conditions (36) allows us to find the expressions of the integration constants

$$\begin{aligned} A_1 &= \frac{i L_c \left(3 f_1 R z_1 I_0 \left(\frac{R f_1}{L_c} \right) - 2 L_c I_1 \left(\frac{R f_1}{L_c} \right) \right)}{f_2 L_c I_0 \left(\frac{R f_2}{L_c} \right) I_1 \left(\frac{R f_1}{L_c} \right) + f_1 z_1 I_0 \left(\frac{R f_1}{L_c} \right) \left(L_c I_1 \left(\frac{R f_2}{L_c} \right) - 2 f_2 R I_0 \left(\frac{R f_2}{L_c} \right) \right)} \frac{\mu_{\text{micro}}}{\mu_e + \mu_{\text{micro}}}, \\ B_1 &= \frac{i L_c \left(f_2 R I_0 \left(\frac{R f_2}{L_c} \right) - 2 L_c I_1 \left(\frac{R f_2}{L_c} \right) \right)}{f_2 L_c I_0 \left(\frac{R f_2}{L_c} \right) I_1 \left(\frac{R f_1}{L_c} \right) + f_1 z_1 I_0 \left(\frac{R f_1}{L_c} \right) \left(L_c I_1 \left(\frac{R f_2}{L_c} \right) - 2 f_2 R I_0 \left(\frac{R f_2}{L_c} \right) \right)} \frac{\mu_{\text{micro}}}{\mu_e + \mu_{\text{micro}}}, \\ z_1 &:= \frac{a_1 + 2 a_3}{3 a_1}. \end{aligned} \quad (43)$$

The classical torque, the higher-order torque, and energy (per unit length dz) expressions are

$$\begin{aligned} M_c(\vartheta) &:= \int_0^{2\pi} \int_0^R \left[\langle \tilde{\sigma} \mathbf{e}_z, \mathbf{e}_\varphi \rangle r \right] r dr d\varphi \\ &= \left[\left(\frac{4 \mu_c f_2 I_2 \left(\frac{R f_1}{L_c} \right) I_2 \left(\frac{R f_2}{L_c} \right) \left(\frac{L_c}{R} \right)^2}{\mu_e f_1 \left(f_1 z_1 I_0 \left(\frac{R f_1}{L_c} \right) \left(2 f_2 I_0 \left(\frac{R f_2}{L_c} \right) - I_1 \left(\frac{R f_2}{L_c} \right) \frac{L_c}{R} \right) - f_2 I_0 \left(\frac{R f_2}{L_c} \right) I_1 \left(\frac{R f_1}{L_c} \right) \frac{L_c}{R} \right)} \right. \right. \\ &\quad + \frac{f_1 z_1 I_0 \left(\frac{R f_1}{L_c} \right) \left(24 I_1 \left(\frac{R f_2}{L_c} \right) \left(\frac{L_c}{R} \right)^3 - 12 f_2 I_0 \left(\frac{R f_2}{L_c} \right) \left(\frac{L_c}{R} \right)^2 - f_2^2 I_1 \left(\frac{R f_2}{L_c} \right) \frac{L_c}{R} + 2 f_2^3 I_0 \left(\frac{R f_2}{L_c} \right) \right)}{f_2^2 \left(f_1 z_1 I_0 \left(\frac{R f_1}{L_c} \right) \left(2 f_2 I_0 \left(\frac{R f_2}{L_c} \right) - I_1 \left(\frac{R f_2}{L_c} \right) \frac{L_c}{R} \right) - f_2 I_0 \left(\frac{R f_2}{L_c} \right) I_1 \left(\frac{R f_1}{L_c} \right) \frac{L_c}{R} \right)} \\ &\quad \left. - \frac{I_1 \left(\frac{R f_1}{L_c} \right) \left(16 I_1 \left(\frac{R f_2}{L_c} \right) \left(\frac{L_c}{R} \right)^4 - 8 f_2 I_0 \left(\frac{R f_2}{L_c} \right) \left(\frac{L_c}{R} \right)^3 + f_2^3 I_0 \left(\frac{R f_2}{L_c} \right) \frac{L_c}{R} \right)}{f_2^2 \left(f_1 z_1 I_0 \left(\frac{R f_1}{L_c} \right) \left(2 f_2 I_0 \left(\frac{R f_2}{L_c} \right) - I_1 \left(\frac{R f_2}{L_c} \right) \frac{L_c}{R} \right) - f_2 I_0 \left(\frac{R f_2}{L_c} \right) I_1 \left(\frac{R f_1}{L_c} \right) \frac{L_c}{R} \right)} \right] \frac{\mu_e \mu_{\text{micro}}}{\mu_e + \mu_{\text{micro}}} I_p \vartheta \\ &= T_c \vartheta, \\ M_m(\vartheta) &:= \int_0^{2\pi} \int_0^R \left[\langle (\mathbf{m} \times \mathbf{e}_z) \mathbf{e}_\varphi, \mathbf{e}_r \rangle - \langle (\mathbf{m} \times \mathbf{e}_z) \mathbf{e}_r, \mathbf{e}_\varphi \rangle \right] r dr d\varphi \\ &= \left[\frac{I_2 \left(\frac{R f_2}{L_c} \right) \left(q_1 I_0 \left(\frac{R f_1}{L_c} \right) \left(\frac{L_c}{R} \right)^2 - q_2 I_1 \left(\frac{R f_1}{L_c} \right) \left(\frac{L_c}{R} \right)^3 \right)}{f_1 z_1 I_0 \left(\frac{R f_1}{L_c} \right) \left(2 f_2 I_0 \left(\frac{R f_2}{L_c} \right) - I_1 \left(\frac{R f_2}{L_c} \right) \frac{L_c}{R} \right) - f_2 I_0 \left(\frac{R f_2}{L_c} \right) I_1 \left(\frac{R f_1}{L_c} \right) \frac{L_c}{R}} \frac{4 \mu \mu_{\text{micro}}}{3 (\mu_e + \mu_{\text{micro}})} \right] I_p \vartheta \\ &= T_m \vartheta, \end{aligned} \quad (44)$$

$$\begin{aligned}
W_{\text{tot}}(\boldsymbol{\vartheta}) &:= \int_0^{2\pi} \int_0^R W(\mathbf{D}\mathbf{u}, \mathbf{P}, \text{Curl}\mathbf{P}) \, r \, dr \, d\varphi \\
&= \frac{1}{2} \left[\left(\frac{4\mu_c f_2 I_2 \left(\frac{Rf_1}{L_c} \right) I_2 \left(\frac{Rf_2}{L_c} \right) \left(\frac{L_c}{R} \right)^2}{\mu_e f_1 \left(f_1 z_1 I_0 \left(\frac{Rf_1}{L_c} \right) \left(2f_2 I_0 \left(\frac{Rf_2}{L_c} \right) - I_1 \left(\frac{Rf_2}{L_c} \right) \frac{L_c}{R} \right) - f_2 I_0 \left(\frac{Rf_2}{L_c} \right) I_1 \left(\frac{Rf_1}{L_c} \right) \frac{L_c}{R} \right)} \right. \right. \\
&\quad + \frac{f_1 z_1 I_0 \left(\frac{Rf_1}{L_c} \right) \left(24I_1 \left(\frac{Rf_2}{L_c} \right) \left(\frac{L_c}{R} \right)^3 - 12f_2 I_0 \left(\frac{Rf_2}{L_c} \right) \left(\frac{L_c}{R} \right)^2 - f_2^2 I_1 \left(\frac{Rf_2}{L_c} \right) \frac{L_c}{R} + 2f_2^3 I_0 \left(\frac{Rf_2}{L_c} \right)}{f_2^2 \left(f_1 z_1 I_0 \left(\frac{Rf_1}{L_c} \right) \left(2f_2 I_0 \left(\frac{Rf_2}{L_c} \right) - I_1 \left(\frac{Rf_2}{L_c} \right) \frac{L_c}{R} \right) - f_2 I_0 \left(\frac{Rf_2}{L_c} \right) I_1 \left(\frac{Rf_1}{L_c} \right) \frac{L_c}{R} \right)} \\
&\quad - \frac{I_1 \left(\frac{Rf_1}{L_c} \right) \left(16I_1 \left(\frac{Rf_2}{L_c} \right) \left(\frac{L_c}{R} \right)^4 - 8f_2 I_0 \left(\frac{Rf_2}{L_c} \right) \left(\frac{L_c}{R} \right)^3 + f_2^3 I_0 \left(\frac{Rf_2}{L_c} \right) \frac{L_c}{R} \right)}{f_2^2 \left(f_1 z_1 I_0 \left(\frac{Rf_1}{L_c} \right) \left(2f_2 I_0 \left(\frac{Rf_2}{L_c} \right) - I_1 \left(\frac{Rf_2}{L_c} \right) \frac{L_c}{R} \right) - f_2 I_0 \left(\frac{Rf_2}{L_c} \right) I_1 \left(\frac{Rf_1}{L_c} \right) \frac{L_c}{R} \right)} \\
&\quad \left. + \frac{4\mu I_2 \left(\frac{Rf_2}{L_c} \right) \left(q_1 I_0 \left(\frac{Rf_1}{L_c} \right) \left(\frac{L_c}{R} \right)^2 - q_2 I_1 \left(\frac{Rf_1}{L_c} \right) \left(\frac{L_c}{R} \right)^3 \right)}{3\mu_e \left(f_1 z_1 I_0 \left(\frac{Rf_1}{L_c} \right) \left(2f_2 I_0 \left(\frac{Rf_2}{L_c} \right) - I_1 \left(\frac{Rf_2}{L_c} \right) \frac{L_c}{R} \right) - f_2 I_0 \left(\frac{Rf_2}{L_c} \right) I_1 \left(\frac{Rf_1}{L_c} \right) \frac{L_c}{R} \right)} \right] \frac{\mu_e \mu_{\text{micro}}}{\mu_e + \mu_{\text{micro}}} I_p \boldsymbol{\vartheta}^2 \\
&= \frac{1}{2} T_W \boldsymbol{\vartheta}^2,
\end{aligned}$$

$$q_1 := 3a_1 f_1 f_2 z_1, \quad q_2 := 2f_2(a_1 - a_3).$$

Again it holds

$$\frac{d}{d\boldsymbol{\vartheta}} W_{\text{tot}}(\boldsymbol{\vartheta}) = M_c(\boldsymbol{\vartheta}) + M_m(\boldsymbol{\vartheta}), \quad \frac{d^2}{d\boldsymbol{\vartheta}^2} W_{\text{tot}}(\boldsymbol{\vartheta}) = T_c + T_m = T_w. \quad (45)$$

Both quantities M_c and W_{tot} are immediately accessible in any higher order generalized continuum model. However, the precise form of M_m is difficult to guess. The latter identity can, therefore, also be seen as an implicit definition of the higher order moment M_m . In the Appendix we will provide an independent way of obtaining the notation for M_m starting from considerations done on the Cosserat model (see Appendix C). We provide again the homogenization relations between the macro-parameters, the meso- (with index $(\cdot)_e$), and the micro-parameters [11, 46, 49]

$$\mu_{\text{macro}} = \frac{\mu_e \mu_{\text{micro}}}{\mu_e + \mu_{\text{micro}}}, \quad \kappa_{\text{macro}} = \frac{\kappa_e \kappa_{\text{micro}}}{\kappa_e + \kappa_{\text{micro}}}, \quad \text{with} \quad \begin{cases} \kappa_i = \frac{2\mu_i + 3\lambda_i}{3}, \\ i = \{e, \text{micro}, \text{macro}\} \end{cases}, \quad (46)$$

which can be used to define the following torsional stiffnesses

$$T_{\text{macro}} = \mu_{\text{macro}} I_p = \frac{\mu_{\text{micro}} \mu_e}{\mu_{\text{micro}} + \mu_e} I_p, \quad T_{\text{micro}} = \mu_{\text{micro}} I_p, \quad T_e = \mu_e I_p. \quad (47)$$

The plots of the torsional stiffness for the classical torque (light blue), the higher-order torque (red), and the torque energy (green) for $\mu_c = \{0, 1/2, \infty\}$ while varying L_c is shown in Fig. 5.

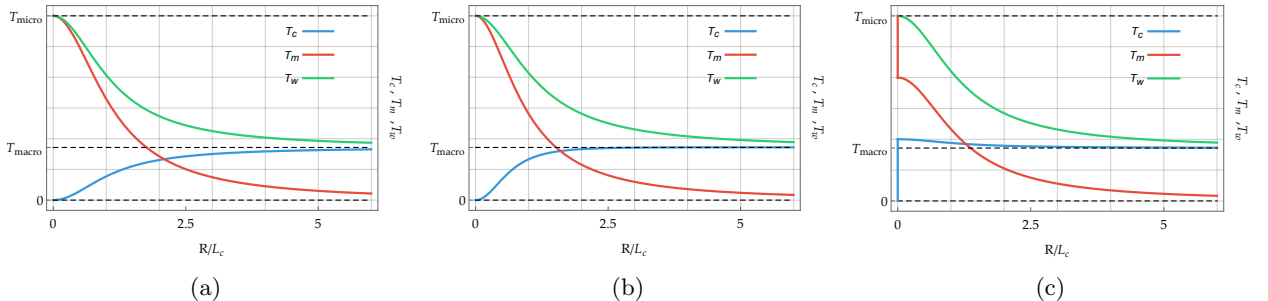


Figure 5: **(Relaxed micromorphic model)** Torsional stiffness for the classical torque T_c , the higher-order torque T_m , and the torque energy T_w while varying L_c for (a) $\mu_c \rightarrow 0$, (b) $\mu_c = 1/2$, and (c) $\mu_c \rightarrow \infty$. The torsional stiffness remains bounded as $L_c \rightarrow \infty$ ($R \rightarrow 0$). The values of the parameters used are: $\mu = 1$, $\mu_e = 1/10$, $\mu_{\text{micro}} = 1/4$, $a_1 = 1/5$, $a_2 = 1/6$, $a_3 = 1/7$, $R = 1$.

It is here highlighted that the torsional stiffness obtainable from the energy T_w is the only stiffness available experimentally.

4.1 Limits

4.1.1 The relaxed micromorphic model with symmetric force stresses ($\mu_c \rightarrow 0$)

$$\begin{aligned}
 W_{\text{tot}}(\boldsymbol{\vartheta}) &:= \int_0^{2\pi} \int_0^R W(\text{Du}, \mathbf{P}, \text{Curl} \mathbf{P}) \, r \, dr \, d\varphi \\
 &= \frac{1}{2} \left[\frac{f_2 I_0 \left(\frac{R f_2}{L_c} \right) \left(v_2 \mu_{\text{micro}} \frac{L_c^2}{R^2} + \mu_e (\mu_e + \mu_{\text{micro}}) \right)}{f_2 I_0 \left(\frac{R f_2}{L_c} \right) - 2 v_1 I_1 \left(\frac{R f_2}{L_c} \right) \frac{L_c}{R}} \right. \\
 &\quad \left. - \frac{2 I_1 \left(\frac{R f_2}{L_c} \right) \left(v_2 \mu_{\text{micro}} \frac{L_c^2}{R^2} + v_1 \mu_e (\mu_e + \mu_{\text{micro}}) \right) \frac{L_c}{R}}{f_2 I_0 \left(\frac{R f_2}{L_c} \right) - 2 v_1 I_1 \left(\frac{R f_2}{L_c} \right) \frac{L_c}{R}} \right] \frac{\mu_{\text{micro}}}{(\mu_e + \mu_{\text{micro}})^2} I_p \boldsymbol{\vartheta}^2,
 \end{aligned} \tag{48}$$

$$v_1 := \frac{a_1 + 2a_3}{a_1 + 8a_3}, \quad v_2 := \frac{24a_1 a_3 \mu}{a_1 + 8a_3}.$$

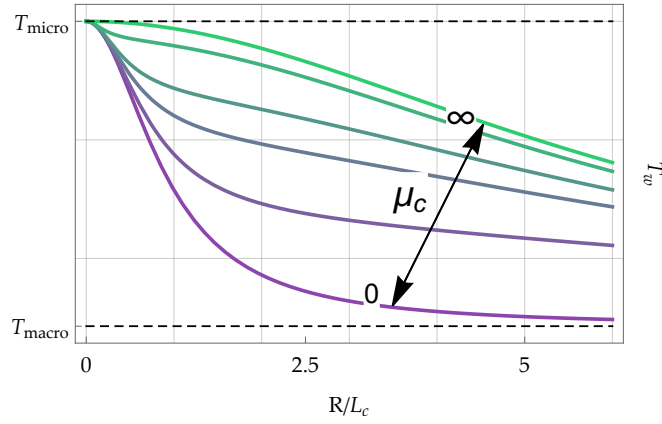


Figure 6: **(Relaxed micromorphic model)** Torsional stiffness for the torque energy while varying L_c , for different values of $\mu_c = \{0, 1/30, 1/10, 1/5, 1, \infty\}$. The torsional stiffness remains bounded as $L_c \rightarrow \infty$ ($R \rightarrow 0$) and the model does not collapse into a linear elastic one. The values of the other parameters used are: $\mu = 1$, $\mu_e = 1/3$, $\mu_{\text{micro}} = 1/4$, $a_1 = 10$, $a_3 = 1/50$, $R = 1$. Here, varying μ_c does not intervene with T_{macro} and T_{micro} .

Note that the torsional stiffness at the micro-scale T_{micro} is here independent of the Cosserat couple modulus μ_c , see (47).

4.1.2 The relaxed micromorphic model with conformal curvature energy ($a_3 = 0$) while varying the Cosserat couple modulus μ_c

In the particular case for which the parameter a_3 is equal to zero the elastic energy turns into

$$\begin{aligned}
 W(\text{Du}, \mathbf{P}, \text{Curl} \mathbf{P}) &= \mu_e \|\text{sym}(\text{Du} - \mathbf{P})\|^2 + \frac{\lambda_e}{2} \text{tr}^2(\text{Du} - \mathbf{P}) + \mu_c \|\text{skew}(\text{Du} - \mathbf{P})\|^2 \\
 &\quad + \mu_{\text{micro}} \|\text{sym} \mathbf{P}\|^2 + \frac{\lambda_{\text{micro}}}{2} \text{tr}^2(\mathbf{P}) + \frac{\mu L_c^2}{2} a_1 \|\text{dev sym Curl} \mathbf{P}\|^2.
 \end{aligned} \tag{49}$$

In this case, the torsional stiffness at the micro scale, namely for $L_c \rightarrow \infty$ ($R \rightarrow 0$)¹, depends also on μ_c

$$\tilde{T} := \lim_{L_c \rightarrow \infty} T_w = \frac{\mu_{\text{micro}} (9\mu_c + \mu_e)}{(9\mu_c + \mu_e) + \mu_{\text{micro}}} I_p. \tag{50}$$

For $\mu_c \rightarrow 0$ we obtain a linear elastic model with stiffness T_{macro} , for $\mu_c \rightarrow \infty$ it is recovered a model that has T_{micro} at the micro-scale, while for intermediate values of $0 < \mu_c < \infty$ a torsional stiffness between T_{macro} and T_{micro} appears.

¹Looking at the analytical solution obtained in (40) we see that the expression $\frac{R}{L_c}$ solely determines the response. Therefore, we can either fix $R > 0$ and send $L_c \rightarrow \infty$, or fix L_c and send $R \rightarrow 0$, having the same effect.

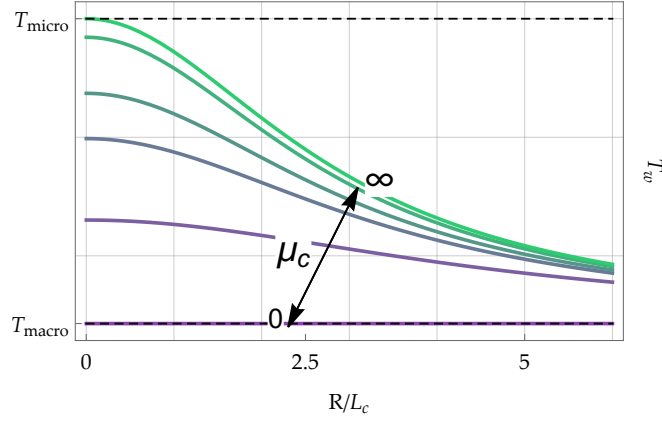


Figure 7: **(Relaxed micromorphic model with conformal curvature energy)** Torsional stiffness for the torque energy while varying L_c , for different values of $\mu_c = \{0, 1/30, 1/10, 1/5, 1, \infty\}$. The torsional stiffness remains bounded as $L_c \rightarrow \infty$ ($R \rightarrow 0$) and the model does not collapse in a linear elastic one beside the case $\mu_c = 0$. The values of the other parameters used are: $\mu = 1$, $\mu_e = 1/3$, $\mu_{\text{micro}} = 1/4$, $a_1 = 2$, $R = 1$. In this case, varying μ_c influences the torsional stiffness also for small specimen size.

We may consider a further limit in (50). It holds

$$\bar{T} := \lim_{\mu_{\text{micro}} \rightarrow \infty} \tilde{T} = (9\mu_c + \mu_e) I_p = (9\mu_c + \mu_{\text{macro}}) I_p, \quad (51)$$

where the last relation for which we have $\mu_e = \mu_{\text{macro}}$ is obtained from (33)₂ taking $\mu_{\text{micro}} \rightarrow \infty$.

4.1.3 The Cosserat model as a limit of the relaxed micromorphic model ($\mu_{\text{micro}} \rightarrow \infty$)

The Cosserat model can be obtained from the relaxed micromorphic model by formally letting $\mu_{\text{micro}} \rightarrow \infty$ and $\kappa_{\text{micro}} \rightarrow \infty$.² From the homogenization formula (46) it is possible to see that for $\mu_{\text{micro}} \rightarrow \mu_{\text{macro}}$ we have $\mu_e \rightarrow \infty$, while $\mu_{\text{macro}} = \mu_e$ for $\mu_{\text{micro}} \rightarrow \infty$, which is the stiffness at the macro-scale for the Cosserat model.

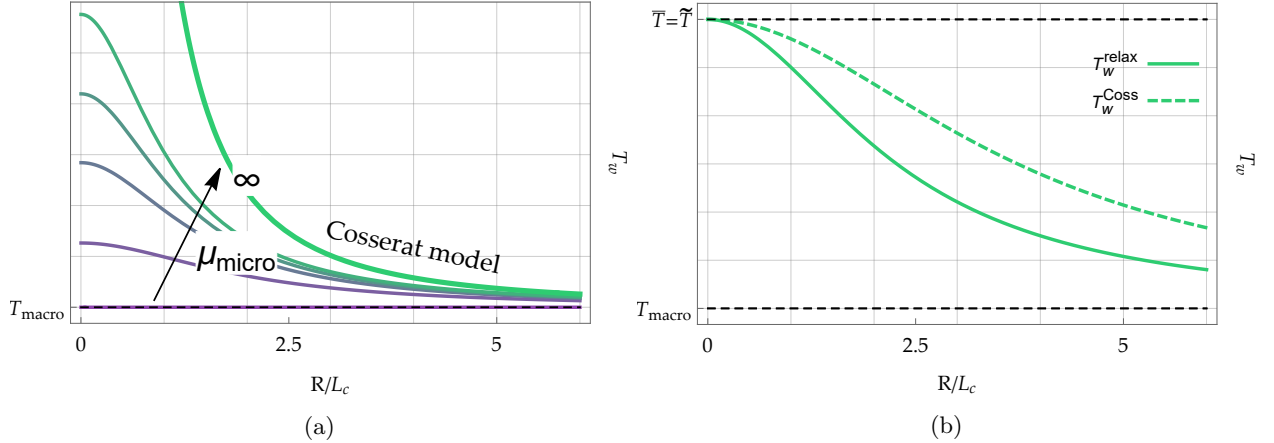


Figure 8: (a) **(Relaxed micromorphic model with full curvature)** Torsional stiffness for the torque energy while varying L_c , for different values of $\mu_{\text{micro}} = \{0, 1/20, 1/7, 1/4, 1/2, \infty\}$. The torsional stiffness becomes unbounded as $L_c \rightarrow \infty$ ($R \rightarrow 0$) when $\mu_{\text{micro}} \rightarrow \infty$. The values of the other parameters used are: $\mu = 1$, $\mu_{\text{macro}} = 1/10$, $\mu_c = 1/2$, $a_1 = 1/5$, $a_3 = 1/7$, $R = 1$. The Cosserat solution appears for $\mu_{\text{micro}} \rightarrow \infty$. (b) **(Cosserat model and relaxed micromorphic model with conformal curvature)**. Torsional stiffness for the torque energy while varying L_c . The torsional stiffness is bounded as $L_c \rightarrow \infty$ ($R \rightarrow 0$). For the Cosserat model we chose $\mu_c = 1/9$ while for the relaxed micromorphic model $\mu_c = 1/2$ and $\mu_{\text{micro}} = 3$ in order to have the same upper bound $\bar{T} = \tilde{T}$. The values of the other parameters used are: $\mu = 1$, $\mu_{\text{macro}} = 1$, $a_1 = 5$, $R = 1$.

²For the torsion problem, κ_{micro} does not intervene.

4.1.4 Sensitivity of the relaxed micromorphic model with respect to the curvature parameters a_1 and a_3 .

Sensitivity study for the relaxed micromorphic model while varying a_1 and a_3 independently.

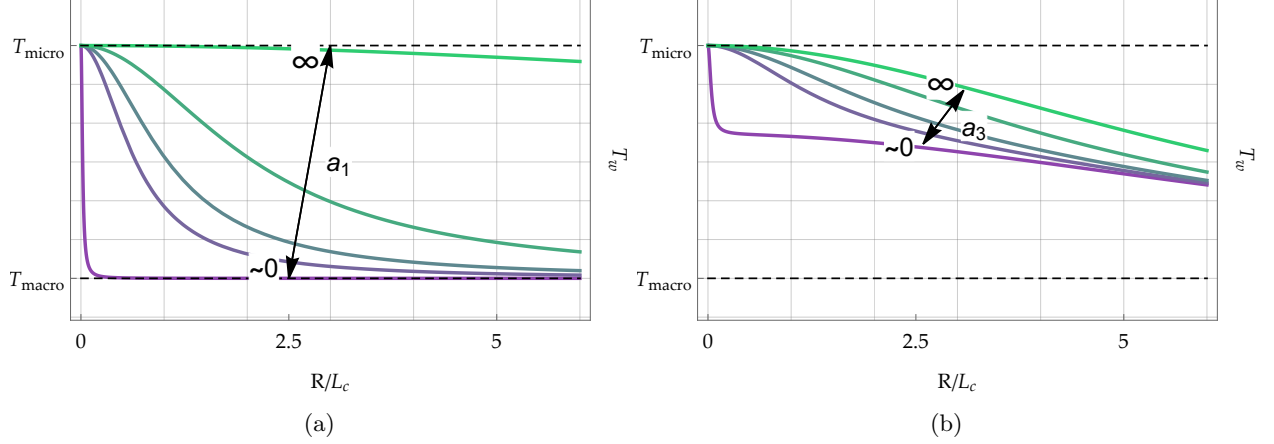


Figure 9: **(Relaxed micromorphic model)** Response of the relaxed micromorphic model while varying (a) the curvature parameter a_1 having $a_3 = 20$ and (b) the curvature parameter a_3 having $a_1 = 20$. The values of the other parameters are $\mu = 1$, $\mu_c = 1/5$, $\mu_e = 1$, $\mu_{\text{micro}} = 1/9$, $R = 1$.

The parametric study represented in Fig. 9 has not been carried out for the limit $a_1 \rightarrow 0$ and $a_3 \rightarrow 0$ since we would have had an indeterminate form for $L_c \rightarrow \infty$, and that is why we used the symbol ~ 0 . The solution of the problem while having $a_3 = 0$ a priori is analyzed carefully in Section 4.1.2, and the solution of the problem while having $a_1 = 0$ a priori make the relaxed model collapse into a classical linear elastic model with torsional stiffness T_{macro} .

4.2 Finite element simulations

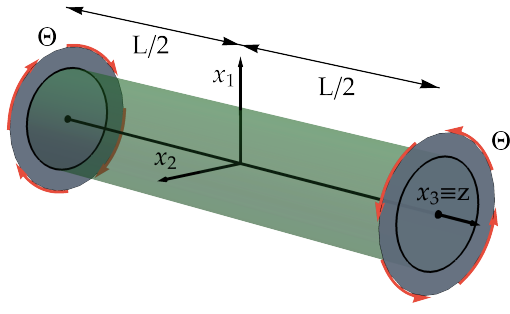
Using finite element analysis as a tool of comparison, in this section we will

- i) test the validity of the solution in terms of the hypothesis of small deformations (i.e., small twist rate);
- ii) discuss the validity of the St.Venant principle for the relaxed micromorphic model.

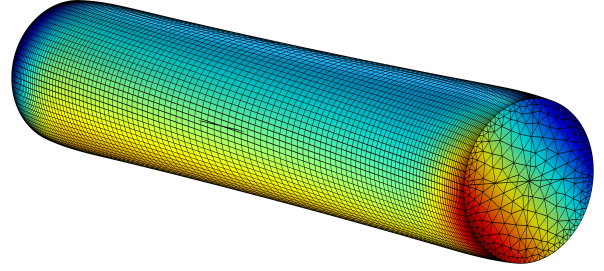
In this analysis we take a finite-size cylindrical rod and we apply opposite and equal finite-rotation at both of its ends ($z = \pm L/2$). Accordingly, the boundary conditions are

$$\begin{aligned} \mathbf{u}(z = \pm L/2) &= \begin{pmatrix} \cos \pm \Theta & \sin \pm \Theta & 0 \\ -\sin \pm \Theta & \cos \pm \Theta & 0 \\ 0 & 0 & 1 \end{pmatrix} \begin{pmatrix} x_1 \\ x_2 \\ L \end{pmatrix} - \begin{pmatrix} x_1 \\ x_2 \\ L \end{pmatrix}, \\ \mathbf{P}(z = \pm L/2) \times \mathbf{e}_1 &= \begin{pmatrix} -P_{12} & P_{11} & 0 \\ -P_{22} & P_{21} & 0 \\ -P_{32} & P_{31} & 0 \end{pmatrix} = \begin{pmatrix} \sin \pm \Theta & \cos \pm \Theta - 1 & 0 \\ 1 - \cos \pm \Theta & \sin \pm \Theta & 0 \\ 0 & 0 & 0 \end{pmatrix} = \mathbf{D}\mathbf{u}(z = \pm L/2) \times \mathbf{e}_1, \end{aligned} \quad (52)$$

where $\mathbf{P}(z) \times \mathbf{e}_1 = \mathbf{D}\mathbf{u}(z) \times \mathbf{e}_1$ are the **consistent boundary conditions** on the tangential part for the micro-distortion tensor \mathbf{P} .



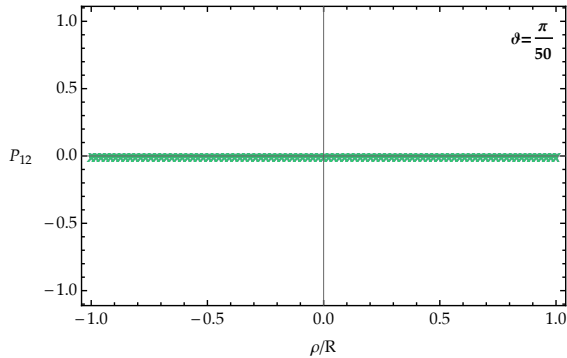
(a)



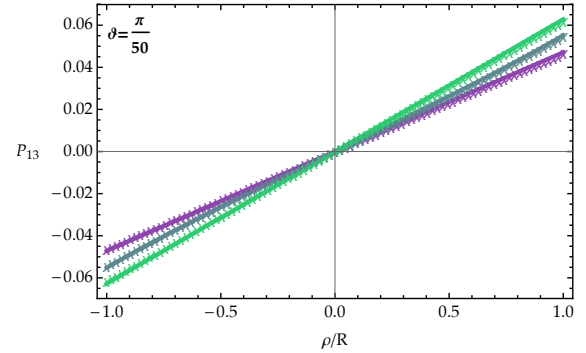
(b)

Figure 10: (a) boundary conditions scheme for a cylindrical rod of length $L = 10$ and radius $R = 1$; (b) deformed rod from the finite-element simulation on which it is mapped how the component of the gradient of the displacement $u_{1,3}$ changes.

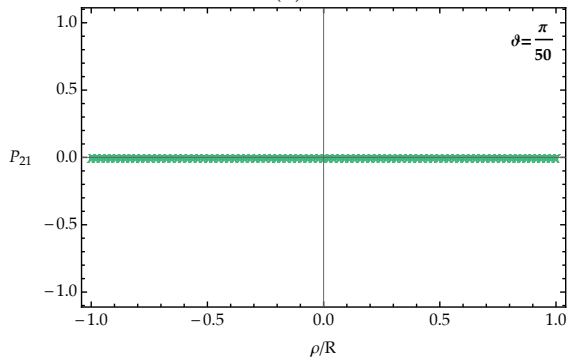
In Fig. 11 it is possible to see how the non identically zero components of the micro-distortion \mathbf{P} vary across the diameter aligned to the x_1 -axis ($\varphi = \pi/2$) of the cross-section placed in the middle of the cylindrical rod ($z = 0$). We chose the middle section in order to study the solution far away enough from the disturbance region on which the boundary conditions have been applied. The values of the components of \mathbf{P} of Fig. 11 (twist rate $\vartheta = \pi/50$) are perfectly in agreement with the analytical solution, confirming the validity of the small-deformation solution obtained in Section 4.



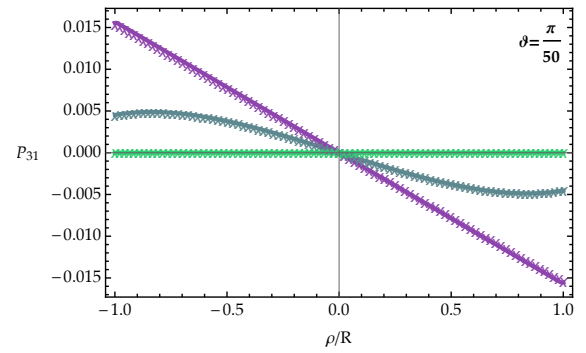
(a)



(b)



(c)



(d)

Figure 11: Plots of the components (a) P_{12} , (b) P_{13} , (c) P_{21} , and (d) P_{31} of the micro-distortion tensor \mathbf{P} at the cross-section $z = 0$. The purple line corresponds to $L_c = 0$, the gray one to $L_c = 1$, and the green one to $L_c = \infty$. The values of the other parameters used are $\mu = 1$, $\mu_c = 1$, $\mu_e = 1$, $\mu_{\text{micro}} = 1$, $a_1 = 1$, $a_3 = 1$, $R = 1$, $\vartheta = \pi/50$, $L = 10$.

Furthermore, in Fig. 12 we show how the solution obtained while applying consistent boundary conditions

converges to the one obtained analytically in a distance from the boundary which is more or less between one radius and one diameter. This is the pinnacle expression of the Saint Venant principle: we have applied not only a finite-rotation instead of a linearized one, but we have also used consistent boundary conditions for \mathbf{P} which we know are different from the correct values that the tangential part of \mathbf{P} should have, and we obtained nevertheless the analytical linearized solution after a rather small boundary layer.

We describe in particular the component P_{31} (other than the component P_{13}) since, due to the consistent boundary conditions, it is forced to start from zero at the lateral boundary. In Fig. 12 we plot this component which are evaluated for the length of the rod on the external surface ($\varphi = \pi/2$ and $r = R$).

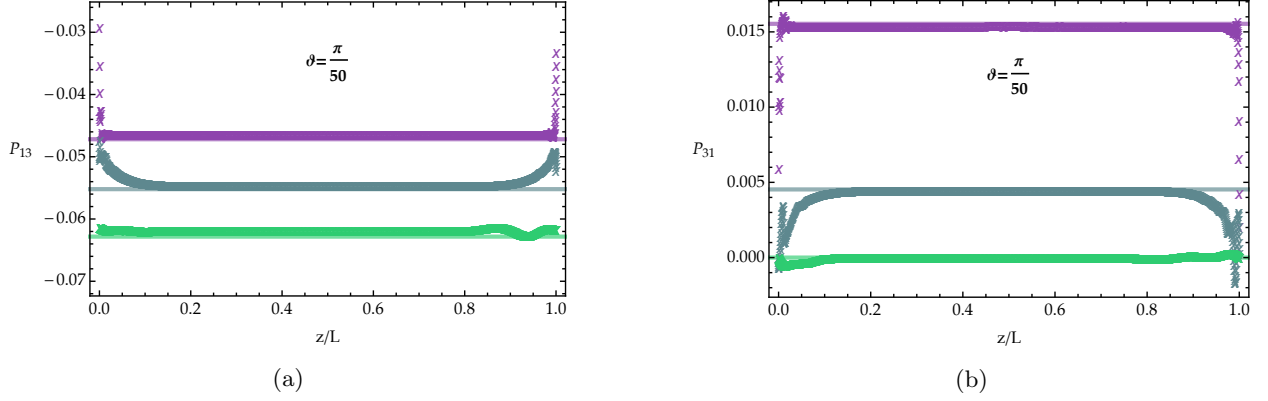


Figure 12: (a) Plot of how the component P_{13} ; (b) and P_{31} vary along a line on the external boundary ($\varphi = \pi/2$ and $r = R$): the solid lines are the analytical solution while the markers are the numerical values obtained thanks to a finite-element analysis. The purple line has been obtained for $L_c = 0$, the gray one for $L_c = 1$, and the green one for $L_c = \infty$. The values of the other parameters used are $\mu = 1$, $\mu_c = 1$, $\mu_e = 1$, $\mu_{\text{micro}} = 1$, $a_1 = 1$, $a_3 = 1$, $R = 1$, $\varphi = \pi/2$. As it can be seen, the solution does not converge stably and not perfectly symmetrically (the mesh is not symmetric) to the analytical one, but nevertheless it converges rapidly.

In Fig. 13 is reported how the component P_{13} vary on the cross section centered in the origin of the reference system ($z = 0$).

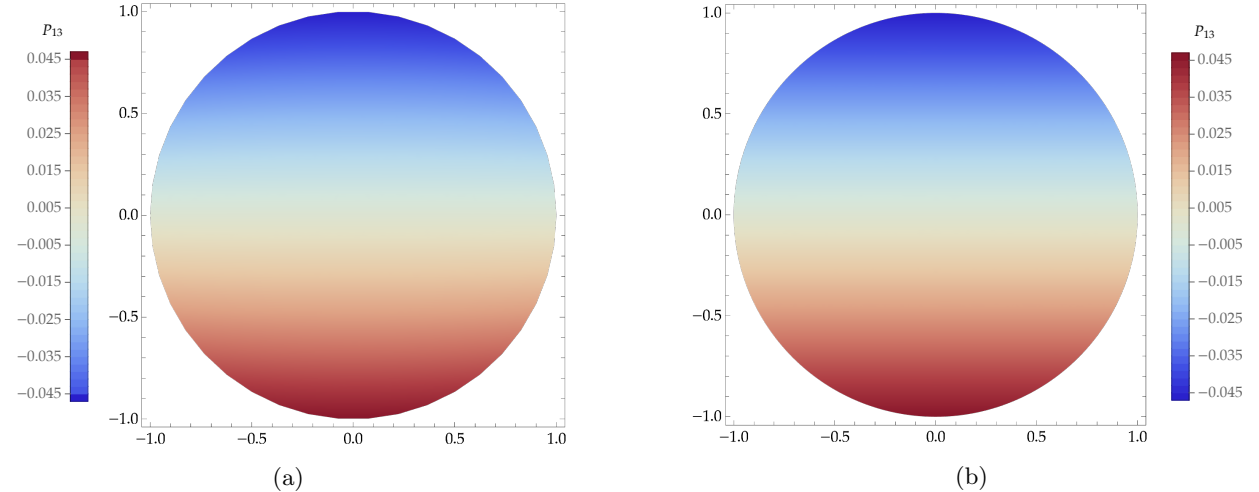


Figure 13: Plots of the component P_{13} across the section placed at $z = 0$ obtained (a) analytically and (b) with the finite-element analysis. The two results are in perfect agreement. The values of the other parameters used are $\mu = 1$, $\mu_c = 1$, $\mu_e = 1$, $\mu_{\text{micro}} = 1$, $a_1 = 1$, $a_3 = 1$, $R = 1$, $\varphi = \pi/2$, $L_c = 1$.

The implications of this results are of great value in the context of the identification of the elastic material parameters: it is clear how to apply consistent boundary conditions on a real sample in a laboratory (Dirichlet hard), and thanks to this results, we now know that our analytical solution is taking place far away enough from the boundary layer.

5 Torsional problem for the isotropic micro-stretch model in dislocation format

In the micro-stretch model in dislocation format [10, 31, 49, 52, 65], contrary to the relaxed micromorphic model, the micro-distortion tensor is devoid from the deviatoric component $\text{dev sym } \mathbf{P} = 0 \Leftrightarrow \mathbf{P} = \mathbf{A} + \omega \mathbf{1}$, $\mathbf{A} \in \mathfrak{so}(3)$, $\omega \in \mathbb{R}$. The expression of the strain energy for this model in dislocation format can be written as [49]:

$$\begin{aligned} W(\mathbf{Du}, \mathbf{A}, \omega, \text{Curl}(\mathbf{A} - \omega \mathbf{1})) \\ = \mu_{\text{macro}} \|\text{dev sym } \mathbf{Du}\|^2 + \frac{\kappa_e}{2} \text{tr}^2(\mathbf{Du} - \omega \mathbf{1}) + \mu_c \|\text{skew}(\mathbf{Du} - \mathbf{A})\|^2 + \frac{9}{2} \kappa_{\text{micro}} \omega^2 \\ + \frac{\mu L_c^2}{2} \left(a_1 \|\text{dev sym } \text{Curl } \mathbf{A}\|^2 + a_2 \|\text{skew } \text{Curl}(\mathbf{A} + \omega \mathbf{1})\|^2 + \frac{a_3}{3} \text{tr}^2(\text{Curl } \mathbf{A}) \right), \end{aligned} \quad (53)$$

since $\text{Curl}(\omega \mathbf{1}) \in \mathfrak{so}(3)$. The equilibrium equations, in the absence of body forces, are then

$$\begin{aligned} \text{Div} \left[\overbrace{2\mu_{\text{macro}} \text{dev sym } \mathbf{Du} + \kappa_e \text{tr}(\mathbf{Du} - \omega \mathbf{1}) \mathbf{1} + 2\mu_c \text{skew}(\mathbf{Du} - \mathbf{A})}^{\tilde{\sigma} :=} \right] &= \mathbf{0}, \\ 2\mu_c \text{skew}(\mathbf{Du} - \mathbf{A}) \\ - \mu L_c^2 \text{skew } \text{Curl} \left(a_1 \text{dev sym } \text{Curl } \mathbf{A} + a_2 \text{skew } \text{Curl}(\mathbf{A} + \omega \mathbf{1}) + \frac{a_3}{3} \text{tr}(\text{Curl } \mathbf{A}) \mathbf{1} \right) &= \mathbf{0}, \\ \text{tr} \left[2\mu_{\text{macro}} \text{dev sym } \mathbf{Du} \right. \\ \left. + \kappa_e \text{tr}(\mathbf{Du} - \omega \mathbf{1}) \mathbf{1} - \kappa_{\text{micro}} \text{tr}(\omega \mathbf{1}) \mathbf{1} - \mu L_c^2 a_2 \text{Curl } \text{skew } \text{Curl}(\omega \mathbf{1} + \mathbf{A}) \right] &= 0. \end{aligned} \quad (54)$$

The boundary conditions at the free surface are

$$\begin{aligned} \tilde{\mathbf{t}}(r = R) &= \tilde{\boldsymbol{\sigma}}(r) \cdot \mathbf{e}_r = \mathbf{0}_{\mathbb{R}^3}, \\ \boldsymbol{\eta}(r = R) &= \text{skew}(\mathbf{m}(r) \cdot \boldsymbol{\epsilon} \cdot \mathbf{e}_r) = \text{skew}(\mathbf{m}(r) \times \mathbf{e}_r) = \mathbf{0}_{\mathbb{R}^3 \times 3}, \\ \gamma(r = R) &= \frac{1}{3} \text{tr}(\mathbf{m}(r) \cdot \boldsymbol{\epsilon} \cdot \mathbf{e}_r) = \frac{1}{3} \text{tr}(\mathbf{m}(r) \times \mathbf{e}_r) = 0. \end{aligned} \quad (55)$$

According with the reference system shown in Fig. 1, the ansatz for the displacement and micro-distortion fields is

$$\begin{aligned} \mathbf{u}(x_1, x_2, x_3) = \mathbf{u}(r, \varphi, z) &= \boldsymbol{\vartheta} \begin{pmatrix} -x_2(r, \varphi) x_3(z) \\ x_1(r, \varphi) x_3(z) \\ 0 \end{pmatrix}, \quad \omega = 0, \\ \mathbf{A}(x_1, x_2, x_3) = \mathbf{A}(r, \varphi, z) &= \frac{\boldsymbol{\vartheta}}{2} \begin{pmatrix} 0 & -2x_3(z) & -g_p(r) x_2(r, \varphi) \\ 2x_3(z) & 0 & g_p(r) x_1(r, \varphi) \\ g_p(r) x_2(r, \varphi) & -g_p(r) x_1(r, \varphi) & 0 \end{pmatrix}. \end{aligned} \quad (56)$$

Since the ansatz requires $\omega = 0$, the micro-stretch model coincides with the Cosserat model which will be presented in the next section.

6 Torsional problem for the isotropic Cosserat continuum

The strain energy for the isotropic Cosserat continuum in dislocation tensor format (curvature expressed in term of $\text{Curl } \mathbf{A}$) can be written as [8, 29, 30, 45, 50, 60, 61, 64]

$$\begin{aligned} W(\mathbf{Du}, \mathbf{A}, \text{Curl } \mathbf{A}) &= \mu_{\text{macro}} \|\text{sym } \mathbf{Du}\|^2 + \frac{\lambda_{\text{macro}}}{2} \text{tr}^2(\mathbf{Du}) + \mu_c \|\text{skew}(\mathbf{Du} - \mathbf{A})\|^2 \\ &+ \frac{\mu L_c^2}{2} \left(a_1 \|\text{dev sym } \text{Curl } \mathbf{A}\|^2 + a_2 \|\text{skew } \text{Curl } \mathbf{A}\|^2 + \frac{a_3}{3} \text{tr}^2(\text{Curl } \mathbf{A}) \right), \end{aligned} \quad (57)$$

where $\mathbf{A} \in \mathfrak{so}(3)$. It is underlined that for the ansatz (61), which will be presented later in this section, it holds that $\text{skew}(\text{Curl } \mathbf{A}) = 0$ (see calculation (39)₂). The equilibrium equations, in the absence of body forces, are therefore the following

$$\begin{aligned} & \text{Div} \overbrace{[2\mu_{\text{macro}} \text{sym} \mathbf{D}\mathbf{u} + \lambda_{\text{macro}} \text{tr}(\mathbf{D}\mathbf{u}) \mathbf{1} + 2\mu_c \text{skew}(\mathbf{D}\mathbf{u} - \mathbf{A})]}^{\tilde{\sigma} :=} = \mathbf{0}, \\ & 2\mu_c \text{skew}(\mathbf{D}\mathbf{u} - \mathbf{A}) - \mu L_c^2 \text{skew} \text{Curl} \left(a_1 \text{dev} \text{sym} \text{Curl} \mathbf{A} + \frac{a_3}{3} \text{tr}(\text{Curl} \mathbf{A}) \mathbf{1} \right) = \mathbf{0}. \end{aligned} \quad (58)$$

The boundary conditions at the free surface are

$$\begin{aligned} \tilde{\mathbf{t}}(r=R) &= \tilde{\boldsymbol{\sigma}}(r) \cdot \mathbf{e}_r = \mathbf{0}_{\mathbb{R}^3}, \\ \boldsymbol{\eta}(r=R) &= \text{skew}(\mathbf{m}(r) \cdot \boldsymbol{\epsilon} \cdot \mathbf{e}_r) = \text{skew}(\mathbf{m}(r) \times \mathbf{e}_r) = \mathbf{0}_{\mathbb{R}^{3 \times 3}}, \end{aligned} \quad (59)$$

where the second order moment stress tensor is now given by

$$\mathbf{m} = \mu L_c^2 \left(a_1 \text{dev} \text{sym} \text{Curl} \mathbf{A} + \frac{a_3}{3} \text{tr}(\text{Curl} \mathbf{A}) \mathbf{1} \right), \quad (60)$$

the expression of $\tilde{\boldsymbol{\sigma}}$ is in (58), \mathbf{e}_r is the radial unit vector, and $\boldsymbol{\epsilon}$ is the Levi-Civita tensor.

According to the reference system shown in Fig. 1, the ansatz for the displacement field and the micro-rotation is

$$\begin{aligned} \mathbf{u}(x_1, x_2, x_3) &= \mathbf{u}(r, \varphi, z) = \boldsymbol{\vartheta} \begin{pmatrix} -x_2(r, \varphi) x_3(z) \\ x_1(r, \varphi) x_3(z) \\ 0 \end{pmatrix}, \\ \mathbf{A}(x_1, x_2, x_3) &= \mathbf{A}(r, \varphi, z) = \frac{\boldsymbol{\vartheta}}{2} \begin{pmatrix} 0 & -2x_3(z) & -g_p(r) x_2(r, \varphi) \\ 2x_3(z) & 0 & g_p(r) x_1(r, \varphi) \\ g_p(r) x_2(r, \varphi) & -g_p(r) x_1(r, \varphi) & 0 \end{pmatrix}, \end{aligned} \quad (61)$$

where, in relation to the ansatz (38), we define $g_p(r) := g_1(r) + g_2(r)$, so that there is only one unknown function to be determined. Substituting the ansatz (61) in (58) the 6 equilibrium equations are equivalent to

$$\begin{aligned} \frac{1}{6} \boldsymbol{\vartheta} \sin \varphi (6r \mu_c (g_p(r) - 1) - \mu L_c^2 (a_1 + 2a_3) (3g_p'(r) + r g_p''(r))) &= 0, \\ \frac{1}{6} \boldsymbol{\vartheta} \cos \varphi (6r \mu_c (g_p(r) - 1) - \mu L_c^2 (a_1 + 2a_3) (3g_p'(r) + r g_p''(r))) &= 0. \end{aligned} \quad (62)$$

It is important to underline that $(58)_1$ is identically satisfied, and that between the two equilibrium equations (62) there is only one independent equation since $(62)_1 = \tan \varphi (62)_2$. The solution of (62) is

$$g_p(r) = 1 - \frac{i A_1 I_1 \left(\frac{r f_1}{L_c} \right)}{r} + \frac{A_2 Y_1 \left(-\frac{i r f_1}{L_c} \right)}{r}, \quad f_1 := \sqrt{\frac{6\mu_c}{(a_1 + 2a_3)\mu}}, \quad (63)$$

where $I_n(\cdot)$ is the *modified Bessel function of the first kind*, $Y_n(\cdot)$ is the *Bessel function of the second kind* (see appendix B for the formal definitions), and A_1, A_2 are integration constants.

The value of A_1 is determined from the boundary conditions (59), where, due to the divergent behaviour of the Bessel function of the second kind at $r = 0$, we have to set $A_2 = 0$ in order to have a continuous solution. The fulfilment of the boundary conditions (59) allows us to find the expressions of the integration constants

$$A_1 = -\frac{i R L_c}{f_1 R z_1 \left(I_0 \left(\frac{R f_1}{L_c} \right) + I_2 \left(\frac{R f_1}{L_c} \right) \right) + z_2 L_c I_1 \left(\frac{R f_1}{L_c} \right)}, \quad z_1 := \frac{a_1 + 2a_3}{3a_1}, \quad z_2 := \frac{4a_3 - a_1}{3a_1}. \quad (64)$$

The classical torque, the higher-order torque, and energy (per unit length dz) expressions are

$$\begin{aligned} M_C(\boldsymbol{\vartheta}) &:= \int_0^{2\pi} \int_0^R [\langle \tilde{\boldsymbol{\sigma}} \mathbf{e}_z, \mathbf{e}_\varphi \rangle r] r dr d\varphi \\ &= \left[\mu_{\text{macro}} + \frac{4\mu_c I_2 \left(\frac{R f_1}{L_c} \right) \frac{L_c^2}{R^2}}{f_1 \left(2 f_1 z_1 I_0 \left(\frac{R f_1}{L_c} \right) + (z_2 - 2z_1) I_1 \left(\frac{R f_1}{L_c} \right) \frac{L_c}{R} \right)} \right] I_p \boldsymbol{\vartheta} = T_C \boldsymbol{\vartheta}, \end{aligned}$$

$$\begin{aligned}
M_{\mathbf{m}}(\boldsymbol{\vartheta}) &:= \int_0^{2\pi} \int_0^R \left[\langle \text{skew}(\mathbf{m} \times \mathbf{e}_z) \mathbf{e}_\varphi, \mathbf{e}_r \rangle - \langle \text{skew}(\mathbf{m} \times \mathbf{e}_z) \mathbf{e}_r, \mathbf{e}_\varphi \rangle \right] r \, dr \, d\varphi \\
&= \left[\frac{2\mu \left(3a_1 f_1 z_1 I_0 \left(\frac{R f_1}{L_c} \right) \frac{L_c^2}{R^2} - 2(a_1 - a_3) I_1 \left(\frac{R f_1}{L_c} \right) \frac{L_c^3}{R^3} \right)}{6f_1 z_1 I_0 \left(\frac{R f_1}{L_c} \right) - 3I_1 \left(\frac{R f_1}{L_c} \right) \frac{L_c}{R}} \right] I_p \boldsymbol{\vartheta} = T_{\mathbf{m}} \boldsymbol{\vartheta}, \tag{65}
\end{aligned}$$

$$\begin{aligned}
W_{\text{tot}}(\boldsymbol{\vartheta}) &:= \int_0^{2\pi} \int_0^R W(\mathbf{D}\mathbf{u}, \mathbf{A}, \text{Curl} \mathbf{A}) \, r \, dr \, d\varphi \\
&= \frac{1}{2} \left[\mu_{\text{macro}} + \frac{4\mu_c I_2 \left(\frac{R f_1}{L_c} \right) \frac{L_c^2}{R^2}}{f_1 \left(2f_1 z_1 I_0 \left(\frac{R f_1}{L_c} \right) + (z_2 - 2z_1) I_1 \left(\frac{R f_1}{L_c} \right) \frac{L_c}{R} \right)} \right. \\
&\quad \left. + \frac{2\mu \left(3a_1 f_1 z_1 I_0 \left(\frac{R f_1}{L_c} \right) \frac{L_c^2}{R^2} - 2(a_1 - a_3) I_1 \left(\frac{R f_1}{L_c} \right) \frac{L_c^3}{R^3} \right)}{6f_1 z_1 I_0 \left(\frac{R f_1}{L_c} \right) - 3I_1 \left(\frac{R f_1}{L_c} \right) \frac{L_c}{R}} \right] I_p \boldsymbol{\vartheta}^2 \\
&= \frac{1}{2} T_W \boldsymbol{\vartheta}^2.
\end{aligned}$$

The validity of (65)₂ for $M_{\mathbf{m}}$ will be shown in the Appendix C. The plot of the torsional stiffness for the classical torque (light blue), the higher-order torque (red), and the torque energy (green) while varying L_c is shown in Fig. 14.

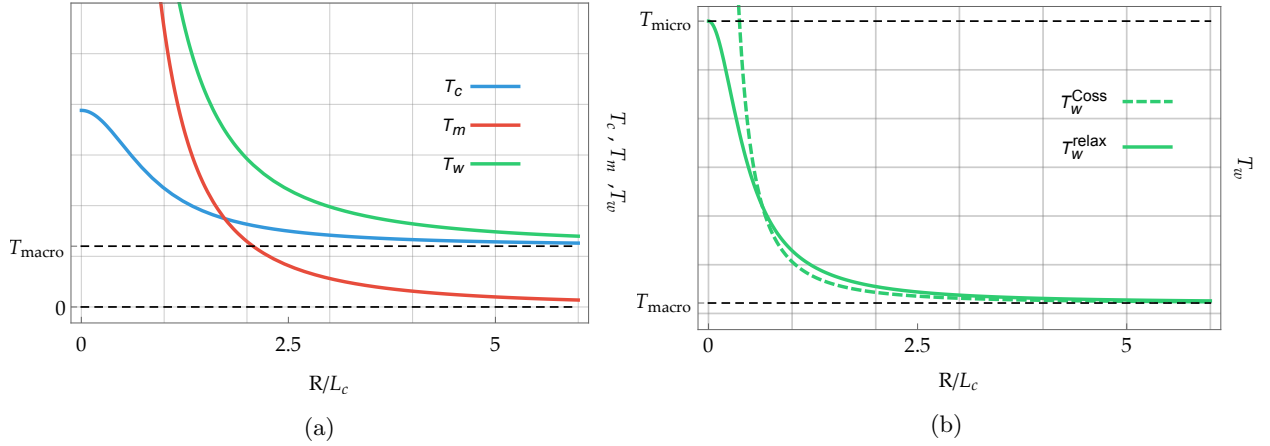


Figure 14: (a) **(Cosserat model with full curvature)** Torsional stiffness for the classical torque T_c , the higher-order torque T_m , and the torque energy T_w while varying L_c . The torsional stiffness is unbounded as $L_c \rightarrow \infty$ ($R \rightarrow 0$). (b) **(Cosserat model with full curvature vs relaxed micromorphic model)** Torsional stiffness for the torque energy (T_w) while varying L_c . Observe that the torsional stiffness remains bounded for the relaxed micromorphic model while it blows up for the Cosserat model as $L_c \rightarrow \infty$ ($R \rightarrow 0$). For best comparison, the characteristic length scale of the Cosserat model has been chosen $L_c^{\text{Coss}} := \frac{L_c^{\text{relax}}}{\sqrt{2}}$. The values of the parameters used are: $\mu = 1$, $\mu_c = 1/2$, $\mu_{\text{macro}} = 1/14$, $\mu_{\text{micro}} = 2$ (just for the relaxed micromorphic model), $a_1 = 1/5$, $a_3 = 1/7$, $R = 1$.

6.1 Cosserat conformal curvature case - bounded stiffness in torsion

In the particular case for which the parameter a_3 is equal to zero the elastic energy turns into

$$\begin{aligned}
W(\mathbf{D}\mathbf{u}, \mathbf{A}, \text{Curl} \mathbf{A}) &= \mu_{\text{macro}} \|\text{sym} \mathbf{D}\mathbf{u}\|^2 + \frac{\lambda_{\text{macro}}}{2} \text{tr}^2(\mathbf{D}\mathbf{u}) + \mu_c \|\text{skew}(\mathbf{D}\mathbf{u} - \mathbf{A})\|^2 \\
&\quad + \frac{\mu L_c^2}{2} a_1 \|\text{dev sym Curl} \mathbf{A}\|^2. \tag{66}
\end{aligned}$$

In terms of $\phi = \text{axl}(\mathbf{A})$, the curvature energy can be written as $\frac{\mu L_c^2}{2} a_1 \|\text{dev sym D axl}(\mathbf{A})\|^2$ which is the conformal curvature case [51]. In this special case, the torsional stiffness remains bounded as $L_c \rightarrow \infty$ ($R \rightarrow 0$), namely $\bar{T} := (9\mu_c + \mu_{\text{macro}}) I_p$, which is consistent with the results in (51).

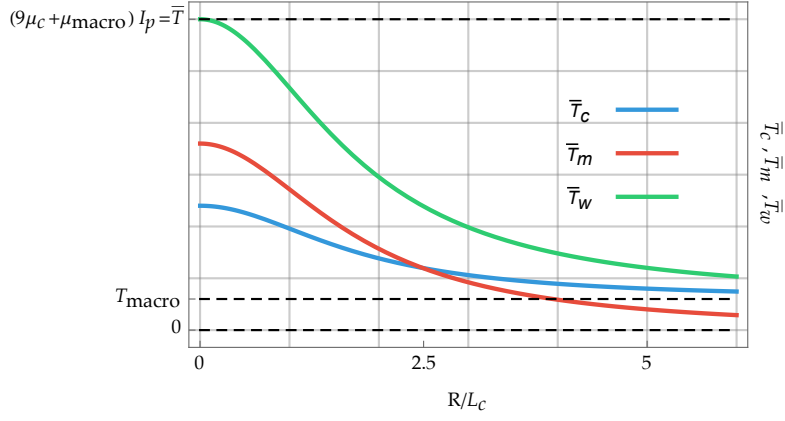


Figure 15: (**Cosserat model with conformal curvature**) Torsional stiffness for the classical torque T_c , the higher-order torque T_m , and the torque energy T_w while varying L_c . The torsional stiffness is bounded as $L_c \rightarrow \infty$ ($R \rightarrow 0$). The values of the parameters used are: $\mu = 1$, $\mu_c = 1/2$, $\mu_{\text{macro}} = 1/2$, $a_1 = 5$, $R = 1$. Here, the Cosserat couple modulus μ_c is clearly related to the value of the stiffness for small specimen size.

6.2 Cosserat limit case $\mu_c \rightarrow \infty$ (indeterminate couple stress model)

$$\begin{aligned} \lim_{\mu_c \rightarrow \infty} M_c(\boldsymbol{\vartheta}) &= \left[\mu_{\text{macro}} + a_1 \mu \frac{L_c^2}{R^2} \right] I_p \boldsymbol{\vartheta} = T_c \boldsymbol{\vartheta}, & \lim_{\mu_c \rightarrow \infty} M_m(\boldsymbol{\vartheta}) &= 2a_1 \mu \frac{L_c^2}{R^2} I_p \boldsymbol{\vartheta} = T_m \boldsymbol{\vartheta}, \quad (67) \\ \lim_{\mu_c \rightarrow \infty} W_{\text{tot}}(\boldsymbol{\vartheta}) &= \frac{1}{2} \left[\mu_{\text{macro}} + 3a_1 \mu \frac{L_c^2}{R^2} \right] I_p \boldsymbol{\vartheta}^2 = \frac{1}{2} T_w \boldsymbol{\vartheta}^2. \end{aligned}$$

It is highlighted that there is *not a one to one correspondence between the torque* obtained as a limit from the Cosserat model (67) and the one obtained using the indeterminate couple stress model from the beginning (78), but of course *the energy (or the sum of the two torques) coincides* and thus the total torque stiffness T_w coincides as well.

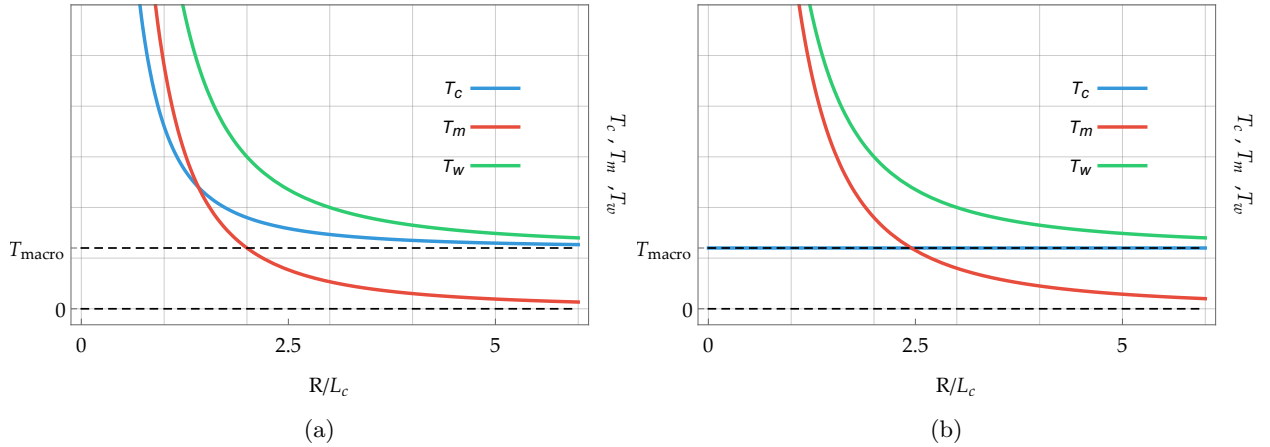


Figure 16: (**Cosserat model vs indeterminate couple stress model**) Comparison of the torsional stiffness for the classical torque T_c , the higher-order torque T_m , and the torque energy T_w while varying L_c for (a) the Cosserat model with $\mu_c \rightarrow \infty$ and for (b) the indeterminate couple stress model. There is not a one to one correspondence between the respective torque but the energy coincides.

6.3 Cosserat limit case $\mu_c \rightarrow 0$.

$$\begin{aligned} \lim_{\mu_c \rightarrow 0} M_c(\boldsymbol{\vartheta}) &= \mu_{\text{macro}} I_p \boldsymbol{\vartheta} = T_c \boldsymbol{\vartheta}, & \lim_{\mu_c \rightarrow 0} M_m(\boldsymbol{\vartheta}) &= \frac{24\mu a_1 a_3}{a_1 + 8a_3} \frac{L_c^2}{R^2} I_p \boldsymbol{\vartheta} = T_m \boldsymbol{\vartheta}, \quad (68) \\ \lim_{\mu_c \rightarrow 0} W_{\text{tot}}(\boldsymbol{\vartheta}) &= \frac{1}{2} \left[\mu_{\text{macro}} + \frac{24\mu a_1 a_3}{a_1 + 8a_3} \frac{L_c^2}{R^2} \right] I_p \boldsymbol{\vartheta}^2 = \frac{1}{2} T_w \boldsymbol{\vartheta}^2. \end{aligned}$$

It is highlighted that the Cosserat model does not collapse into a classical linear elastic model for $\mu_c \rightarrow 0$, but it remains proportional to $(L_c/R)^2$ eq.(68). In this case, the Cosserat model behaves similarly to the indeterminate couple stress model eq.(67) or eq.(78), and it collapses into this model (both the energy and the torques) by formally letting $a_3 \rightarrow \infty$ as it can be seen from equations (67) and (68).

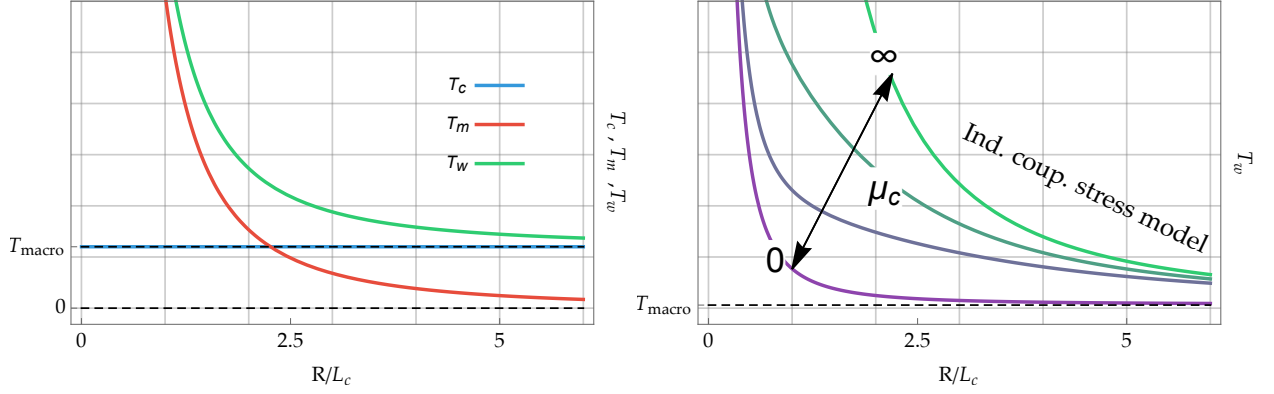


Figure 17: **(Cosserat model)** (a) Torsional stiffness for the classical torque T_c , the higher-order torque T_m , and the torque energy T_w while varying L_c for the limit $\mu_c \rightarrow 0$. The model does not collapse into a classical linear elastic one. The values of the material parameter used are $\mu = 1$, $\mu_e = 1/10$, $a_1 = 1/5$, $a_3 = 1/7$, $R = 1$. (b) Sensitivity study on how the Cosserat model behaves while varying $\mu_c = \{0, 1/3, 1, \infty\}$: for $\mu_c \rightarrow \infty$ we recover the indeterminate couple stress model, while for $\mu_c \rightarrow 0$ we still have a non linear relation between T_w and R/L_c since a classical linear elastic model is not attained (see eq.(68)). The values of the material parameter used are $\mu = 1$, $\mu_e = 1/10$, $a_1 = 12$, $a_3 = 1/20$, $R = 1$.

6.4 Sensitivity of the Cosserat model with respect to the curvature parameters a_1 and a_3 .

Here, we study the sensitivity for the Cosserat model while varying a_1 and a_3 independently.

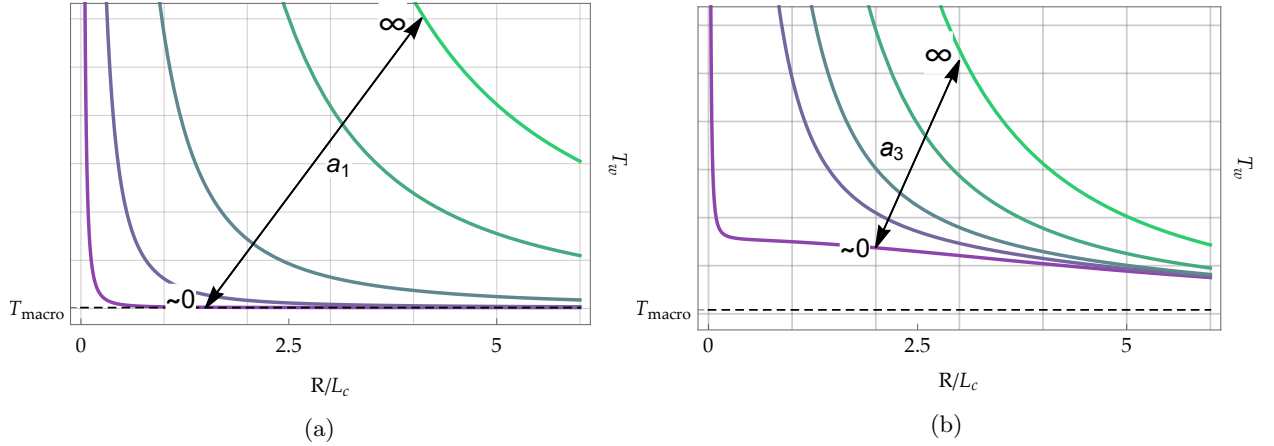


Figure 18: **(Cosserat model)** Response of the Cosserat model while varying (a) the curvature parameter a_1 having $a_3 = 20$ and (b) the curvature parameter a_3 having $a_1 = 20$. The values of the other parameters are $\mu = 1$, $\mu_c = 1/5$, $\mu_{\text{macro}} = 1/10$, $R = 1$.

The parametric study represented in Fig. 18 has not been carried out for the limit $a_1 \rightarrow 0$ and $a_3 \rightarrow 0$ since we would have had an indeterminate form for $L_c \rightarrow \infty$, and that is why we used the symbol ~ 0 . The solution of the problem while having $a_3 = 0$ a priori is analyzed carefully in Section 6.1, and the solution of the problem while having $a_1 = 0$ a priori makes the relaxed micromorphic model collapse into a classical linear elastic model with torsional stiffness T_{macro} . It is also highlighted that the Cosserat model collapses into the indeterminate couple stress model for $a_3 \rightarrow \infty$ also in this more general case for which μ_c is arbitrary.

7 Torsional problem for the isotropic micro-void model in dislocation tensor format

The strain energy for the isotropic micro-void continuum in dislocation tensor format can be written as [9, 60]

$$W(\mathbf{Du}, \omega, \text{Curl}(\omega \mathbf{1})) = \mu_{\text{macro}} \|\text{dev sym } \mathbf{Du}\|^2 + \frac{\kappa_e}{2} \text{tr}^2(\mathbf{Du} - \omega \mathbf{1}) + \frac{\kappa_{\text{micro}}}{2} \text{tr}^2(\omega \mathbf{1}) + \frac{\mu L_c^2}{2} a_2 \|\text{Curl}(\omega \mathbf{1})\|^2. \quad (69)$$

Here, $\omega : \mathbb{R}^3 \rightarrow \mathbb{R}$ is the additional scalar micro-void degree of freedom [9]. The equilibrium equations, in the absence of body forces, are³

$$\begin{aligned} \text{Div} \left[\overbrace{2\mu_{\text{macro}} \text{dev sym } \mathbf{Du} + \kappa_e \text{tr}(\mathbf{Du} - \omega \mathbf{1}) \mathbf{1}}^{\tilde{\sigma} :=} \right] &= \mathbf{0}, \\ \frac{1}{3} \text{tr} [\tilde{\sigma} - \kappa_{\text{micro}} \text{tr}(\omega \mathbf{1}) \mathbf{1} - \mu L_c^2 a_2 \text{Curl} \text{Curl}(\omega \mathbf{1})] &= 0. \end{aligned} \quad (70)$$

The boundary conditions at the free surface are

$$\begin{aligned} \tilde{\mathbf{t}}(r = R) &= \tilde{\sigma}(r) \cdot \mathbf{e}_r = \mathbf{0}_{\mathbb{R}^3}, \\ \eta(r = R) &= \frac{1}{3} \text{tr}(\mathbf{m}(r) \cdot \boldsymbol{\epsilon} \cdot \mathbf{e}_r) = \frac{1}{3} \text{tr}(\mathbf{m}(r) \times \mathbf{e}_r) = 0. \end{aligned} \quad (71)$$

According with the reference system shown in Fig. 1, the ansatz for the displacement field and the function ω have to be

$$\mathbf{u}(x_1, x_2) = \begin{pmatrix} -x_2 x_3 \\ x_1 x_3 \\ 0 \end{pmatrix}, \quad \omega(x_2) \mathbf{1} = \begin{pmatrix} 0 & 0 & 0 \\ 0 & 0 & 0 \\ 0 & 0 & 0 \end{pmatrix}. \quad (72)$$

which clearly reduce the model to a classical linear elastic one. No further calculation will be carried on and the reader is referred to Section 3.

8 Torsional problem for the isotropic couple stress continuum

The indeterminate couple stress model [19, 22, 32, 48, 55, 68, 69] appears by letting formally the Cosserat couple modulus $\mu_c \rightarrow \infty$. This implies the constraint $\mathbf{A} = \text{skew } \mathbf{Du} \in \mathfrak{so}(3)$. It is highlighted that for the torsional problem, we do not have any unknown fields in this model since the displacement \mathbf{u} is known a priori.⁴

Since $\text{tr}(\text{Curl skew } \mathbf{Du}) = \|\text{skew Curl skew } \mathbf{Du}\|^2 = 0$ in terms of the ansatz (77), the indeterminate couple stress elastic energy for the torsion can be written as

$$W(\mathbf{Du}, \text{Curl skew } \mathbf{Du}) = \mu_{\text{macro}} \|\text{sym } \mathbf{Du}\|^2 + \frac{\lambda_{\text{macro}}}{2} \text{tr}^2(\mathbf{Du}) + \frac{\mu L_c^2}{2} a_1 \|\text{sym Curl skew } \mathbf{Du}\|^2. \quad (73)$$

The equilibrium equations, in the absence of body forces, are⁵

$$\text{Div} [2\mu_{\text{macro}} \text{sym } \mathbf{Du} + \lambda_{\text{macro}} \text{tr}(\mathbf{Du}) \mathbf{1} + \mu L_c^2 \text{skew Curl}(a_1 \text{dev sym Curl skew } \mathbf{Du})] = \mathbf{0}, \quad (74)$$

while the (highly non-trivial) boundary traction conditions on the free surface are (for more details see [22, 48])

$$\begin{aligned} \tilde{\mathbf{t}}(r = R) &= \pm \left\{ \left(\tilde{\sigma} - \frac{1}{2} \text{Anti}(\text{Div } \mathbf{m}) \right) \cdot \mathbf{e}_r - \frac{1}{2} \mathbf{e}_r \times \text{D}[\langle \mathbf{e}_r, \text{sym } \mathbf{m} \cdot \mathbf{e}_r \rangle] \right. \\ &\quad \left. - \frac{1}{2} \text{D}[\text{Anti}((\mathbf{1} - \mathbf{e}_r \otimes \mathbf{e}_r) \cdot \mathbf{m} \cdot \mathbf{e}_r) \cdot (\mathbf{1} - \mathbf{e}_r \otimes \mathbf{e}_r)] : (\mathbf{1} - \mathbf{e}_r \otimes \mathbf{e}_r) \right\} = \mathbf{0}, \\ (\mathbf{1} - \mathbf{e}_r \otimes \mathbf{e}_r) \cdot \boldsymbol{\eta}(r = R) &= \pm (\mathbf{1} - \mathbf{e}_r \otimes \mathbf{e}_r) \cdot \text{Anti}[(\mathbf{1} - \mathbf{e}_r \otimes \mathbf{e}_r) \cdot \mathbf{m} \cdot \mathbf{e}_r] \cdot \mathbf{e}_r = \mathbf{0}, \\ \boldsymbol{\pi}(r = R) &= \pm \left(\text{Anti}[(\mathbf{1} - \mathbf{e}_r \otimes \mathbf{e}_r) \cdot \mathbf{m} \cdot \mathbf{e}_r]^+ - \text{Anti}[(\mathbf{1} - \mathbf{e}_r \otimes \mathbf{e}_r) \cdot \mathbf{m} \cdot \mathbf{e}_r]^- \right) \cdot \mathbf{e}_\varphi = \mathbf{0}, \end{aligned} \quad (75)$$

³Where $\kappa_e = \frac{2\mu_e + 3\lambda_e}{3}$ and $\kappa_{\text{micro}} = \frac{2\mu_{\text{micro}} + 3\lambda_{\text{micro}}}{3}$ are the meso- and the micro-scale 3D bulk modulus.

⁴Since we can show that the classical torsion displacement solution satisfies the external balance equation (74) as well as the higher order traction boundary conditions (75).

⁵Using Nye's formula [19] $\text{Curl } \mathbf{A} = \text{tr}[(\text{D axl } \mathbf{A})^T] - (\text{D axl } \mathbf{A})^T$ for $\mathbf{A} \in \mathfrak{so}(3)$ we can rewrite $\text{Curl skew } \mathbf{Du} = -(\text{D axl}(\text{skew } \mathbf{Du}))^T = \frac{1}{2} \text{D curl } \mathbf{u}$, since $\text{tr}(\text{Curl skew } \mathbf{Du}) = 0$.

where $\tilde{\boldsymbol{\sigma}} = 2\mu_e \text{sym } \mathbf{D}\mathbf{u} + \lambda_e \text{tr}(\mathbf{D}\mathbf{u}) \mathbf{1}$ is the symmetric force stress tensor, \mathbf{e}_r is the radial unit vector, and the non-symmetric second order moment stress is

$$\mathbf{m} = \mu L_c^2 (a_1 \text{dev sym Curl skew } \mathbf{D}\mathbf{u} + a_2 \text{skew Curl skew } \mathbf{D}\mathbf{u}) . \quad (76)$$

The term $(\text{Anti}[(\mathbf{1} - \mathbf{e}_r \otimes \mathbf{e}_r) \cdot \mathbf{m} \cdot \mathbf{e}_r]^+ - \text{Anti}[(\mathbf{1} - \mathbf{e}_r \otimes \mathbf{e}_r) \cdot \mathbf{m} \cdot \mathbf{e}_r]^-)$ is the measure of the discontinuity of $\text{Anti}[(\mathbf{1} - \mathbf{e}_r \otimes \mathbf{e}_r) \cdot \mathbf{m} \cdot \mathbf{e}_r]$ across the boundary.

According to the reference system shown in Fig. 1, the ansatz for the displacement field and consequently the skew-symmetric part of the gradient of the displacement are

$$\mathbf{u}(x_1, x_2) = \boldsymbol{\vartheta} \begin{pmatrix} -x_2 x_3 \\ x_1 x_3 \\ 0 \end{pmatrix} \Rightarrow \text{skew } \mathbf{D}\mathbf{u} = \frac{\boldsymbol{\vartheta}}{2} \begin{pmatrix} 0 & -2x_3 & -x_2 \\ 2x_3 & 0 & x_1 \\ x_2 & -x_1 & 0 \end{pmatrix} . \quad (77)$$

Since the ansatz is completely known, it is possible to check that both the equilibrium equations (74) and the boundary conditions (75) are identically satisfied⁶, and it is possible then to evaluate directly the classical torque, the higher-order torque, and the energy.

The classical torque, the higher-order torque, and energy (per unit length dz) expressions are

$$M_C(\boldsymbol{\vartheta}) := \int_0^{2\pi} \int_0^R [\langle \tilde{\boldsymbol{\sigma}} \mathbf{e}_z, \mathbf{e}_\varphi \rangle r] r dr d\varphi = \mu_e I_p \boldsymbol{\vartheta} = T_C \boldsymbol{\vartheta} ,$$

$$\begin{aligned} M_M(\boldsymbol{\vartheta}) &:= \int_0^{2\pi} \int_0^R [\langle (\mathbf{m} \times \mathbf{e}_z) \mathbf{e}_\varphi, \mathbf{e}_r \rangle - \langle (\mathbf{m} \times \mathbf{e}_z) \mathbf{e}_r, \mathbf{e}_\varphi \rangle + \langle (\mathbf{m} \times \mathbf{e}_r) \mathbf{e}_\varphi, \mathbf{e}_z \rangle - \langle (\mathbf{m} \times \mathbf{e}_r) \mathbf{e}_z, \mathbf{e}_\varphi \rangle] r dr d\varphi \\ &= 3a_1 \mu \frac{L_c^2}{R^2} I_p \boldsymbol{\vartheta} = T_M \boldsymbol{\vartheta} , \end{aligned} \quad (78)$$

$$W_{\text{tot}}(\boldsymbol{\vartheta}) := \int_0^{2\pi} \int_0^R W(\mathbf{D}\mathbf{u}, \text{Curl skew } \mathbf{D}\mathbf{u}) r dr d\varphi = \frac{1}{2} \left[\mu_{\text{macro}} + 3a_1 \mu \frac{L_c^2}{R^2} \right] I_p \boldsymbol{\vartheta}^2 = \frac{1}{2} T_W \boldsymbol{\vartheta}^2 .$$

The plot of the torsional stiffness for the classical torque, the higher-order torque, and the torque energy while varying L_c is shown in Fig. 19.

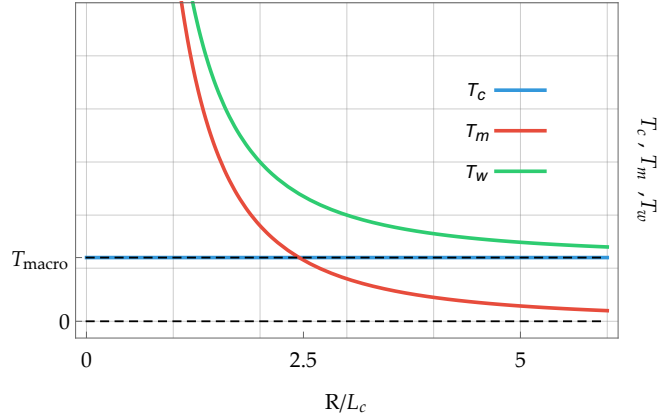


Figure 19: (**Indeterminate couple stress model**) Torsional stiffness for the classical torque T_C , the higher-order torque T_M , and the torque energy T_W while varying L_c . The torsional stiffness is unbounded as $L_c \rightarrow \infty$ ($R \rightarrow 0$). The values of the parameters used are: $\mu = 1$, $\mu_e = 1/3$, $a_1 = 1/5$, $R = 1$.

8.1 Torsional problem for the modified and the “pseudo”-consistent isotropic couple stress model

The **modified couple stress model** [19, 41, 43, 48, 54] consists in choosing $a_1 > 0$, $a_2 = 0$ and leads to a symmetric couple stress tensor while the (**“pseudo”**)-**consistent couple stress model** [21] appears for $a_1 = 0$, $a_2 > 0$ and leads to a skew symmetric stress tensor \mathbf{m} .

⁶In Hadjesfandiari and Dargush [22] the discussion of higher traction boundary conditions seems to be missing some terms in (75), letting the authors erroneously conclude that the classical displacement pure torsion solution does not satisfy the higher order boundary conditions.

Since $\text{tr}(\text{Curl skew } \mathbf{D}\mathbf{u}) = \|\text{skew Curl skew } \mathbf{D}\mathbf{u}\|^2 = 0$, the term $\|\text{dev sym Curl skew } \mathbf{D}\mathbf{u}\|^2$ is the only non zero component in the curvature energy, the form of the energy remains the same. This implies that, for the torsion problem, the **modified couple stress model** coincides with the **indeterminate couple stress model**, and that the (“pseudo”)-consistent couple stress model reduces to a classical linear elastic model without size-effects. According to the notation [21], the constitutive law can be written as⁷

$$\tilde{\boldsymbol{\sigma}} = 2\mu_{\text{macro}} \text{sym } \mathbf{D}\mathbf{u} + \lambda_{\text{macro}} \text{tr}(\mathbf{D}\mathbf{u}) \mathbf{1}, \quad \mathbf{m} = \eta (\text{D curl } \mathbf{u})^T + \eta' \text{D curl } \mathbf{u}. \quad (79)$$

where according to the classical Cosserat notation (see Appendix C)

$$\eta = \beta = \mu_{\text{macro}} \frac{L_c^2}{2} \frac{a_1 - a_2}{2}, \quad \eta' = \gamma = \mu_{\text{macro}} \frac{L_c^2}{2} \frac{a_1 + a_2}{2}. \quad (80)$$

In this notation, the modified couple stress model appears for $\eta = \eta'$ and the “pseudo”-consistent couple stress model appears for $\eta = -\eta'$.

9 Torsional problem for the classical isotropic micromorphic continuum without mixed terms

The strain energy for the isotropic micromorphic continuum without mixed terms ($\langle \text{sym } \mathbf{P}, \text{sym } (\mathbf{D}\mathbf{u} - \mathbf{P}) \rangle$, etc.) and simplified isotropic curvature can be written as

$$\begin{aligned} W(\mathbf{D}\mathbf{u}, \mathbf{P}, \mathbf{D}\mathbf{P}) &= \mu_e \|\text{dev sym } (\mathbf{D}\mathbf{u} - \mathbf{P})\|^2 + \frac{\kappa_e}{2} \text{tr}^2(\mathbf{D}\mathbf{u} - \mathbf{P}) + \mu_c \|\text{skew } (\mathbf{D}\mathbf{u} - \mathbf{P})\|^2 \\ &+ \mu_{\text{micro}} \|\text{dev sym } \mathbf{P}\|^2 + \frac{\kappa_{\text{micro}}}{2} \text{tr}^2(\mathbf{P}) \\ &+ \frac{\mu L_c^2}{2} \left(a_1 \|\text{D}(\text{dev sym } \mathbf{P})\|^2 + a_2 \|\text{D}(\text{skew } \mathbf{P})\|^2 + \frac{2}{9} a_3 \|\text{D}(\text{tr}(\mathbf{P}) \mathbf{1})\|^2 \right). \end{aligned} \quad (81)$$

The equilibrium equations, in the absence of body forces, are the following

$$\begin{aligned} \text{Div} \left[\overbrace{2\mu_e \text{dev sym } (\mathbf{D}\mathbf{u} - \mathbf{P}) + \kappa_e \text{tr}(\mathbf{D}\mathbf{u} - \mathbf{P}) \mathbf{1} + 2\mu_c \text{skew } (\mathbf{D}\mathbf{u} - \mathbf{P})}^{\tilde{\boldsymbol{\sigma}} :=} \right] &= \mathbf{0}, \\ \tilde{\boldsymbol{\sigma}} - 2\mu_{\text{micro}} \text{dev sym } \mathbf{P} - \kappa_{\text{micro}} \text{tr}(\mathbf{P}) \mathbf{1} \\ &+ \mu L_c^2 \left[a_1 \text{dev sym } \boldsymbol{\Delta} \mathbf{P} + a_2 \text{skew } \boldsymbol{\Delta} \mathbf{P} + \frac{2}{9} a_3 \text{tr}(\boldsymbol{\Delta} \mathbf{P}) \mathbf{1} \right] = \mathbf{0}, \end{aligned} \quad (82)$$

where $\boldsymbol{\Delta} \mathbf{P} \in \mathbb{R}^{3 \times 3}$ is taken component-wise. The boundary conditions at the external surfaces are

$$\tilde{\mathbf{t}}(r=R) = \tilde{\boldsymbol{\sigma}}(r) \cdot \mathbf{e}_r = \mathbf{0}_{\mathbb{R}^3}, \quad \boldsymbol{\eta}(r=R) = \mathbf{m}(r) \cdot \mathbf{e}_r = \mathbf{0}_{\mathbb{R}^{3 \times 3}}, \quad (83)$$

where

$$\mathbf{m} = \mu L_c^2 \left[a_1 \text{D}(\text{dev sym } \mathbf{P}) + a_2 \text{D}(\text{skew } \mathbf{P}) + \frac{2}{9} a_3 \text{D}(\text{tr}(\mathbf{S}) \mathbf{1}) \right] \quad (84)$$

is the third order moment stress tensor, the expression of $\tilde{\boldsymbol{\sigma}}$ is given in (82), and \mathbf{e}_r is the radial unit vector. According with the reference system shown in Fig. 1, the ansatz for the displacement field and the micro-distortion is

$$\begin{aligned} \mathbf{u}(x_1, x_2, x_3) &= \mathbf{u}(r, \varphi, z) = \boldsymbol{\vartheta} \begin{pmatrix} -x_2(r, \varphi) x_3(z) \\ x_1(r, \varphi) x_3(z) \\ 0 \end{pmatrix}, \\ \mathbf{P}(x_1, x_2, x_3) &= \mathbf{P}(r, \varphi, z) = \boldsymbol{\vartheta} \begin{pmatrix} 0 & -x_3(z) & -g_2(r) x_2(r, \varphi) \\ x_3(z) & 0 & g_2(r) x_1(r, \varphi) \\ g_1(r) x_2(r, \varphi) & -g_1(r) x_1(r, \varphi) & 0 \end{pmatrix}. \end{aligned} \quad (85)$$

⁷Setting $a_1 \mu_{\text{macro}} L_c^2 = 8\eta$ we obtain the rigidity as $T_W := \frac{a^2}{d\boldsymbol{\vartheta}^2} W_{\text{tot}}(\boldsymbol{\vartheta}) = \mu_{\text{macro}} \left(1 + 24 \frac{\eta}{\mu_{\text{macro}}} \frac{1}{R^2}\right) I_p$. In (44) of Hadjesfandiari and Dargush [22] we have the relation $\ell^2 = \frac{\eta}{\mu_{\text{macro}}}$, while in (55) we have the formula $T_W = \mu_{\text{macro}} \left(1 + 24 \left(\frac{\ell}{R}\right)^2\right) I_p = \mu_{\text{macro}} \left(1 + 24 \frac{\eta}{\mu_{\text{macro}}} \frac{1}{R^2}\right) I_p$.

Substituting the ansatz (85) in (82) the 12 equilibrium equations are equivalent to

$$\begin{aligned}
& \frac{1}{2} \vartheta \sin \varphi \left(\rho \left(\mu L_c^2 ((a_1 - a_2) g_1''(\rho) - (a_1 + a_2) g_2''(\rho)) + 2\mu_c (g_1(\rho) + g_2(\rho) - 1) \right. \right. \\
& \quad \left. \left. - 2(\mu_e + \mu_{\text{micro}}) (g_1(\rho) - g_2(\rho)) - 2\mu_e + 3\mu L_c^2 ((a_1 - a_2) g_1'(\rho) - (a_1 + a_2) g_2'(\rho)) \right) \right) = 0, \\
& \frac{1}{2} \vartheta \cos \varphi \left(\rho \left(\mu L_c^2 ((a_2 - a_1) g_1''(\rho) + (a_1 + a_2) g_2''(\rho)) - 2\mu_c (g_1(\rho) + g_2(\rho) - 1) \right. \right. \\
& \quad \left. \left. + 2(\mu_e + \mu_{\text{micro}}) (g_1(\rho) - g_2(\rho)) + 2\mu_e + 3\mu L_c^2 ((a_2 - a_1) g_1'(\rho) + (a_1 + a_2) g_2'(\rho)) \right) \right) = 0, \quad (86) \\
& \frac{1}{2} \vartheta \sin \varphi \left(\rho \left(\mu L_c^2 ((a_1 + a_2) g_1''(\rho) + (a_2 - a_1) g_2''(\rho)) - 2(\mu_c (g_1(\rho) + g_2(\rho) - 1) \right. \right. \\
& \quad \left. \left. + (\mu_e + \mu_{\text{micro}}) (g_1(\rho) - g_2(\rho))) - 2\mu_e + 3\mu L_c^2 ((a_1 + a_2) g_1'(\rho) + (a_2 - a_1) g_2'(\rho)) \right) \right) = 0, \\
& \frac{1}{2} \vartheta \cos \varphi \left(\rho \left(\mu L_c^2 ((a_1 - a_2) g_2''(\rho) - (a_1 + a_2) g_1''(\rho)) + 2(\mu_c (g_1(\rho) + g_2(\rho) - 1) \right. \right. \\
& \quad \left. \left. + (\mu_e + \mu_{\text{micro}}) (g_1(\rho) - g_2(\rho))) + 2\mu_e + 3\mu L_c^2 ((a_1 - a_2) g_2'(\rho) - (a_1 + a_2) g_1'(\rho)) \right) \right) = 0.
\end{aligned}$$

It is important to underline that (82)₁ is identically satisfied, and that between the four equilibrium equations (86) there are only two that are linearly independent since: (86)₁ = tan φ (86)₂ and (86)₃ = tan φ (86)₄.

It is also pointed out that the two remaining linearly independent equations (86)_{1,3} can be uncoupled⁸ and have the form of the Bessel ODE if we take their sum and difference, while being careful of substituting $g_p(r) := g_1(r) + g_2(r)$ and $g_m(r) := g_1(r) - g_2(r)$ along with their derivatives:

$$\begin{aligned}
\vartheta \sin \varphi \left(a_1 \mu L_c^2 (3g_m'(\rho) + \rho g_m''(\rho)) - 2\rho \mu_e (g_m(\rho) + 1) - 2\rho g_m(\rho) \mu_{\text{micro}} \right) &= 0, \\
\vartheta \sin \varphi \left(2\rho \mu_c (g_p(\rho) - 1) - a_2 \mu L_c^2 (3g_p'(\rho) + \rho g_p''(\rho)) \right) &= 0.
\end{aligned} \quad (87)$$

Since $g_1(r) := \frac{g_p(r) + g_m(r)}{2}$ and $g_2(r) := \frac{g_p(r) - g_m(r)}{2}$, the solution in terms of $g_1(r)$ and $g_2(r)$ of (87) is

$$\begin{aligned}
g_1(r) &= \frac{1}{2} \left(1 - \frac{i A_1 I_1 \left(\frac{r f_2}{L_c} \right) - A_2 Y_1 \left(-i \frac{r f_2}{L_c} \right) + i B_1 I_1 \left(\frac{r f_1}{L_c} \right) - B_2 Y_1 \left(-i \frac{r f_1}{L_c} \right)}{r} - \frac{\mu_e}{\mu_e + \mu_{\text{micro}}} \right), \\
g_2(r) &= \frac{1}{2} \left(1 + \frac{i A_1 I_1 \left(\frac{r f_2}{L_c} \right) - A_2 Y_1 \left(-i \frac{r f_2}{L_c} \right) - i B_1 I_1 \left(\frac{r f_1}{L_c} \right) + B_2 Y_1 \left(-i \frac{r f_1}{L_c} \right)}{r} + \frac{\mu_e}{\mu_e + \mu_{\text{micro}}} \right), \quad (88) \\
f_1 &:= \sqrt{\frac{2\mu_c}{a_2 \mu}}, \quad f_2 := \sqrt{\frac{2(\mu_e + \mu_{\text{micro}})}{a_1 \mu}},
\end{aligned}$$

where $I_n(\cdot)$ is the *modified Bessel function of the first kind*, $Y_n(\cdot)$ is the *Bessel function of the second kind* (see appendix B for the formal definitions), and A_1, B_1, A_2, B_2 are integration constants.

The values of A_1, B_1 are determined thanks to the boundary conditions (83), while, due to the divergent behaviour of the Bessel function of the second kind at $r = 0$, we have to set $A_2 = 0$ and $B_2 = 0$ in order to have a continuous solution. The fulfilment of the boundary conditions (83) allows us to find the expressions of the integration constants

$$A_1 = \frac{2i L_c \mu_e}{f_2 (\mu_e + \mu_{\text{micro}}) \left(I_0 \left(\frac{R f_2}{L_c} \right) + I_2 \left(\frac{R f_2}{L_c} \right) \right)}, \quad B_1 = -\frac{2i L_c}{f_1 \left(I_0 \left(\frac{R f_1}{L_c} \right) + I_2 \left(\frac{R f_1}{L_c} \right) \right)}. \quad (89)$$

The classical torque, the higher-order torque, and energy (per unit length dz) expressions are

$$\begin{aligned}
M_C(\vartheta) &:= \int_0^{2\pi} \int_0^R \left[\langle \tilde{\sigma} \mathbf{e}_z, \mathbf{e}_\varphi \rangle r \right] r dr d\varphi \\
&= \left[\left(\frac{8\mu_c I_2 \left(\frac{R f_1}{L_c} \right)}{f_1^2 I_0 \left(\frac{R f_1}{L_c} \right) + f_1^2 I_2 \left(\frac{R f_1}{L_c} \right)} + \frac{8\mu_e^2 I_2 \left(\frac{R f_2}{L_c} \right)}{(\mu_e + \mu_{\text{micro}}) \left(f_2^2 I_0 \left(\frac{R f_2}{L_c} \right) + f_2^2 I_2 \left(\frac{R f_2}{L_c} \right) \right)} \right) \frac{L_c^2}{R^2} + \frac{\mu_e \mu_{\text{micro}}}{\mu_e + \mu_{\text{micro}}} \right] I_p \vartheta \\
&= T_C \vartheta, \\
M_M(\vartheta) &:= \int_0^{2\pi} \int_0^R \left[\langle (\mathbf{m} \mathbf{e}_z) \mathbf{e}_\varphi, \mathbf{e}_r \rangle - \langle (\mathbf{m} \mathbf{e}_z) \mathbf{e}_r, \mathbf{e}_\varphi \rangle \right] r dr d\varphi = 4a_2 \mu \frac{L_c^2}{R^2} I_p \vartheta = T_M \vartheta,
\end{aligned}$$

⁸That this uncoupling takes place at all seems to be connected to the chosen form of the curvature energy. It remains unclear at present whether this feature holds for the most general isotropic curvature expression as well.

$$\begin{aligned}
W_{\text{tot}}(\boldsymbol{\vartheta}) &:= \int_0^{2\pi} \int_0^R W(\mathbf{D}\mathbf{u}, \mathbf{P}, \mathbf{D}\mathbf{P}) \, r \, dr \, d\varphi \\
&= \frac{1}{2} \left[\left(\frac{8\mu_c I_2 \left(\frac{Rf_1}{L_c} \right)}{f_1^2 I_0 \left(\frac{Rf_1}{L_c} \right) + f_1^2 I_2 \left(\frac{Rf_1}{L_c} \right)} + \frac{8\mu_e^2 I_2 \left(\frac{Rf_2}{L_c} \right)}{(\mu_e + \mu_{\text{micro}}) \left(f_2^2 I_0 \left(\frac{Rf_2}{L_c} \right) + f_2^2 I_2 \left(\frac{Rf_2}{L_c} \right) \right)} \right) \frac{L_c^2}{R^2} \right. \\
&\quad \left. + \underbrace{\frac{\mu_e \mu_{\text{micro}}}{\mu_e + \mu_{\text{micro}}}}_{\mu_{\text{macro}}} + 4a_2 \mu \frac{L_c^2}{R^2} \right] I_p \boldsymbol{\vartheta}^2 = \frac{1}{2} T_W \boldsymbol{\vartheta}^2,
\end{aligned} \tag{90}$$

and again it holds,

$$\frac{d}{d\boldsymbol{\vartheta}} W_{\text{tot}}(\boldsymbol{\vartheta}) = M_c(\boldsymbol{\vartheta}) + M_m(\boldsymbol{\vartheta}), \quad \frac{d^2}{d\boldsymbol{\vartheta}^2} W_{\text{tot}}(\boldsymbol{\vartheta}) = T_c + T_m = T_W. \tag{91}$$

It is underlined that the boundary conditions for the micromorphic model are consistent with the relaxed micromorphic model's one, being careful of changing $\mathbf{m} e_z$ with $\mathbf{m} \times e_z$. The plot of the torsional stiffness for the classical torque (light blue), the higher-order torque (red), and the torque energy (green) while varying L_c is shown in Fig. 20.

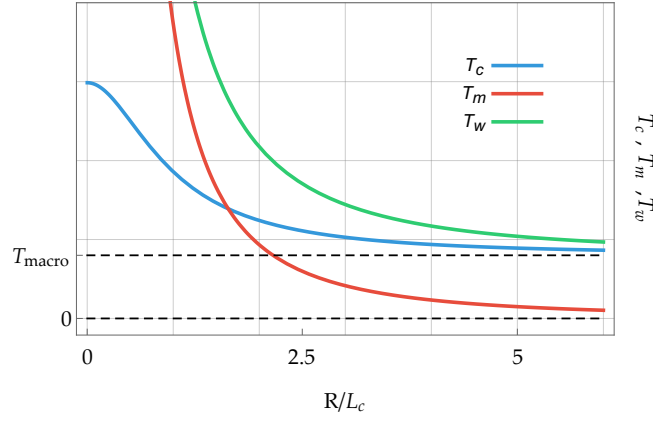


Figure 20: (**Micromorphic model**, classical case) Torsional stiffness for the classical torque T_c , the higher-order torque T_m , and the torque energy T_W while varying L_c . The torsional stiffness is unbounded as $L_c \rightarrow \infty$ ($R \rightarrow 0$). The values of the parameters used are: $\mu = 1$, $\mu_e = 1/3$, $\mu_{\text{micro}} = 1/4$, $\mu_c = 1/5$, $a_1 = 1/5$, $a_2 = 1/6$, $R = 1$.

9.1 Limits

9.1.1 The classical micromorphic model with symmetric forces stresses ($\mu_c \rightarrow 0$): nothing special

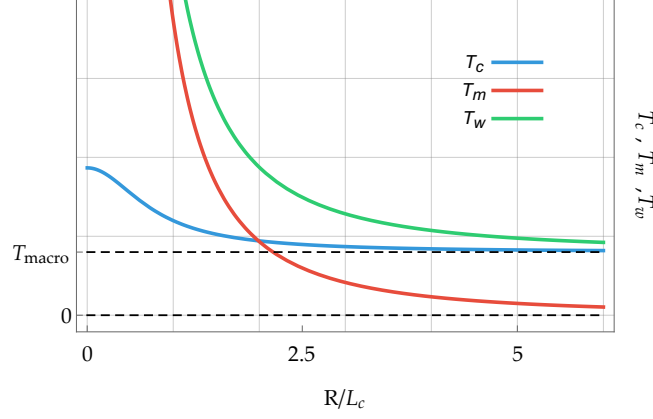


Figure 21: (**Micromorphic model**) Torsional stiffness for the torque energy while varying L_c , for different values of $\mu_c = \{0, 1/30, 1/10, 1/5, 1, \infty\}$. The torsional stiffness remains bounded as $L_c \rightarrow \infty$ ($R \rightarrow 0$) and the model does not collapse in a linear elastic one. The values of the other parameters used are: $\mu = 1$, $\mu_e = 1/3$, $\mu_{\text{micro}} = 1/4$, $a_1 = 2$, $a_3 = 1/20$, $R = 1$.

9.1.2 The classical micromorphic model with reduced curvature energy ($a_2 = 0$)

The classical micromorphic model with reduced curvature energy ($a_2 = 0$) collapses into the micro-strain model (Section 10 with $\text{sym}P$) thus becoming independent with respect to the Cosserat couple modulus μ_c (see (47) for the different stiffnesses expressions).

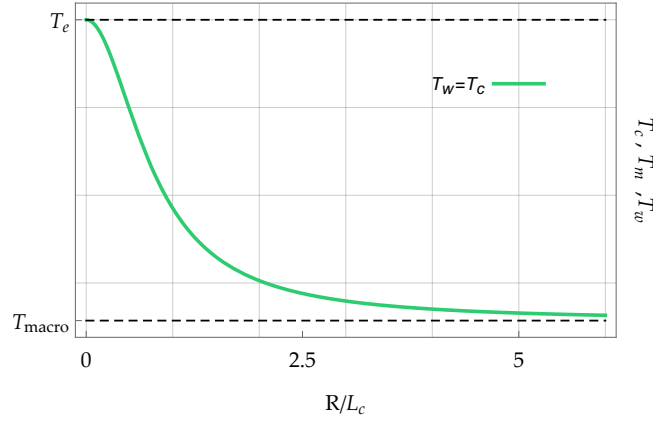


Figure 22: (**Micromorphic model**) Torsional stiffness for the torque energy while varying L_c , for different values of $\mu_c = \{0, 1/30, 1/10, 1/5, 1, \infty\}$. The torsional stiffness remains bounded as $L_c \rightarrow \infty$ ($R \rightarrow 0$) and the model does not collapse in a linear elastic one. The values of the other parameters used are: $\mu = 1$, $\mu_e = 1/3$, $\mu_{\text{micro}} = 1/4$, $a_1 = 2$, $a_3 = 1/20$, $R = 1$. In this case, the stiffness for arbitrary small sample size is governed by T_e and not T_{micro} . The reason for this is explained in Appendix D.

10 Torsional problem for the micro-strain model without mixed terms

The micro-strain model [13, 25] is a particular case of the classical Mindlin-Eringen model, in which it is assumed a priori that the micro-distortion remains symmetric, $\mathbf{P} = \mathbf{S} \in \text{Sym}(3)$.⁹

A torsion solution for a more general case with mixed terms has been derived in [24], but here we employ a reduced isotropic curvature expression to make the calculations more manageable.

⁹Shaat [66] uses the micro-strain model with mixed terms and a degenerate curvature expression in $D\mathbf{S}$, omitting $S_{11,1}$, $S_{22,2}$, and $S_{33,3}$.

It is underlined that the micro-strain model cannot be obtained as a limit case of the relaxed micromorphic model and vice versa, although there are some similarities. The strain energy which we consider is

$$W(\mathbf{Du}, \mathbf{S}, \mathbf{DS}) = \mu_e \|\text{dev}(\text{sym } \mathbf{Du} - \mathbf{S})\|^2 + \frac{\kappa_e}{2} \text{tr}^2(\mathbf{Du} - \mathbf{S}) + \mu_{\text{micro}} \|\text{dev } \mathbf{S}\|^2 + \frac{\kappa_{\text{micro}}}{2} \text{tr}^2(\mathbf{S}) \quad (92)$$

$$+ \frac{\mu L_c^2}{2} \left(a_1 \|\mathbf{D}(\text{dev } \mathbf{S})\|^2 + \frac{2}{9} a_3 \|\mathbf{D}(\text{tr}(\mathbf{S}) \mathbf{1})\|^2 \right).$$

The chosen 2-parameter curvature expression represents a simplified isotropic curvature (the full isotropic curvature for the micro-strain model would still counts 8 parameters [5]). In this form, the micro-strain model can be obtained from the classical micromorphic model (Section 9), in general, by setting $\mu_c = 0$ and $a_2 = 0$. For the torsion problem, the condition $a_2 = 0$ alone is sufficient.

It is underlined that for the ansatz (96), which will be presented later in this section, it holds $\text{tr}(\mathbf{S}) = 0$. The equilibrium equations, in the absence of body forces, are therefore the following

$$\begin{aligned} \text{Div} \left[\overbrace{2\mu_e \text{dev}(\text{sym } \mathbf{Du} - \mathbf{S}) + \kappa_e \text{tr}(\mathbf{Du} - \mathbf{S}) \mathbf{1}}^{\tilde{\boldsymbol{\sigma}} :=} \right] &= \mathbf{0}, \\ 2\mu_e \text{dev}(\text{sym } \mathbf{Du} - \mathbf{S}) + \kappa_e \text{tr}(\mathbf{Du} - \mathbf{S}) \mathbf{1} - 2\mu_{\text{micro}} \text{dev } \mathbf{S} - \kappa_{\text{micro}} \text{tr}(\mathbf{S}) \mathbf{1} \\ &+ \mu L_c^2 \text{sym Div} \left[a_1 \mathbf{D}(\text{dev } \mathbf{S}) + \frac{2}{9} a_3 \mathbf{D}(\text{tr}(\mathbf{S}) \mathbf{1}) \right] = \mathbf{0}. \end{aligned} \quad (93)$$

The boundary conditions at the external free surfaces are

$$\tilde{\mathbf{t}}(r = R) = \tilde{\boldsymbol{\sigma}}(r) \cdot \mathbf{e}_r = \mathbf{0}_{\mathbb{R}^3}, \quad \boldsymbol{\eta}(r = R) = \text{sym}(\mathbf{m}(r) \cdot \mathbf{e}_r) = \mathbf{0}_{\mathbb{R}^{3 \times 3}}, \quad (94)$$

where

$$\mathbf{m} = \mu L_c^2 \left[a_1 \mathbf{D}(\text{dev } \mathbf{S}) + \frac{2}{9} a_3 \mathbf{D}(\text{tr}(\mathbf{S}) \mathbf{1}) \right] \quad (95)$$

is the third order moment stress tensor, the expression of $\tilde{\boldsymbol{\sigma}}$ is in (93), \mathbf{e}_r is the radial unit vector. According with the reference system shown in Fig. 1, the ansatz for the displacement field and the micro-distortion is

$$\begin{aligned} \mathbf{u}(r, \varphi, z) &= \boldsymbol{\vartheta} \begin{pmatrix} -x_2(r, \varphi) x_3(z) \\ x_1(r, \varphi) x_3(z) \\ 0 \end{pmatrix}, \\ \mathbf{S}(r, \varphi, z) &= \frac{\boldsymbol{\vartheta}}{2} \begin{pmatrix} 0 & 0 & g_m(r) x_2(r, \varphi) \\ 0 & 0 & -g_m(r) x_1(r, \varphi) \\ g_m(r) x_2(r, \varphi) & -g_m(r) x_1(r, \varphi) & 0 \end{pmatrix}, \end{aligned} \quad (96)$$

where, in relation to the ansatz (38), $g_m(r) := g_1(r) - g_2(r)$. Substituting the ansatz (96) in (93) the 9 equilibrium equation are equivalent to

$$\begin{aligned} \frac{1}{2} \boldsymbol{\vartheta} \sin \varphi (a_1 \mu L_c^2 (3g'_m(r) + r g''_m(r)) - 2r \mu_e (g_m(r) + 1) - 2r g_m(r) \mu_{\text{micro}}) &= 0, \\ -\frac{1}{2} \boldsymbol{\vartheta} \cos \varphi (a_1 \mu L_c^2 (3g'_m(r) + r g''_m(r)) - 2r \mu_e (g_m(r) + 1) - 2r g_m(r) \mu_{\text{micro}}) &= 0. \end{aligned} \quad (97)$$

Between the two equilibrium equations (97) there is only one independent equation since $(97)_1 = -\tan \varphi (97)_2$. The solution of (97) is

$$g_m(r) = \frac{A_2 Y_1 \left(-\frac{ir f_1}{L_c} \right) - i A_1 I_1 \left(\frac{r f_1}{L_c} \right)}{r} - \frac{\mu_e}{\mu_e + \mu_{\text{micro}}}, \quad f_1 := \sqrt{\frac{2(\mu_e + \mu_{\text{micro}})}{a_1 \mu}}, \quad (98)$$

where $I_n(\cdot)$ is the *modified Bessel function of the first kind*, $Y_n(\cdot)$ is the *Bessel function of the second kind* (see appendix B for the formal definitions), and A_1, A_2 are integration constants.

The value of A_1 is determined thanks to the boundary conditions (94), while, due to the divergent behaviour of the Bessel function of the second kind at $r = 0$, we have to set $A_2 = 0$ in order to have a continuous solution. The fulfilment of the boundary conditions (94) allows us to find the expressions of the integration constants

$$A_1 = \frac{2i L_c}{I_0 \left(\frac{R f_1}{L_c} \right) + I_2 \left(\frac{R f_1}{L_c} \right)} \frac{\mu_e}{f_1 (\mu_e + \mu_{\text{micro}})}. \quad (99)$$

The classical torque, the higher-order torque, and the energy (per unit length dz) expressions are

$$\begin{aligned}
M_C(\boldsymbol{\vartheta}) &:= \int_0^{2\pi} \int_0^R \left[\langle \tilde{\boldsymbol{\sigma}} \mathbf{e}_z, \mathbf{e}_\varphi \rangle r \right] r dr d\varphi \\
&= \left[\frac{\mu_e \mu_{\text{micro}}}{\mu_e + \mu_{\text{micro}}} + \frac{\mu_e^2 \mu a_1}{(\mu_e + \mu_{\text{micro}})^2} \frac{4 I_2 \left(\frac{R f_1}{L_c} \right)}{I_0 \left(\frac{R f_1}{L_c} \right) + I_2 \left(\frac{R f_1}{L_c} \right)} \frac{L_c^2}{R^2} \right] I_p \boldsymbol{\vartheta} = T_C \boldsymbol{\vartheta}, \\
M_M(\boldsymbol{\vartheta}) &:= \int_0^{2\pi} \int_0^R \left[\langle \text{sym}(\mathbf{m} \mathbf{e}_z) \mathbf{e}_\varphi, \mathbf{e}_r \rangle - \langle \text{sym}(\mathbf{m} \mathbf{e}_z) \mathbf{e}_r, \mathbf{e}_\varphi \rangle \right] r dr d\varphi = 0, \\
W_{\text{tot}}(\boldsymbol{\vartheta}) &:= \int_0^{2\pi} \int_0^R W(\mathbf{D}\mathbf{u}, \mathbf{S}, \mathbf{D}\mathbf{S}) r dr d\varphi \\
&= \frac{1}{2} \left[\underbrace{\frac{\mu_e \mu_{\text{micro}}}{\mu_e + \mu_{\text{micro}}}}_{\mu_{\text{macro}}} + \frac{\mu_e^2 \mu a_1}{(\mu_e + \mu_{\text{micro}})^2} \frac{4 I_2 \left(\frac{R f_1}{L_c} \right)}{I_0 \left(\frac{R f_1}{L_c} \right) + I_2 \left(\frac{R f_1}{L_c} \right)} \frac{L_c^2}{R^2} \right] I_p \boldsymbol{\vartheta}^2 = \frac{1}{2} T_W \boldsymbol{\vartheta}^2.
\end{aligned} \tag{100}$$

The plot of the torsional stiffness for the classical torque, the higher-order torque, and the torque energy while varying L_c is shown in Fig. 14. Since the higher-order torque is zero and the following relation holds

$$\frac{d}{d\boldsymbol{\vartheta}} W_{\text{tot}}(\boldsymbol{\vartheta}) = M_C(\boldsymbol{\vartheta}) + M_M(\boldsymbol{\vartheta}) = M_C(\boldsymbol{\vartheta}), \quad \frac{d^2}{d\boldsymbol{\vartheta}^2} W_{\text{tot}}(\boldsymbol{\vartheta}) = T_C + T_M = T_C = T_W, \tag{101}$$

only the plot of the energy (per unit length dz) while changing L_c is shown in Fig. 23

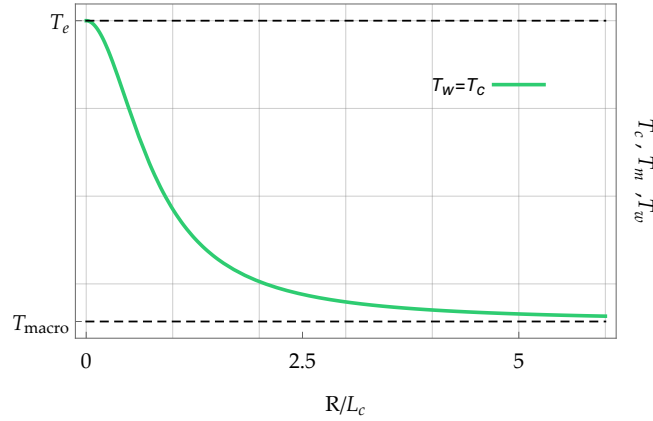


Figure 23: (**Micro-strain model**) Torque energy T_W while varying L_c . Observe that the torsional stiffness remains bounded as $L_c \rightarrow \infty$ ($R \rightarrow 0$). The values of the parameters used are: $\mu_e = 1/3$, $\mu_{\text{micro}} = 1/4$, $\mu = 1$, $a_1 = 1/5$. In this case, the stiffness for arbitrary small sample size is governed by T_e and not T_{micro} .

The energy of the model remains bounded, as for the shear and bending problem [60, 61], since for both problems the higher-order moments are zero, and this does not create a conflict with the boundary condition as $L_c \rightarrow \infty$ (see (47) for the different stiffnesses expressions). Note that there is no simple way to a-priori guess that the small size torsional response is given by T_e since $\mathbf{S} \in \text{Sym}(3)$ is not easily seen to be zero. In Appendix D we show that the variational limit for $L_c \rightarrow \infty$ is indeed realized by $\mathbf{S}(\mathbf{x}) = \bar{\mathbf{S}} = \mathbf{0}$ and this shows that the limit stiffness is given by T_e .

11 Torsional problem for the second gradient continuum

The expression of the most general isotropic strain energy for the second gradient continuum is [42, 54]

$$\begin{aligned}
W(\mathbf{D}\mathbf{u}, \mathbf{D}^2\mathbf{u}) &= \mu_{\text{macro}} \|\text{sym } \mathbf{D}\mathbf{u}\|^2 + \frac{\lambda_{\text{macro}}}{2} \text{tr}^2(\mathbf{D}\mathbf{u}) \\
&\quad + \hat{a}_1 \chi_{iik} \chi_{kjj} + \hat{a}_2 \chi_{ijj} \chi_{ikk} + \hat{a}_3 \chi_{iik} \chi_{jjk} + \hat{a}_4 \chi_{ijk} \chi_{ijk} + \hat{a}_5 \chi_{ijk} \chi_{kji},
\end{aligned} \tag{102}$$

where $\boldsymbol{\chi} = \mathbf{D}^2 \mathbf{u}$ ($\chi_{ijk} = \frac{\partial^2 u_k}{\partial x_i \partial x_j}$). The expression we are going to use in the following is a simplified isotropic strain energy with three curvature parameters

$$W(\mathbf{Du}, \mathbf{D}^2 \mathbf{u}) = \mu_{\text{macro}} \|\text{sym } \mathbf{Du}\|^2 + \frac{\lambda_{\text{macro}}}{2} \text{tr}^2(\mathbf{Du}) \quad (103)$$

$$+ \frac{\mu L_c^2}{2} \left(a_1 \left\| \mathbf{D}(\text{dev } \text{sym } \mathbf{Du}) \right\|^2 + a_2 \left\| \mathbf{D}(\text{skew } \mathbf{Du}) \right\|^2 + \frac{2}{9} a_3 \left\| \mathbf{D}(\text{tr}(\mathbf{Du}) \mathbf{1}) \right\|^2 \right).$$

The equilibrium equation, in the absence of body forces, is

$$\text{Div} \left[2\mu_{\text{macro}} \text{sym } \mathbf{Du} + \lambda_{\text{macro}} \text{tr}(\mathbf{Du}) \mathbf{1} \right. \quad (104)$$

$$\left. - \mu L_c^2 \left(a_1 \text{dev } \text{sym } \boldsymbol{\Delta}(\mathbf{Du}) + a_2 \text{skew } \boldsymbol{\Delta}(\mathbf{Du}) + \frac{2}{9} a_3 \text{tr}(\boldsymbol{\Delta}(\mathbf{Du})) \mathbf{1} \right) \right] = \mathbf{0},$$

where $\boldsymbol{\Delta}(\mathbf{Du}) \in \mathbb{R}^{3 \times 3}$ is taken component-wise. The non-trivial boundary conditions at the free surface are

$$\begin{aligned} \tilde{\mathbf{t}}(r=R) &= \tilde{\boldsymbol{\sigma}} \mathbf{e}_r + [(\mathbf{e}_r \otimes \mathbf{e}_r) : \boldsymbol{\nabla} \mathbf{m}] \mathbf{e}_r - 2 [(\mathbf{1} - \mathbf{e}_r \otimes \mathbf{e}_r) : \boldsymbol{\nabla} \mathbf{m}] \mathbf{e}_r \quad (105) \\ &\quad + \left([(\mathbf{1} - \mathbf{e}_r \otimes \mathbf{e}_r) : \boldsymbol{\nabla} \mathbf{e}_r] (\mathbf{e}_r \otimes \mathbf{e}_r) - [(\mathbf{1} - \mathbf{e}_r \otimes \mathbf{e}_r) (\boldsymbol{\nabla} \mathbf{e}_r)^T] \right) : \mathbf{m} = \mathbf{0}_{\mathbb{R}^3}, \\ \tilde{\boldsymbol{\eta}}(r=R) &= (\mathbf{e}_r \otimes \mathbf{e}_r) : \mathbf{m} = \mathbf{0}_{\mathbb{R}^3},^{10} \end{aligned}$$

where, since the boundary surface is smooth, one set of boundary condition is identically satisfied (see [41, 42] for all the details). According to the reference system shown in Fig. 1, the ansatz for the displacement field and consequently the gradient of the displacement are

$$\mathbf{u}(x_1, x_2) = \boldsymbol{\vartheta} \begin{pmatrix} -x_2 & x_3 \\ x_1 & x_3 \\ 0 \end{pmatrix} \Rightarrow \mathbf{Du} = \frac{\boldsymbol{\vartheta}}{2} \begin{pmatrix} 0 & -2x_3 & -2x_2 \\ 2x_3 & 0 & 2x_1 \\ 0 & 0 & 0 \end{pmatrix}. \quad (106)$$

Since the ansatz is completely known, it is possible to check that the equilibrium equation (104) and the boundary conditions (106) are identically satisfied and it is possible to evaluate directly the classical torque, the higher-order torque, and the energy.

The classical torque, the higher-order torque, and energy (per unit length dz) expressions are

$$\begin{aligned} M_{\text{C}}(\boldsymbol{\vartheta}) &:= \int_0^{2\pi} \int_0^R [\langle \tilde{\boldsymbol{\sigma}} \mathbf{e}_z, \mathbf{e}_\varphi \rangle r] r \, dr \, d\varphi = \mu_{\text{macro}} I_p \boldsymbol{\vartheta} = T_{\text{C}} \boldsymbol{\vartheta}, \\ M_{\text{M}}(\boldsymbol{\vartheta}) &:= \int_0^{2\pi} \int_0^R [\langle (\mathbf{m} \mathbf{e}_z) \mathbf{e}_r, \mathbf{e}_\varphi \rangle - \langle (\mathbf{m} \mathbf{e}_z) \mathbf{e}_\varphi, \mathbf{e}_r \rangle + \langle (\mathbf{m} \mathbf{e}_r) \mathbf{e}_z, \mathbf{e}_\varphi \rangle - \langle (\mathbf{m} \mathbf{e}_\varphi) \mathbf{e}_z, \mathbf{e}_r \rangle] r \, dr \, d\varphi \\ &= 2\mu(a_1 + 3a_2) \frac{L_c^2}{R^2} I_p \boldsymbol{\vartheta} = T_{\text{M}} \boldsymbol{\vartheta}, \\ W_{\text{tot}}(\boldsymbol{\vartheta}) &:= \int_0^{2\pi} \int_0^R W(\mathbf{Du}, \mathbf{D}^2 \mathbf{u}) \, r \, dr \, d\varphi = \frac{1}{2} \left[\mu_{\text{macro}} + 2\mu(a_1 + 3a_2) \frac{L_c^2}{R^2} \right] I_p \boldsymbol{\vartheta}^2 = \frac{1}{2} T_{\text{W}} \boldsymbol{\vartheta}^2. \quad (107) \end{aligned}$$

The plot of the torsional stiffness for the classical torque (light blue), the higher-order torque (red), and the torque energy (green) while varying L_c is shown in Fig. 24.

¹⁰In index notation $(\mathbf{1} - \mathbf{e}_r \otimes \mathbf{e}_r) : \boldsymbol{\nabla} \mathbf{m} = (\delta_{ip} - n_i n_p) m_{ijk,p}$.

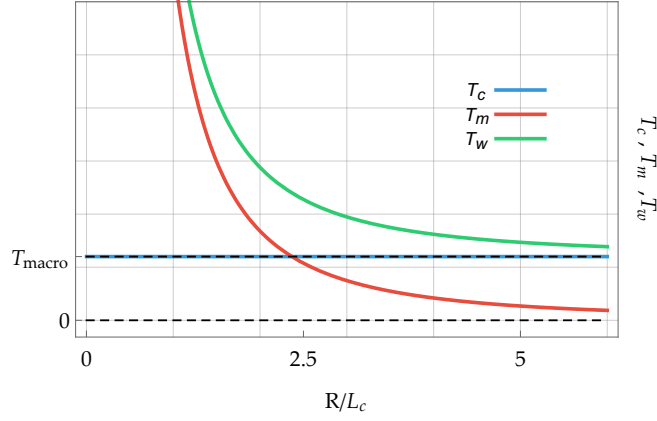


Figure 24: **(Second gradient model)** Torsional stiffness for the classical torque T_c , the higher-order torque T_m , and the torque energy T_w while varying L_c . The torsional stiffness is unbounded as $L_c \rightarrow \infty$ ($R \rightarrow 0$). The values of the parameters used are: $\mu = 1$, $\mu_{\text{macro}} = 1/4$, $a_1 = 1/5$, $a_3 = 1/6$, $R = 1$.

11.1 The strain gradient continuum as a limit of the micro-strain model

If we let $\mu_e, \kappa_e \rightarrow \infty$ in the micro-strain model, we obtain in the limit a strain gradient model with elastic energy

$$W(\mathbf{Du}, \mathbf{D} \text{sym} \mathbf{Du}) = \mu_{\text{macro}} \|\text{sym} \mathbf{Du}\|^2 + \frac{\lambda_{\text{macro}}}{2} \text{tr}^2(\mathbf{Du}) + \frac{\mu L_c^2}{2} \left(a_1 \|\mathbf{D}(\text{dev} \text{sym} \mathbf{Du})\|^2 + a_3 \|\mathbf{D}(\text{tr}(\mathbf{Du}) \mathbf{1})\|^2 \right). \quad (108)$$

Since $\text{tr}(\mathbf{Du}) = 0$ for our ansatz (14), the equilibrium equations, in the absence of body forces, are

$$\text{Div} \left[2\mu_{\text{macro}} \text{sym} \mathbf{Du} + \lambda_{\text{macro}} \text{tr}(\mathbf{Du}) \mathbf{1} - \mu L_c^2 a_1 \text{dev} \text{sym} \mathbf{\Delta}(\mathbf{Du}) \right] = \mathbf{0}, \quad (109)$$

where $\mathbf{\Delta}(\mathbf{Du}) \in \mathbb{R}^{3 \times 3}$ is taken component-wise.

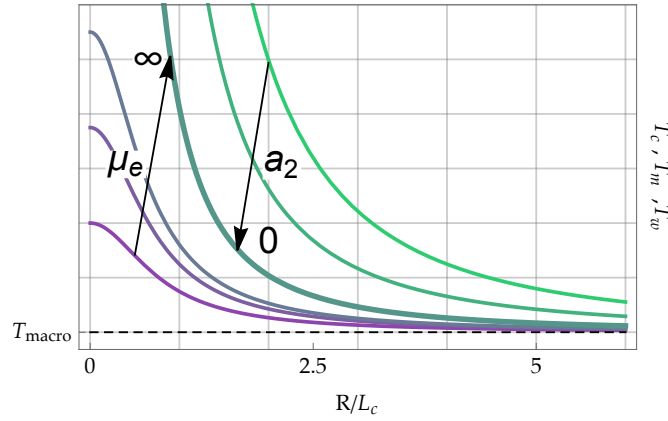


Figure 25: The purplish curves show how the micro-strain model particularises to the strain gradient model for $\mu_e \rightarrow \infty$ (the following set has been used $\mu_e = \{1/3, 1/2, 2/3, \infty\}$). The greenish curves show how the choice of $a_2 = 0$ guarantees the formal equivalence (which is however always substantially true) between the second gradient model and the strain gradient model [42] (the following set has been used $a_2 = \{1/4, 1/10, 0\}$). The values of the other parameters used are: $\mu = 1$, $\mu_{\text{macro}} = 1/7$, $a_1 = 1/5$, $R = 1$.

12 Ad-hoc model containing Cosserat and micro-strain effects

Given $\mathbf{S} \in \text{Sym}(3)$ and $\mathbf{A} \in \mathfrak{so}(3)$, the strain energy which we consider now is

$$\begin{aligned} W(\mathbf{D}\mathbf{u}, \mathbf{A}, \mathbf{S}, \text{Curl } \mathbf{A}, \mathbf{D}\mathbf{S}) = & \mu_e \|\text{sym } \mathbf{D}\mathbf{u} - \mathbf{S}\|^2 + \frac{\lambda_e}{2} \text{tr}^2(\mathbf{D}\mathbf{u} - \mathbf{S}) + \mu_c \|\text{skew}(\mathbf{D}\mathbf{u} - \mathbf{A})\|^2 \\ & + \mu_{\text{micro}} \|\text{dev } \mathbf{S}\|^2 + \frac{\kappa_{\text{micro}}}{2} \text{tr}^2(\mathbf{S}) \\ & + \frac{\mu L_c^2}{2} \left(a_1 \|\text{dev sym Curl } \mathbf{A}\|^2 + \frac{a_3}{3} \text{tr}^2(\text{Curl } \mathbf{A}) + a_4 \|\mathbf{D}(\text{dev } \mathbf{S})\|^2 \right), \end{aligned} \quad (110)$$

since $\|\text{skew Curl } \mathbf{A}\|^2 = \|\mathbf{D}(\text{skew } \mathbf{S})\|^2 = \|\mathbf{D}(\text{tr}(\mathbf{S}) \mathbf{1})\|^2 = 0$ in terms of the ansatz (114).

The equilibrium equations, in the absence of body forces, are the following

$$\begin{aligned} \text{Div} \left[\overbrace{2\mu_e (\text{sym } \mathbf{D}\mathbf{u} - \mathbf{S}) + \lambda_e \text{tr}(\mathbf{D}\mathbf{u} - \mathbf{S}) \mathbf{1} + 2\mu_c (\text{skew } \mathbf{D}\mathbf{u} - \mathbf{A})}^{\tilde{\boldsymbol{\sigma}} :=} \right] &= \mathbf{0}, \\ 2\mu_c \text{skew}(\mathbf{D}\mathbf{u} - \mathbf{A}) - \mu L_c^2 \text{skew Curl} \left(a_1 \text{dev sym Curl } \mathbf{A} + \frac{a_3}{3} \text{tr}(\text{Curl } \mathbf{A}) \mathbf{1} \right) &= \mathbf{0} \\ 2\mu_e (\text{sym } \mathbf{D}\mathbf{u} - \mathbf{S}) + \lambda_e \text{tr}(\mathbf{D}\mathbf{u} - \mathbf{S}) \mathbf{1} - 2\mu_{\text{micro}} \mathbf{S} - \lambda_{\text{micro}} \text{tr}(\mathbf{S}) \mathbf{1} + \mu L_c^2 a_4 \text{sym } \mathbf{D}(\text{dev } \mathbf{S}) &= \mathbf{0}. \end{aligned} \quad (111)$$

The boundary conditions at the external free surfaces are

$$\begin{aligned} \tilde{\mathbf{t}}(r=R) &= \tilde{\boldsymbol{\sigma}}(r) \cdot \mathbf{e}_r = \mathbf{0}_{\mathbb{R}^3}, \\ \boldsymbol{\eta}_b(r=R) &= \text{skew}(\mathbf{m}(r) \cdot \boldsymbol{\epsilon} \cdot \mathbf{e}_r) = \text{skew}(\mathbf{m}(r) \times \mathbf{e}_r) = \mathbf{0}_{\mathbb{R}^3 \times 3}, \\ \boldsymbol{\eta}_a(r=R) &= \text{sym}(\mathbf{m}(r) \cdot \mathbf{e}_r) = \mathbf{0}_{\mathbb{R}^3 \times 3}, \end{aligned} \quad (112)$$

where

$$\begin{aligned} \mathbf{m} &= \mu L_c^2 \left(a_1 \text{dev sym Curl } \mathbf{A} + \frac{a_3}{3} \text{tr}(\text{Curl } \mathbf{A}) \mathbf{1} \right), \\ \mathbf{m} &= \mu L_c^2 a_4 \mathbf{D}(\text{dev } \mathbf{S}), \end{aligned} \quad (113)$$

is the second and third order moment stress tensor respectively, the expression of $\tilde{\boldsymbol{\sigma}}$ is in (111), \mathbf{e}_r is the radial unit vector. According with the reference system shown in Fig. 1, the ansatz for the displacement field and the micro-distortion is

$$\begin{aligned} \mathbf{u}(r, \varphi, z) &= \boldsymbol{\vartheta} \begin{pmatrix} -x_2(r, \varphi) x_3(z) \\ x_1(r, \varphi) x_3(z) \\ 0 \end{pmatrix}, \\ \mathbf{A}(r, \varphi, z) &= \frac{\boldsymbol{\vartheta}}{2} \begin{pmatrix} 0 & -2x_3(z) & -g_p(r) x_2(r, \varphi) \\ 2x_3(z) & 0 & g_p(r) x_1(r, \varphi) \\ g_p(r) x_2(r, \varphi) & -g_p(r) x_1(r, \varphi) & 0 \end{pmatrix}, \\ \mathbf{S}(r, \varphi, z) &= \frac{\boldsymbol{\vartheta}}{2} \begin{pmatrix} 0 & 0 & g_m(r) x_2(r, \varphi) \\ 0 & 0 & -g_m(r) x_1(r, \varphi) \\ g_m(r) x_2(r, \varphi) & -g_m(r) x_1(r, \varphi) & 0 \end{pmatrix}, \end{aligned} \quad (114)$$

where, in relation to the ansatz (38), $g_m(r) := g_1(r) - g_2(r)$ and $g_p(r) := g_1(r) + g_2(r)$. Substituting the ansatz (114) in (111) the 15 equilibrium equation are equivalent to

$$\begin{aligned} \frac{1}{6} \boldsymbol{\vartheta} \sin \varphi (6r \mu_c (g_p(r) - 1) - \mu L_c^2 (a_1 + 2a_3) (3g_p'(r) + r g_p''(r))) &= 0, \\ \frac{1}{6} \boldsymbol{\vartheta} \cos \varphi (6r \mu_c (g_p(r) - 1) - \mu L_c^2 (a_1 + 2a_3) (3g_p'(r) + r g_p''(r))) &= 0, \\ \frac{1}{2} \boldsymbol{\vartheta} \sin \varphi (a_4 \mu L_c^2 (3g_m'(r) + r g_m''(r)) - 2r \mu_e (g_m(r) + 1) - 2r g_m(r) \mu_{\text{micro}}) &= 0, \\ -\frac{1}{2} \boldsymbol{\vartheta} \cos \varphi (a_4 \mu L_c^2 (3g_m'(r) + r g_m''(r)) - 2r \mu_e (g_m(r) + 1) - 2r g_m(r) \mu_{\text{micro}}) &= 0. \end{aligned} \quad (115)$$

Between the two equilibrium equations (115) there are only two independent equation since $(115)_1 = -\tan \varphi$ $(115)_2$ and $(115)_3 = \tan \varphi$ $(115)_4$. The solution of (115) is

$$g_p(r) = 1 - \frac{i A_1 I_1 \left(\frac{r f_1}{L_c} \right)}{r} + \frac{A_2 Y_1 \left(-\frac{i r f_1}{L_c} \right)}{r}, \quad f_1 := \sqrt{\frac{6\mu_c}{(a_1 + 2a_3)\mu}}, \quad (116)$$

$$g_m(r) = \frac{A_2 Y_1 \left(-\frac{i r f_2}{L_c} \right) - i A_1 I_1 \left(\frac{r f_2}{L_c} \right)}{r} - \frac{\mu_e}{\mu_e + \mu_{\text{micro}}}, \quad f_2 := \sqrt{\frac{2(\mu_e + \mu_{\text{micro}})}{a_4 \mu}}, \quad (117)$$

where $I_n(\cdot)$ is the *modified Bessel function of the first kind*, $Y_n(\cdot)$ is the *Bessel function of the second kind* (see appendix B for the formal definitions), and A_1, A_2, A_3, A_4 are integration constants.

The values of A_1 and A_2 are determined thanks to the boundary conditions (112), while, due to the divergent behaviour of the Bessel function of the second kind at $r = 0$, we have to set $A_2 = A_4 = 0$ in order to have a continuous solution. The fulfilment of the boundary conditions (112) allows us to find the expressions of the integration constants

$$\begin{aligned} A_1 &= -\frac{i R L_c}{f_1 R z_1 \left(I_0 \left(\frac{R f_1}{L_c} \right) + I_2 \left(\frac{R f_1}{L_c} \right) \right) + z_2 L_c I_1 \left(\frac{R f_1}{L_c} \right)}, & z_1 &:= \frac{a_1 + 2a_3}{3a_1}, \\ A_3 &= \frac{2i L_c}{I_0 \left(\frac{R f_2}{L_c} \right) + I_2 \left(\frac{R f_2}{L_c} \right)} \frac{\mu_e}{f_2 (\mu_e + \mu_{\text{micro}})}, & z_2 &:= \frac{4a_3 - a_1}{3a_1}. \end{aligned} \quad (118)$$

The classical torque, the higher-order torque, and the energy (per unit length dz) expressions are

$$\begin{aligned} M_C(\boldsymbol{\vartheta}) &:= \int_0^{2\pi} \int_0^R \left[\langle \tilde{\boldsymbol{\sigma}} \mathbf{e}_z, \mathbf{e}_\varphi \rangle r \right] r dr d\varphi \\ &= \left[\frac{4\mu_c I_2 \left(\frac{R f_1}{L_c} \right) \frac{L_c^2}{R^2}}{f_1 \left(2 f_1 z_1 I_0 \left(\frac{R f_1}{L_c} \right) + (z_2 - 2z_1) I_1 \left(\frac{R f_1}{L_c} \right) \frac{L_c}{R} \right)} \right. \\ &\quad \left. + \frac{\mu_e \mu_{\text{micro}}}{\mu_e + \mu_{\text{micro}}} + \frac{\mu_e^2 \mu a_4}{(\mu_e + \mu_{\text{micro}})^2} \frac{4 I_2 \left(\frac{R f_2}{L_c} \right)}{I_0 \left(\frac{R f_2}{L_c} \right) + I_2 \left(\frac{R f_2}{L_c} \right)} \frac{L_c^2}{R^2} \right] I_p \boldsymbol{\vartheta} = T_C \boldsymbol{\vartheta}, \\ M_M(\boldsymbol{\vartheta}) &:= \int_0^{2\pi} \int_0^R \left[\underbrace{\langle \text{sym}(\mathbf{m} \mathbf{e}_z) \mathbf{e}_\varphi, \mathbf{e}_r \rangle - \langle \text{sym}(\mathbf{m} \mathbf{e}_z) \mathbf{e}_r, \mathbf{e}_\varphi \rangle}_{\text{micro-strain component}} \right. \\ &\quad \left. + \underbrace{\langle \text{skew}(\mathbf{m} \times \mathbf{e}_z) \mathbf{e}_\varphi, \mathbf{e}_r \rangle - \langle \text{skew}(\mathbf{m} \times \mathbf{e}_z) \mathbf{e}_r, \mathbf{e}_\varphi \rangle}_{\text{Cosserat component}} \right] r dr d\varphi \\ &= \left[\frac{2\mu \left(3a_1 f_1 z_1 I_0 \left(\frac{R f_1}{L_c} \right) \frac{L_c^2}{R^2} - 2(a_1 - a_3) I_1 \left(\frac{R f_1}{L_c} \right) \frac{L_c^3}{R^3} \right)}{6f_1 z_1 I_0 \left(\frac{R f_1}{L_c} \right) - 3I_1 \left(\frac{R f_1}{L_c} \right) \frac{L_c}{R}} \right] = T_M \boldsymbol{\vartheta}, \quad (119) \\ W_{\text{tot}}(\boldsymbol{\vartheta}) &:= \int_0^{2\pi} \int_0^R W(\mathbf{D}\mathbf{u}, \mathbf{A}, \mathbf{S}, \text{Curl } \mathbf{A}, \mathbf{D}\mathbf{S}) r dr d\varphi \\ &= \frac{1}{2} \left[\frac{4\mu_c I_2 \left(\frac{R f_1}{L_c} \right) \frac{L_c^2}{R^2}}{f_1 \left(2 f_1 z_1 I_0 \left(\frac{R f_1}{L_c} \right) + (z_2 - 2z_1) I_1 \left(\frac{R f_1}{L_c} \right) \frac{L_c}{R} \right)} \right. \\ &\quad + \frac{\mu_e \mu_{\text{micro}}}{\mu_e + \mu_{\text{micro}}} + \frac{\mu_e^2 \mu a_4}{(\mu_e + \mu_{\text{micro}})^2} \frac{4 I_2 \left(\frac{R f_2}{L_c} \right)}{I_0 \left(\frac{R f_2}{L_c} \right) + I_2 \left(\frac{R f_2}{L_c} \right)} \frac{L_c^2}{R^2} \\ &\quad \left. + \frac{2\mu \left(3a_1 f_1 z_1 I_0 \left(\frac{R f_1}{L_c} \right) \frac{L_c^2}{R^2} - 2(a_1 - a_3) I_1 \left(\frac{R f_1}{L_c} \right) \frac{L_c^3}{R^3} \right)}{6f_1 z_1 I_0 \left(\frac{R f_1}{L_c} \right) - 3I_1 \left(\frac{R f_1}{L_c} \right) \frac{L_c}{R}} \right] I_p \boldsymbol{\vartheta}^2 = \frac{1}{2} T_W \boldsymbol{\vartheta}^2. \end{aligned}$$

It is highlighted that, like for the micro-strain model (Section 10), the higher order torque contribution $\langle (\mathbf{m} \mathbf{e}_z) \mathbf{e}_\varphi, \mathbf{e}_\varphi \rangle$ is equal to zero. The plot of the torsional stiffness for the classical torque, the higher-order torque, and the torque energy while varying L_c is shown in Fig. 26. Again, it holds

$$\frac{d}{d\boldsymbol{\vartheta}} W_{\text{tot}}(\boldsymbol{\vartheta}) = M_C(\boldsymbol{\vartheta}) + M_M(\boldsymbol{\vartheta}), \quad \frac{d^2}{d\boldsymbol{\vartheta}^2} W_{\text{tot}}(\boldsymbol{\vartheta}) = T_C + T_M = T_W. \quad (120)$$

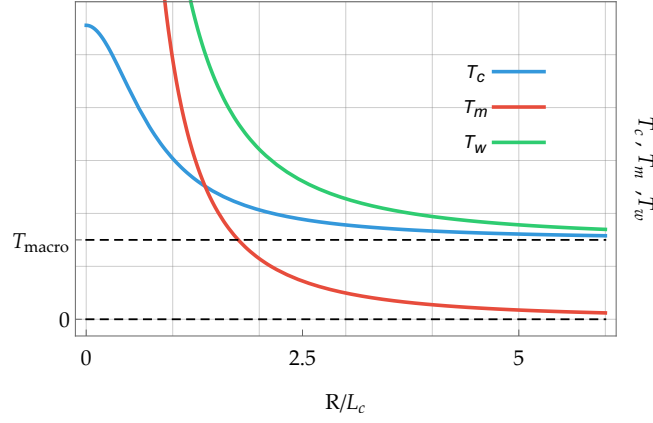


Figure 26: (**Ad-hoc model**) Torsional stiffness for the classical torque T_c , the higher-order torque T_m , and the torque energy T_w while varying L_c . The torsional stiffness is unbounded as $L_c \rightarrow \infty$ ($R \rightarrow 0$) due to the Cosserat effects. The values of the parameters used are: $\mu = 1$, $\mu_c = 1/2$, $\mu_e = 1/3$, $\mu_{\text{micro}} = 1/4$, $a_1 = 1/5$, $a_3 = 1/6$, $a_4 = 1/7$, $R = 1$.

13 Summary and conclusions

We have derived the analytical expressions of the torsional rigidity for a family of generalized continua capable of modelling size-dependence in the sense that more slender specimens are comparatively stiffer. We only consider (simplified) isotropic expressions so as to better compare the different models with each other. For example, a strain gradient continuum, by construction, does not have mixed energy terms. Therefore, we omitted these terms in all models. Excluding the mixed terms like $\langle \text{sym } D\mathbf{u}, \text{sym } D\mathbf{u} - \mathbf{P} \rangle$ also simplifies considerably the investigation of positive definiteness. Indeed, all presented models are positive definite if the usual relations

$$\begin{aligned} \mu_{\text{macro}} &> 0, & \kappa_{\text{macro}} &= \frac{2\mu_{\text{macro}} + 3\lambda_{\text{macro}}}{3} > 0, \\ \mu_{\text{micro}} &> 0, & \kappa_{\text{micro}} &= \frac{2\mu_{\text{micro}} + 3\lambda_{\text{micro}}}{3} > 0, \\ \mu_{\text{micro}} > \mu_{\text{macro}} &\implies \mu_e > 0, & \kappa_e &= \frac{2\mu_e + 3\lambda_e}{3} > 0. \end{aligned} \quad (121)$$

are satisfied together with individual positivity of all curvature parameters. In all cases, the displacement follows the classical pure torsion solution. Despite the conceptual simplicity of the models, we observe already a delicate interplay between the used kinematics and the assumed curvature energy expression. For example, let us compare the relaxed micromorphic model with the micro-strain model (Section 10). Both models have a similar looking lower order energy term (if the Cosserat couple modulus $\mu_c \equiv 0$), but different kinematics and different curvature energy. For arbitrary slender specimens, the torsional stiffness of the micro-strain model is governed by μ_e , whereas the torsional stiffness of the relaxed micromorphic model is determined by μ_{micro} . Thus, the physical interpretation of the material parameters in both models is completely different. This is surprising at first glance but the reason for this response is finally explained in Appendix D.

In the end, the more restricted the used kinematics, the less viable a model may become. In this respect, only the full micromorphic kinematics degree of freedom (12 DOFS) can be advised. In addition, the curvature energy should not intervene too strongly. For example, penalizing a full gradient $D\mathbf{P}$ in the curvature energy of the classical micromorphic model leads to a stiffness singularity for arbitrary slender specimens, while penalizing only $\text{Curl } \mathbf{P}$ in the relaxed micromorphic model does not show the same singular response. Moreover, in the relaxed micromorphic model the interpretation of the lower order material parameters (μ_e , μ_{micro} , μ_{micro} , etc.) does not in principle change when different curvature energies are considered. In the end, it is therefore the relaxed micromorphic model that produces sensible and consistent response in all considered cases. It remains to be investigated if, together with the previously developed solution for bending and shear [60, 61], the present analytical solution allows to identify the complete set of micromorphic parameters of a material from bending, shear and torsion experiments at specimens with different diameters.

Acknowledgements. Angela Madeo acknowledges support from the European Commission through the funding of the ERC Consolidator Grant META-LEGO, N° 101001759. Angela Madeo and Gianluca Rizzi acknowledge funding from the French Research Agency

ANR, “METASMARK” (ANR-17CE08-0006). Angela Madeo and Gianluca Rizzi acknowledge support from IDEXLYON in the framework of the “Programme Investissement d’Avenir” ANR-16-IDEX-0005. Hassam Khan acknowledges the support of the German Academic Exchange Service (DAAD) and the Higher Education Commission of Pakistan (HEC). Ionel Dumitrel Ghiba acknowledges support from a grant of the Romanian Ministry of Research and Innovation, CNCS-UEFISCDI, project number PN-III-P1-1.1-TE-2019-0348, Contract No. TE 8/2020, within PNCDI III. Patrizio Neff acknowledges support in the framework of the DFG-Priority Programme 2256 “Variational Methods for Predicting Complex Phenomena in Engineering Structures and Materials”, Neff 902/10-1, Project-No. 440935806.

References

- [1] A. Aivaliotis, A. Daouadji, G. Barbagallo, D. Tallarico, P. Neff, and A. Madeo. Microstructure-related Stoneley waves and their effect on the scattering properties of a 2d Cauchy/relaxed-micromorphic interface. *Wave Motion*, 90:99–120, 2019.
- [2] A. Aivaliotis, D. Tallarico, M.V. d’Agostino, A. Daouadji, P. Neff, and A. Madeo. Frequency-and angle-dependent scattering of a finite-sized meta-structure via the relaxed micromorphic model. *Archive for Applied Mechanics*, 20:1073–1096, 2020.
- [3] H. Altenbach, W.H. Müller, and B.E. Abali. *Higher Gradient Materials and Related Generalized Continua*. Springer, 2019.
- [4] W.B. Anderson and R.S. Lakes. Size effects due to Cosserat elasticity and surface damage in closed-cell polymethacrylimide foam. *Journal of Materials Science*, 29(24):6413–6419, 1994.
- [5] G. Barbagallo, A. Madeo, M.V. d’Agostino, R. Abreu, I.D. Ghiba, and P. Neff. Transparent anisotropy for the relaxed micromorphic model: macroscopic consistency conditions and long wave length asymptotics. *International Journal of Solids and Structures*, 120:7–30, 2017.
- [6] S. Bauer, P. Neff, D. Pauly, and G. Starke. Dev-Div-and DevSym-DevCurl-inequalities for incompatible square tensor fields with mixed boundary conditions. *ESAIM: Control, Optimisation and Calculus of Variations*, 22(1):112–133, 2016.
- [7] E. Bulgariu and I.D. Ghiba. On the thermal stresses in anisotropic porous cylinders. *Discrete and Continuous Dynamical Systems-S*, 6(6):1539, 2013.
- [8] E. Cosserat and F. Cosserat. *Théorie des corps déformables*. A. Hermann et fils (reprint 2009), Paris, 1909.
- [9] S.C. Cowin and J.W. Nunziato. Linear elastic materials with voids. *Journal of Elasticity*, 13(2):125–147, 1983.
- [10] S. De Cicco and L. Nappa. Torsion and flexure of microstretch elastic circular cylinders. *International Journal of Engineering Science*, 35(6):573–583, 1997.
- [11] M.V. d’Agostino, G. Barbagallo, I.D. Ghiba, B. Eidel, P. Neff, and A. Madeo. Effective description of anisotropic wave dispersion in mechanical band-gap metamaterials via the relaxed micromorphic model. *Journal of Elasticity*, 39:299–329, 2020.
- [12] A.C. Eringen. *Microcontinuum Field Theories*. Springer, Heidelberg, 1999.
- [13] S. Forest and R. Sievert. Nonlinear microstrain theories. *International Journal of Solids and Structures*, 43(24):7224–7245, 2006.
- [14] R.D. Gauthier and W.E. Jahsman. A quest for micropolar elastic constants. *Journal of Applied Mechanics*, 42(2):369–374, 1975.
- [15] I. D. Ghiba, S. Owczarek, and P. Neff. Existence results for non-homogeneous boundary conditions in the relaxed micromorphic model. *Mathematical Methods in the Applied Sciences*, 44(2):2040–2049, 2021.
- [16] I.D. Ghiba. Semi-inverse solution for Saint-Venant’s problem in the theory of porous elastic materials. *European Journal of Mechanics-A/Solids*, 27(6):1060–1074, 2008.
- [17] I.D. Ghiba. On the deformation of transversely isotropic porous elastic circular cylinder. *Archives of Mechanics*, 61(5):407–421, 2009.
- [18] I.D. Ghiba. Saint-venant’s principle. *Encyclopedia of Thermal Stresses*, pages 4255–4264, 2014.
- [19] I.D. Ghiba, P. Neff, A. Madeo, and I. Münch. A variant of the linear isotropic indeterminate couple-stress model with symmetric local force-stress, symmetric nonlocal force-stress, symmetric couple-stresses and orthogonal boundary conditions. *Mathematics and Mechanics of Solids*, 22(6):1221–1266, 2017.
- [20] I.D. Ghiba, P. Neff, A. Madeo, L. Placidi, and G. Rosi. The relaxed linear micromorphic continuum: existence, uniqueness and continuous dependence in dynamics. *Mathematics and Mechanics of Solids*, 20(10):1171–1197, 2014.
- [21] A.R. Hadjesfandiari and G.F. Dargush. Couple stress theory for solids. *International Journal of Solids and Structures*, 48(18):2496–2510, 2011.
- [22] A.R. Hadjesfandiari and G.F. Dargush. Comparison of theoretical elastic couple stress predictions with physical experiments for pure torsion. *arXiv preprint arXiv:1605.02556*, 2016.
- [23] S. Hassanpour and G.R. Heppler. Micropolar elasticity theory: a survey of linear isotropic equations, representative notations, and experimental investigations. *Mathematics and Mechanics of Solids*, 22(2):224–242, 2017.
- [24] G. Hütter. Application of a microstrain continuum to size effects in bending and torsion of foams. *International Journal of Engineering Science*, 101:81–91, 2016.
- [25] G. Hütter, U. Mühlich, and M. Kuna. Micromorphic homogenization of a porous medium: elastic behavior and quasi-brittle damage. *Continuum Mechanics and Thermodynamics*, 27(6):1059–1072, 2015.
- [26] D. Ieşan. On Saint-Venant’s problem. *Archive for Rational Mechanics and Analysis*, 91(4):363–373, 1986.
- [27] D. Ieşan. *Saint-Venant’s Problem*, volume 1279. Springer, 2006.
- [28] D. Ieşan. *Classical and Generalized Models of Elastic Rods*. CRC Press, 2008.
- [29] R. Izadi, M. Tuna, P. Trovalusci, and E. Ghavanloo. Torsional characteristics of carbon nanotubes: Micropolar elasticity models and molecular dynamics simulation. *Nanomaterials*, 11(2), 2021.
- [30] J. Jeong, H. Ramézani, I. Münch, and P. Neff. A numerical study for linear isotropic Cosserat elasticity with conformally invariant curvature. *Zeitschrift für Angewandte Mathematik und Mechanik*, 89(7):552–569, 2009.
- [31] N. Kirchner and P. Steinmann. Mechanics of extended continua: modeling and simulation of elastic microstretch materials. *Computational Mechanics*, 40(4):651–666, 2007.
- [32] W.T. Koiter. Couple stresses in the theory of elasticity: I and II. *Proc. Kon. Ned. Akad. Wetensch. Ser. B*, 67:17–44, 1964.
- [33] R. Lakes and W.J. Drugan. Bending of a Cosserat elastic bar of square cross section: Theory and experiment. *Journal of Applied Mechanics*, 82(9), 2015.
- [34] R.S. Lakes. Webpage. <http://silver.neep.wisc.edu/~lakes/>.
- [35] R.S. Lakes. Experimental methods for study of Cosserat elastic solids and other generalized elastic continua. *Continuum Models for Materials with Microstructure*, 70:1–25, 1995.
- [36] P. Lewintan, S. Müller, and P. Neff. Korn inequalities for incompatible tensor fields in three space dimensions with conformally invariant dislocation energy. *to appear in Calculus of Variations and Partial Differential Equations*, 2021, (arXiv:2011.10573).

- [37] P. Lewintan and P. Neff. Nečas-Lions lemma reloaded: An L^p -version of the generalized Korn inequality for incompatible tensor fields. *arXiv preprint: 1912.08447*, 2019.
- [38] P. Lewintan and P. Neff. L^p -trace-free generalized Korn inequalities for incompatible tensor fields in three space dimensions. *to appear in Zeitschrift für Angewandte Mathematik und Physik (ZAMP)*, 2021, (arXiv:2004.05981).
- [39] S. Lurie, Y. Solyaev, A. Volkov, and D. Volkov-Bogorodskiy. Bending problems in the theory of elastic materials with voids and surface effects. *Mathematics and Mechanics of Solids*, 23(5):787–804, 2018.
- [40] A. Madeo, G. Barbagallo, M. Collet, M.V. d’Agostino, M. Miniaci, and P. Neff. Relaxed micromorphic modeling of the interface between a homogeneous solid and a band-gap metamaterial: New perspectives towards metastructural design. *Mathematics and Mechanics of Solids*, 23(12):1485–1506, 2018.
- [41] A. Madeo, I.D. Ghiba, P. Neff, and I. Münch. A new view on boundary conditions in the Grioli-Koiter-Mindlin-Toupin indeterminate couple stress model. *European Journal of Mechanics-A/Solids*, 59:294–322, 2016.
- [42] R.D. Mindlin. Micro-structure in linear elasticity. *Archive for Rational Mechanics and Analysis*, 16(1):51–78, 1964.
- [43] I. Münch, P. Neff, A. Madeo, and I.D. Ghiba. The modified indeterminate couple stress model: Why Yang et al.’s arguments motivating a symmetric couple stress tensor contain a gap and why the couple stress tensor may be chosen symmetric nevertheless. *Zeitschrift für Angewandte Mathematik und Mechanik*, 97(12):1524–1554, 2017.
- [44] P. Neff. Existence of minimizers for a finite-strain micromorphic elastic solid. *Proceedings of the Royal Society of Edinburgh: Section A Mathematics*, 136(05):997–1012, 2006.
- [45] P. Neff. The Cosserat couple modulus for continuous solids is zero viz the linearized Cauchy-stress tensor is symmetric. *Zeitschrift für Angewandte Mathematik und Mechanik*, 86(11):892–912, 2006.
- [46] P. Neff, B. Eidel, M.V. d’Agostino, and A. Madeo. Identification of scale-independent material parameters in the relaxed micromorphic model through model-adapted first order homogenization. *Journal of Elasticity*, 139:269–298, 2020.
- [47] P. Neff, I.D. Ghiba, M. Lazar, and A. Madeo. The relaxed linear micromorphic continuum: well-posedness of the static problem and relations to the gauge theory of dislocations. *The Quarterly Journal of Mechanics and Applied Mathematics*, 68(1):53–84, 2014.
- [48] P. Neff, I.D. Ghiba, A. Madeo, and I. Münch. Correct traction boundary conditions in the indeterminate couple stress model. *arXiv preprint arXiv:1504.00448*, 2015.
- [49] P. Neff, I.D. Ghiba, A. Madeo, L. Placidi, and G. Rosi. A unifying perspective: the relaxed linear micromorphic continuum. *Continuum Mechanics and Thermodynamics*, 26(5):639–681, 2014.
- [50] P. Neff and J. Jeong. A new paradigm: the linear isotropic Cosserat model with conformally invariant curvature energy. *Zeitschrift für Angewandte Mathematik und Mechanik*, 89(2):107–122, 2009.
- [51] P. Neff, J. Jeong, and A. Fischle. Stable identification of linear isotropic Cosserat parameters: bounded stiffness in bending and torsion implies conformal invariance of curvature. *Acta Mechanica*, 211(3-4):237–249, 2010.
- [52] P. Neff, J. Jeong, I. Münch, and H. Ramezani. Mean field modeling of isotropic random Cauchy elasticity versus microstretch elasticity. *Zeitschrift für angewandte Mathematik und Physik*, 60(3):479–497, 2009.
- [53] P. Neff, J. Jeong, I. Münch, and H. Ramézani. Linear Cosserat elasticity, Conformal Curvature and Bounded Stiffness. In *Mechanics of Generalized Continua*, pages 55–63. Springer, 2010.
- [54] P. Neff, J. Jeong, and H. Ramézani. Subgrid interaction and micro-randomness – Novel invariance requirements in infinitesimal gradient elasticity. *International Journal of Solids and Structures*, 46(25-26):4261–4276, 2009.
- [55] P. Neff, I. Münch, I.D. Ghiba, and A. Madeo. On some fundamental misunderstandings in the indeterminate couple stress model. A comment on recent papers of AR Hadjesfandiari and GF Dargush. *International Journal of Solids and Structures*, 81:233–243, 2016.
- [56] P. Neff, D. Pauly, and K.J. Witsch. Poincaré meets Korn via Maxwell: extending Korn’s first inequality to incompatible tensor fields. *Journal of Differential Equations*, 258(4):1267–1302, 2015.
- [57] S. Owczarek, I. D. Ghiba, and P. Neff. A note on local higher regularity in the dynamic linear relaxed micromorphic model. *arXiv:2006.05448*, to appear in *Mathematical Methods in the Applied Sciences*, 2021.
- [58] A. Reuß. Berechnung der Fließgrenze von Mischkristallen auf Grund der Plastizitätsbedingung für Einkristalle. *Zeitschrift für Angewandte Mathematik und Mechanik*, 9(1):49–58, 1929.
- [59] G. Rizzi, M. Collet, F. Demore, B. Eidel, P. Neff, and A. Madeo. Exploring metamaterials’ structures through the relaxed micromorphic model: switching an acoustic screen into an acoustic absorber. *Frontiers in Materials*, 7:354, 2021.
- [60] G. Rizzi, G. Hütter, A. Madeo, and P. Neff. Analytical solutions of the simple shear problem for micromorphic models and other generalized continua. *Archive of Applied Mechanics*, 20:1–18, 2021.
- [61] G. Rizzi, G. Hütter, A. Madeo, and P. Neff. Analytical solutions of the cylindrical bending problem for the relaxed micromorphic continuum and other generalized continua. *Continuum Mechanics and Thermodynamics*, pages 1–35, 2021, (arXiv:2012.10391).
- [62] G. Rizzi, D. Tallarico, P. Neff, and A. Madeo. Towards the conception of complex engineering meta-structures: relaxed-micromorphic modelling of mechanical diodes. *to appear in Wave Motion*, 2021, (arXiv:2012.11192).
- [63] G. Romano, R. Barretta, and M. Diaco. Micromorphic continua: non-redundant formulations. *Continuum Mechanics and Thermodynamics*, 28(6):1659–1670, 2016.
- [64] Z. Rueger and R.S. Lakes. Strong Cosserat elasticity in a transversely isotropic polymer lattice. *Physical Review Letters*, 120(6):065501, 2018.
- [65] A. Scalia. Extension, bending and torsion of anisotropic microstretch elastic cylinders. *Mathematics and Mechanics of Solids*, 5(1):31–40, 2000.
- [66] M. Shaat. A reduced micromorphic model for multiscale materials and its applications in wave propagation. *Composite Structures*, 201:446–454, 2018.
- [67] A. Sky, M. Neunteufel, I. Münch, J. Schoeberl, and P. Neff. A hybrid $H^1 \times H(\text{curl})$ finite element formulation for a relaxed micromorphic continuum model of antiplane shear. *to appear in Computational Mechanics*, 2021, (arXiv:2009.13397).
- [68] P. Tong, F. Yang, D.C.C. Lam, and J. Wang. *Size effects of hair-sized structures–torsion*, volume 261. 2004.
- [69] G.C. Tsias and J.T. Katsikadelis. A new microstructure-dependent Saint–Venant torsion model based on a modified couple stress theory. *European Journal of Mechanics-A/Solids*, 30(5):741–747, 2011.
- [70] G.N. Watson. *A Treatise on the Theory of Bessel Functions*. Cambridge University Press, 1995.

A Cylindrical coordinates

The relation between the derivatives for a vector field $\mathbf{u}(\mathbf{x})$, $\hat{\mathbf{u}}(\mathbf{r})$ and a second order tensor $\mathbf{P}(\mathbf{x})$, $\hat{\mathbf{P}}(\mathbf{r})$ with respect an orthogonal set of coordinates $\mathbf{x} = \{x_1, x_2, x_3\}$ and a cylindrical set of coordinates $\mathbf{r} = \{r, \varphi, z\}$ are the following

$$\nabla_{\mathbf{x}} \mathbf{u}(\mathbf{x}) = (\nabla_{\mathbf{r}} \hat{\mathbf{u}}(\mathbf{r})) Q^{(1)}, \quad \nabla_{\mathbf{x}} \mathbf{P}(\mathbf{x}) = (\nabla_{\mathbf{r}} \hat{\mathbf{P}}(\mathbf{r})) Q^{(1)}, \quad (122)$$

$$u_{i,j} = \hat{u}_{i,\alpha} Q_{\alpha j}^{(1)}, \quad P_{ij,k} = \hat{P}_{ij,\alpha} Q_{\alpha k}^{(1)}, \quad (123)$$

where

$$Q^{(1)} = (\nabla_{\mathbf{r}} \mathbf{x}(\mathbf{r}))^{-1} = \begin{pmatrix} \cos \varphi & \sin \varphi & 0 \\ -\frac{\sin \varphi}{r} & \frac{\cos \varphi}{r} & 0 \\ 0 & 0 & 1 \end{pmatrix}, \quad (124)$$

and

$$\nabla_{\mathbf{x}}^2 \mathbf{u}(\mathbf{x}) = (\nabla_{\mathbf{r}}^2 \hat{\mathbf{u}}(\mathbf{r})) : Q^{(2)} + (\nabla_{\mathbf{r}} \hat{\mathbf{u}}(\mathbf{r})) Q^{(3)}, \quad \nabla_{\mathbf{x}} \mathbf{P}(\mathbf{x}) = (\nabla_{\mathbf{r}}^2 \hat{\mathbf{P}}(\mathbf{r})) : Q^{(2)} + (\nabla_{\mathbf{r}} \hat{\mathbf{P}}(\mathbf{r})) Q^{(3)}. \quad (125)$$

$$u_{i,jk} = \hat{u}_{i,\alpha\beta} Q_{\alpha\beta jk} + \hat{u}_{i,\alpha} Q_{\alpha jk}, \quad P_{ij,kl} = \hat{P}_{ij,\alpha\beta} Q_{\alpha\beta kl} + \hat{P}_{ij,\alpha} Q_{\alpha kl}. \quad (126)$$

$$Q^{(2)} = \begin{pmatrix} \begin{pmatrix} \cos^2 \varphi & \sin \varphi \cos \varphi & 0 \\ \sin \varphi \cos \varphi & \sin^2 \varphi & 0 \\ 0 & 0 & 0 \end{pmatrix} & \begin{pmatrix} -\frac{\sin \varphi \cos \varphi}{2r} & \frac{\cos(2\varphi)}{2r} & 0 \\ \frac{\cos(2\varphi)}{2r} & \frac{\sin \varphi \cos \varphi}{r} & 0 \\ 0 & 0 & 0 \end{pmatrix} & \begin{pmatrix} 0 & 0 & \frac{\cos \varphi}{2} \\ 0 & 0 & \frac{\sin \varphi}{2} \\ \frac{\cos \varphi}{2} & \frac{\sin \varphi}{2} & 0 \end{pmatrix} \\ \begin{pmatrix} -\frac{\sin \varphi \cos \varphi}{2r} & \frac{\cos(2\varphi)}{2r} & 0 \\ \frac{\cos(2\varphi)}{2r} & \frac{\sin \varphi \cos \varphi}{r} & 0 \\ 0 & 0 & 0 \end{pmatrix} & \begin{pmatrix} \frac{\sin^2 \varphi}{r^2} & -\frac{\sin \varphi \cos \varphi}{r^2} & 0 \\ -\frac{\sin \varphi \cos \varphi}{r^2} & \frac{\cos^2 \varphi}{r^2} & 0 \\ 0 & 0 & 0 \end{pmatrix} & \begin{pmatrix} 0 & 0 & -\frac{\sin \varphi}{2r} \\ 0 & 0 & \frac{\cos \varphi}{2r} \\ -\frac{\sin \varphi}{2r} & \frac{\cos \varphi}{2r} & 0 \end{pmatrix} \\ \begin{pmatrix} 0 & 0 & \frac{\cos \varphi}{2} \\ 0 & 0 & \frac{\sin \varphi}{2} \\ \frac{\cos \varphi}{2} & \frac{\sin \varphi}{2} & 0 \end{pmatrix} & \begin{pmatrix} 0 & 0 & -\frac{\sin \varphi}{2r} \\ 0 & 0 & \frac{\cos \varphi}{2r} \\ -\frac{\sin \varphi}{2r} & \frac{\cos \varphi}{2r} & 0 \end{pmatrix} & \begin{pmatrix} 0 & 0 & 0 \\ 0 & 0 & 0 \\ 0 & 0 & 1 \end{pmatrix} \end{pmatrix},$$

$$Q^{(3)} = \begin{pmatrix} \begin{pmatrix} \frac{\sin^2 \varphi}{r} \\ -\frac{\sin \varphi \cos \varphi}{r} \\ 0 \end{pmatrix} & \begin{pmatrix} -\frac{\sin \varphi \cos \varphi}{r} \\ \frac{\cos^2 \varphi}{r} \\ 0 \end{pmatrix} & \begin{pmatrix} 0 \\ 0 \\ 0 \end{pmatrix} \\ \begin{pmatrix} \frac{\sin(2\varphi)}{r^2} \\ -\frac{\cos(2\varphi)}{r^2} \\ 0 \end{pmatrix} & \begin{pmatrix} -\frac{\cos(2\varphi)}{r^2} \\ \frac{\sin(2\varphi)}{r^2} \\ 0 \end{pmatrix} & \begin{pmatrix} 0 \\ 0 \\ 0 \end{pmatrix} \\ \begin{pmatrix} 0 \\ 0 \\ 0 \end{pmatrix} & \begin{pmatrix} 0 \\ 0 \\ 0 \end{pmatrix} & \begin{pmatrix} 0 \\ 0 \\ 0 \end{pmatrix} \end{pmatrix}. \quad (127)$$

B Bessel functions

The *Bessel functions* are the solutions $y(x)$ of the Bessel differential equation [70]

$$x^2 \frac{d^2 y}{dx^2} + x \frac{dy}{dx} + (x^2 - \alpha^2)y = 0. \quad (128)$$

For the particular case in which $\alpha = n$ is an integer, the solution of (128) can be expressed as a linear combination of the Bessel function of the *first* $J_n(x)$ and *second* $Y_n(x)$ kind

$$y(x) = A_1 J_n(x) + A_2 Y_n(x), \quad (129)$$

whose definitions are

$$J_n(x) = \int_0^\pi \cos(n\tau - x \sin(\tau)) d\tau, \quad Y_n(x) = \frac{J_n(x) \cos(n\pi) - J_{-n}(x)}{\sin(n\pi)}. \quad (130)$$

Moreover, the *modified Bessel functions of the first kind* is defined as $I_n(x) = i^{-n} J_n(ix)$.

C Classical Cosserat formulation in micro-rotation vector format

An overview of the different classical notations for the Cosserat model has been given in [23]. In [50] we have presented the correspondence between the Cosserat model expressed in dislocation format (Curl of the skew symmetric micro-distortion tensor) and in its classical formulation (gradient of the micro-rotation vector ϕ). The relation between the coefficients in the two notations is

$$\begin{aligned} \alpha &= \frac{\mu L_c^2}{2} \frac{1}{3} (4a_3 - a_1), & \beta &= \frac{\mu L_c^2}{2} \frac{a_1 - a_2}{2}, & \gamma &= \frac{\mu L_c^2}{2} \frac{a_1 + a_2}{2}, \\ a_1 &= \frac{\gamma + \beta}{\mu L_c^2}, & a_2 &= \frac{\gamma - \beta}{\mu L_c^2}, & a_3 &= \frac{3\alpha + \beta + \gamma}{4\mu L_c^2}. \end{aligned} \quad (131)$$

Setting $\phi := \text{axl}(\mathbf{A})$ and taking into account (131), the expression of the strain energy for the isotropic Cosserat continuum can be equivalently expressed as

$$\begin{aligned} W(\mathbf{Du}, \mathbf{A}, \text{Curl } \mathbf{A}) &= \mu_{\text{macro}} \|\text{sym } \mathbf{Du}\|^2 + \frac{\lambda_{\text{macro}}}{2} \text{tr}^2(\mathbf{Du}) + \mu_c \|\text{skew } \mathbf{Du} - \mathbf{A}\|^2 \\ &\quad + \underbrace{\frac{\mu L_c^2}{2} \left(a_1 \|\text{dev sym Curl } \mathbf{A}\|^2 + a_2 \|\text{skew Curl } \mathbf{A}\|^2 + \frac{a_3}{3} \text{tr}^2(\text{Curl } \mathbf{A}) \right)}_{\text{dislocation tensor format}} \\ &= W(\mathbf{Du}, \phi, \text{D}\phi) = \mu_{\text{macro}} \|\text{sym } \mathbf{Du}\|^2 + \frac{\lambda_{\text{macro}}}{2} \text{tr}^2(\mathbf{Du}) + \frac{\mu_c}{2} \|\text{curl } \mathbf{u} - 2\phi\|^2 \\ &\quad + \underbrace{\frac{1}{2} \left(\alpha \text{tr}^2(\text{D}\phi) + \beta \langle \text{D}\phi^T, \text{D}\phi \rangle + \gamma \|\text{D}\phi\|^2 \right)}_{\text{classical micro-rotation vector format}}, \end{aligned} \quad (132)$$

since

$$\|\text{skew } \mathbf{D}\mathbf{u} - \mathbf{A}\|^2 = 2 \|\text{axl}(\text{skew } \mathbf{D}\mathbf{u} - \text{Anti}(\boldsymbol{\phi}))\|^2 = 2 \left\| \frac{1}{2} \text{curl } \mathbf{u} - \boldsymbol{\phi} \right\|^2 = \frac{1}{2} \|\text{curl } \mathbf{u} - 2\boldsymbol{\phi}\|^2. \quad (133)$$

The equilibrium equations, in the absence of body forces, in the classical notation are

$$\begin{aligned} \text{Div} [2\mu_{\text{macro}} \text{sym } \mathbf{D}\mathbf{u} + \lambda_{\text{macro}} \text{tr}(\mathbf{D}\mathbf{u}) \mathbf{1}] - \mu_c \text{curl} [\text{curl } \mathbf{u} - 2\boldsymbol{\phi}] &= \mathbf{0}, \\ \text{Div} [\alpha \text{tr}(\mathbf{D}\boldsymbol{\phi}) \mathbf{1} + \beta (\mathbf{D}\boldsymbol{\phi})^T + \gamma \mathbf{D}\boldsymbol{\phi}] + 2\mu_c (\text{curl } \mathbf{u} - 2\boldsymbol{\phi}) &= \mathbf{0}. \end{aligned} \quad (134)$$

The boundary conditions at the free surface are

$$\tilde{\mathbf{t}}(r=R) = \tilde{\boldsymbol{\sigma}}(r) \cdot \mathbf{e}_r = \mathbf{0}_{\mathbb{R}^3}, \quad \bar{\boldsymbol{\eta}}(r=R) = \bar{\mathbf{m}}(r) \cdot \mathbf{e}_r = \mathbf{0}_{\mathbb{R}^{3 \times 3}}, \quad (135)$$

where

$$\tilde{\boldsymbol{\sigma}} = 2\mu_{\text{macro}} \text{sym } \mathbf{D}\mathbf{u} + \lambda_{\text{macro}} \text{tr}(\mathbf{D}\mathbf{u}) \mathbf{1} + 2\mu_c (\text{skew } \mathbf{D}\mathbf{u} - \text{Anti}(\boldsymbol{\phi})), \quad (136)$$

\mathbf{e}_r is the radial unit vector, and the second-order moment stress tensor

$$\bar{\mathbf{m}} = \alpha \text{tr}(\mathbf{D}\boldsymbol{\phi}) \mathbf{1} + \beta (\mathbf{D}\boldsymbol{\phi})^T + \gamma \mathbf{D}\boldsymbol{\phi}. \quad (137)$$

According to the reference system shown in Fig. 1, the ansatz for the displacement field and the micro-rotation vector turns into

$$\mathbf{u}(x_1, x_2, x_3) = \mathbf{u}(r, \varphi, z) = \boldsymbol{\vartheta} \begin{pmatrix} -x_2(r, \varphi) x_3(z) \\ x_1(r, \varphi) x_3(z) \\ 0 \end{pmatrix}, \quad \boldsymbol{\phi}(x_1, x_2, x_3) = \boldsymbol{\phi}(r, \varphi, z) = \frac{\boldsymbol{\vartheta}}{2} \begin{pmatrix} -g_p(r) x_1(r, \varphi) \\ -g_p(r) x_2(r, \varphi) \\ 2x_3(z) \end{pmatrix}, \quad (138)$$

Substituting the ansatz (138) in (134) the equilibrium equations are equivalent to

$$\begin{aligned} -\frac{1}{2} \boldsymbol{\vartheta} \cos \varphi (4\rho \mu_c (g(\rho) - 1) - (\alpha + \beta + \gamma) (3g'(\rho) + \rho g''(\rho))) &= 0, \\ -\frac{1}{2} \boldsymbol{\vartheta} \sin \varphi (4\rho \mu_c (g(\rho) - 1) - (\alpha + \beta + \gamma) (3g'(\rho) + \rho g''(\rho))) &= 0, \end{aligned} \quad (139)$$

which are completely equivalent to (62) in Section 6 once used the relations (131). Since also the boundary conditions (135) are equivalent to the boundary condition (59) in Section 6, further calculations are avoided. Here, we recall the relations between the two moment stress tensors expressed in the classical format ($\bar{\mathbf{m}}$) and in the dislocation format (\mathbf{m})

$$\text{dev sym } \mathbf{m} = -\text{dev sym } \bar{\mathbf{m}}, \quad \text{skew } \mathbf{m} = \text{skew } \bar{\mathbf{m}}, \quad \text{tr } \mathbf{m} = \frac{1}{2} \text{tr } \bar{\mathbf{m}}, \quad (140)$$

where $\text{skew } \mathbf{m} = \text{skew } \bar{\mathbf{m}} = \mathbf{0}$ for the torsional problem, and

$$\mathbf{m} = \mu L_c^2 \left(a_1 \text{dev sym Curl } \mathbf{A} + \frac{a_3}{3} \text{tr}(\text{Curl } \mathbf{A}) \mathbf{1} \right), \quad \bar{\mathbf{m}} = \alpha \text{tr}(\mathbf{D}(\text{axl}(\mathbf{A}))) \mathbf{1} + \beta (\mathbf{D}(\text{axl}(\mathbf{A})))^T + \gamma \mathbf{D}(\text{axl}(\mathbf{A})), \quad (141)$$

It is also interesting to show the relation between the two higher-order torques expressed in terms of \mathbf{m} and $\bar{\mathbf{m}}$, respectively. First, we observe

$$\langle \text{skew}(\mathbf{m} \times \mathbf{e}_z) \mathbf{e}_\varphi, \mathbf{e}_r \rangle - \langle \text{skew}(\mathbf{m} \times \mathbf{e}_z) \mathbf{e}_r, \mathbf{e}_\varphi \rangle = \langle (\mathbf{m} \times \mathbf{e}_z) \mathbf{e}_\varphi, \mathbf{e}_r \rangle - \langle (\mathbf{m} \times \mathbf{e}_z) \mathbf{e}_r, \mathbf{e}_\varphi \rangle, \quad (142)$$

which does not holds component-wise.¹¹

Using that the cross product between two unit vectors gives the third one, and

$$(\mathbf{m} \times \mathbf{v}) \mathbf{w} = \mathbf{m} (\mathbf{v} \times \mathbf{w}) \quad \forall \mathbf{v}, \mathbf{w} \in \mathbb{R}^3 \quad \text{and} \quad \forall \mathbf{m} \in \mathbb{R}^{3 \times 3}, \quad (143)$$

it is possible to write

$$\langle (\mathbf{m} \times \mathbf{e}_z) \mathbf{e}_\varphi, \mathbf{e}_r \rangle - \langle (\mathbf{m} \times \mathbf{e}_z) \mathbf{e}_r, \mathbf{e}_\varphi \rangle = \langle \mathbf{m} (\mathbf{e}_\varphi \times \mathbf{e}_z), \mathbf{e}_r \rangle - \langle \mathbf{m} (\mathbf{e}_r \times \mathbf{e}_z), \mathbf{e}_\varphi \rangle = -[\langle \mathbf{m} \mathbf{e}_r, \mathbf{e}_r \rangle + \langle \mathbf{m} \mathbf{e}_\varphi, \mathbf{e}_\varphi \rangle]. \quad (144)$$

Since $(\mathbf{e}_r \otimes \mathbf{e}_r + \mathbf{e}_\varphi \otimes \mathbf{e}_\varphi + \mathbf{e}_z \otimes \mathbf{e}_z) = \mathbf{1}$ we may convert the double dot-product into a dyadic product as follows

$$-[\langle \mathbf{m} \mathbf{e}_r, \mathbf{e}_r \rangle + \langle \mathbf{m} \mathbf{e}_\varphi, \mathbf{e}_\varphi \rangle] = -\langle \mathbf{m}, (\mathbf{e}_r \otimes \mathbf{e}_r + \mathbf{e}_\varphi \otimes \mathbf{e}_\varphi) \rangle = -\langle \mathbf{m}, (\mathbf{1} - \mathbf{e}_z \otimes \mathbf{e}_z) \rangle. \quad (145)$$

Substituting the relation (140) between \mathbf{m} and $\bar{\mathbf{m}}$ we have

$$-\langle \mathbf{m}, (\mathbf{1} - \mathbf{e}_z \otimes \mathbf{e}_z) \rangle = -\left\langle \left(-\text{dev } \bar{\mathbf{m}} + \text{skew } \bar{\mathbf{m}} + \frac{1}{3} \frac{\text{tr}(\bar{\mathbf{m}})}{2} \mathbf{1} \right), (\mathbf{1} - \mathbf{e}_z \otimes \mathbf{e}_z) \right\rangle. \quad (146)$$

Since $\langle \mathbf{1}, \mathbf{1} \rangle = 3$, $\langle \mathbf{1}, (\mathbf{e}_z \otimes \mathbf{e}_z) \rangle = 1$, and $\bar{\mathbf{m}}$ is decomposed into its three orthogonal components (except for multiplying factors) we can write

$$-\left\langle \left(-\text{dev } \bar{\mathbf{m}} + \text{skew } \bar{\mathbf{m}} + \frac{1}{3} \frac{\text{tr}(\bar{\mathbf{m}})}{2} \mathbf{1} \right), \underbrace{(\mathbf{1} - \mathbf{e}_z \otimes \mathbf{e}_z)}_{\in \text{Sym}(3)} \right\rangle = -\left\langle \left(-\text{dev } \bar{\mathbf{m}} + \frac{1}{3} \frac{\text{tr}(\bar{\mathbf{m}})}{2} \mathbf{1} \right), \underbrace{(\mathbf{1} - \mathbf{e}_z \otimes \mathbf{e}_z)}_{\in \text{Sym}(3)} \right\rangle = \quad (147)$$

$$\langle \text{dev } \bar{\mathbf{m}}, (\mathbf{1} - \mathbf{e}_z \otimes \mathbf{e}_z) \rangle - \frac{1}{3} \frac{\text{tr}(\bar{\mathbf{m}})}{2} [3 - 1] = -\langle \text{dev } \bar{\mathbf{m}}, \mathbf{e}_z \otimes \mathbf{e}_z \rangle - \frac{1}{3} \text{tr}(\bar{\mathbf{m}}) = \quad (148)$$

$$-\langle \text{dev } \bar{\mathbf{m}}, \mathbf{e}_z \otimes \mathbf{e}_z \rangle - \frac{1}{3} \text{tr}(\bar{\mathbf{m}}) \langle \mathbf{1}, \mathbf{e}_z \otimes \mathbf{e}_z \rangle = -\langle \text{dev } \bar{\mathbf{m}} + \frac{1}{3} \text{tr}(\bar{\mathbf{m}}) \mathbf{1}, \mathbf{e}_z \otimes \mathbf{e}_z \rangle = \langle \bar{\mathbf{m}}, \mathbf{e}_z \otimes \mathbf{e}_z \rangle = -\langle \bar{\mathbf{m}} \mathbf{e}_z, \mathbf{e}_z \rangle = -\bar{m}_{zz}. \quad (149)$$

¹¹The values of the four terms for a generic second order tensor \mathbf{m} are: $\langle \text{skew}(\mathbf{m} \times \mathbf{e}_z) \mathbf{e}_\varphi, \mathbf{e}_r \rangle = \frac{1}{2} (m_{11} + m_{22})$, $\langle \text{skew}(\mathbf{m} \times \mathbf{e}_z) \mathbf{e}_r, \mathbf{e}_\varphi \rangle = -\frac{1}{2} (m_{11} + m_{22})$, $\langle (\mathbf{m} \times \mathbf{e}_z) \mathbf{e}_\varphi, \mathbf{e}_r \rangle = m_{22} \sin^2 \varphi + m_{11} \cos^2 \varphi + (m_{12} + m_{21}) \sin \varphi \cos \varphi$, $\langle (\mathbf{m} \times \mathbf{e}_z) \mathbf{e}_r, \mathbf{e}_\varphi \rangle = -m_{22} \cos^2 \varphi - m_{11} \sin^2 \varphi + (m_{12} + m_{21}) \sin \varphi \cos \varphi$. Note that $\langle \text{skew}(\mathbf{m} \times \mathbf{e}_z) \mathbf{e}_\varphi, \mathbf{e}_r \rangle \neq \langle (\mathbf{m} \times \mathbf{e}_z) \mathbf{e}_\varphi, \mathbf{e}_r \rangle$ and $\langle \text{skew}(\mathbf{m} \times \mathbf{e}_z) \mathbf{e}_r, \mathbf{e}_\varphi \rangle \neq \langle (\mathbf{m} \times \mathbf{e}_z) \mathbf{e}_r, \mathbf{e}_\varphi \rangle$.

The last relation is a pure algebraic relation valid for all $\mathbf{m}, \bar{\mathbf{m}}$ related by (138) and $\mathbf{e}_r, \mathbf{e}_\varphi, \mathbf{e}_z$ are given in (11). Thus, we have shown that

$$\langle \text{skew}(\mathbf{m} \times \mathbf{e}_z) \mathbf{e}_\varphi, \mathbf{e}_r \rangle - \langle \text{skew}(\mathbf{m} \times \mathbf{e}_z) \mathbf{e}_r, \mathbf{e}_\varphi \rangle = \bar{\mathbf{m}}_{zz}. \quad (150)$$

This solution is valid for a generic second order tensor and for a generic vector triplet. Using (149), we finally see that

$$\int_{\Gamma} \bar{\mathbf{m}}_{zz} r \, dr \, d\varphi = \int_{\Gamma} \left[\langle \text{skew}(\mathbf{m} \times \mathbf{e}_z) \mathbf{e}_\varphi, \mathbf{e}_r \rangle - \langle \text{skew}(\mathbf{m} \times \mathbf{e}_z) \mathbf{e}_r, \mathbf{e}_\varphi \rangle \right] r \, dr \, d\varphi. \quad (151)$$

The ratio Ω between the Cosserat torsional stiffness and the classical value that can be found e.g. in [4, 14, 35] is

$$\begin{aligned} \Omega &= 1 + 6 \left(\frac{\ell_t}{R} \right)^2 \left[\frac{1 - 4/3 \Psi \chi}{1 - \Psi \chi} \right], & \ell_t^2 &= \frac{\beta + \gamma}{2\mu_{\text{macro}}}, & \Psi &= \frac{\beta + \gamma}{\alpha + \beta + \gamma}, \\ \chi &= \frac{I_1(pR)}{pRI_0(pR)}, & p^2 &= \frac{4\mu_c}{\alpha + \beta + \gamma}, & N^2 &= \frac{\mu_c}{\mu_{\text{macro}} + \mu_c}. \end{aligned} \quad (152)$$

where ℓ_t is the *characteristic length for torsion*, Ψ is the polar ratio, N is the *Cosserat coupling number*, α, β , and γ are the curvature coefficients in the classical Cosserat formulation, μ_{macro} is the classical Cauchy shear modulus, μ_c is the Cosserat couple modulus, and I_n is the modified Bessel function of the first kind of order n .

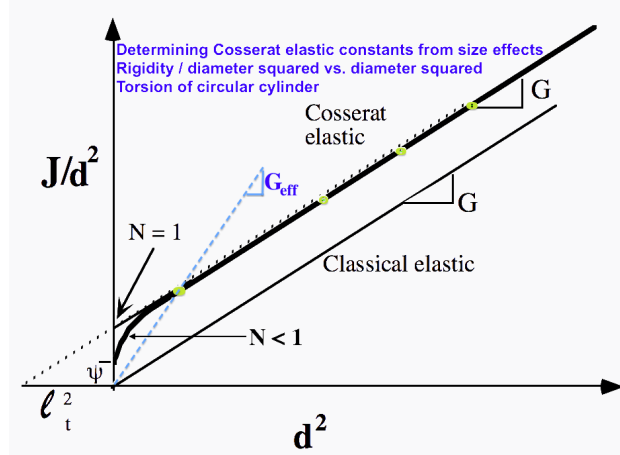


Figure 27: For comparison, the figure has been taken from Lakes [35]. Here, $G = \mu_{\text{macro}}$ denotes the classical shear modulus and $N \rightarrow 1$ corresponds to $\mu_c \rightarrow \infty$.

To go from (65) to (152) we have to use the relations (131), while remembering to incorporate the term μL_c^2 (the terms not reported do not change between the two notations)

$$\Omega = 1 + 6 \left(\frac{\ell_t}{R} \right)^2 \left[\frac{1 - 4/3 \Psi \chi}{1 - \Psi \chi} \right], \quad \ell_t^2 = \frac{a_1}{2\mu_{\text{macro}}}, \quad \Psi = \frac{3a_1}{2a_1 + 4a_3}, \quad p^2 = \frac{6\mu_c}{a_1 + 2a_3}. \quad (153)$$

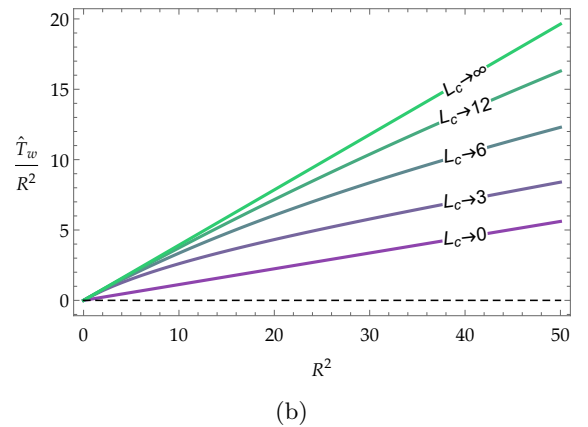
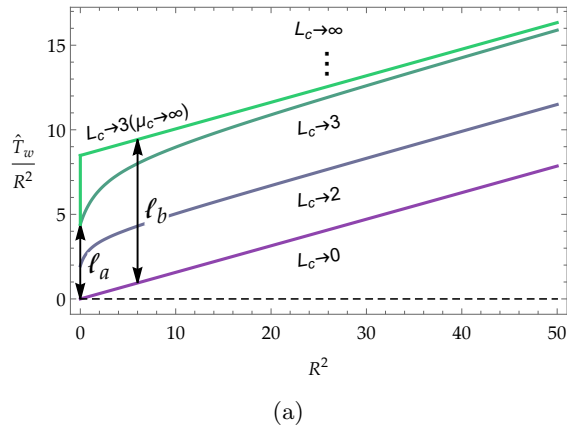


Figure 28: (a) Cosserat model; (b) relaxed micromorphic model. The values of the coefficient used are: $\mu = 1$, $\mu_c = 1/2$, $\mu_{\text{macro}} = 1/14$, $\mu_{\text{micro}} = 1/4$, $a_1 = 1/5$, $a_3 = 1/37$.

In Fig. 28 we report how the torsional stiffness divided by the radius of the cylindrical rod squared (\hat{T}_w/R^2) vary with respect to the radius squared R^2 for the Cosserat model and the relaxed micromorphic model where

$$\ell_a = \mu L_c^2 12\pi \frac{a_1 a_3}{a_1 + 8a_3} = \frac{\pi(\beta + \gamma)(3\alpha + \beta + \gamma)}{2\alpha + \beta + \gamma}, \quad \ell_b = \mu L_c^2 \frac{3}{2} \pi a_1 = \frac{3}{2} \pi(\beta + \gamma). \quad (154)$$

It is highlighted that the Cosserat model do not tend to a classical linear elastic model for $\mu_c \rightarrow 0$ as it can be seen from eq.(153) or eq.(68).

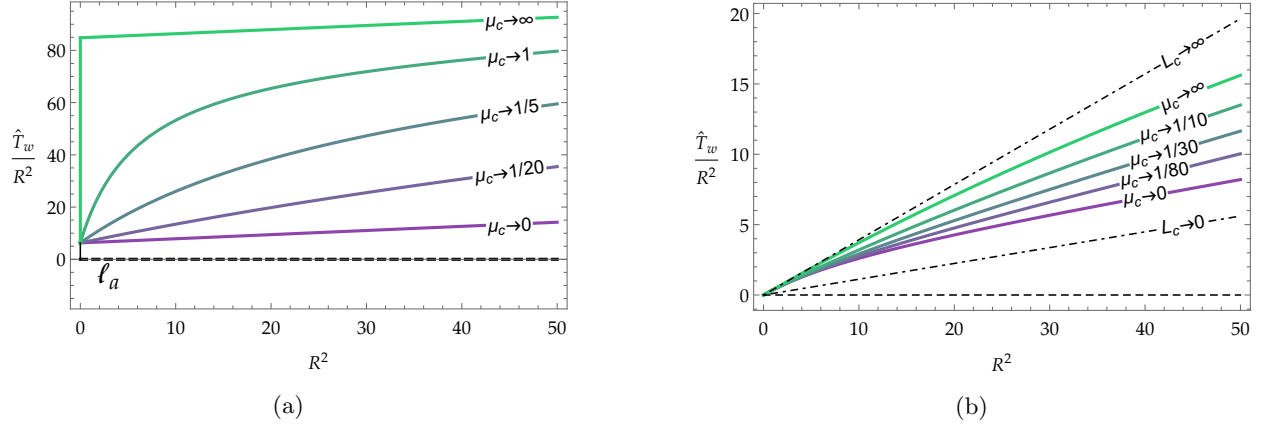


Figure 29: (a) Cosserat model; (b) relaxed micromorphic model. The values of the coefficient used are: $\mu = 1$, $\mu_{\text{macro}} = 1/14$, $\mu_{\text{micro}} = 1/4$, $a_1 = 2$, $a_3 = 1/50$, $L_c = 3$. In the Cosserat model, the solution for $\mu_c \rightarrow \infty$ (the indeterminate couple stress model) shows a jump.

It is underlined that for the relaxed micromorphic model the stiffness is bounded by the one obtained for $L_c \rightarrow 0$ (macro) and $L_c \rightarrow \infty$ (micro): the macro-stiffness ($L_c \rightarrow 0$) is the limit to which all curves with finite L_c tend asymptotically to for $R^2 \rightarrow \infty$ (this limit has been cut in order make possible to distinguish all the curves), while the micro-stiffness ($L_c \rightarrow \infty$) is the limit to which all the curves tend asymptotically to for $R^2 \rightarrow 0$.

D Ad-hoc minimization for $L_c \rightarrow \infty$ in the full micromorphic model and in the micro-strain model

Looking at the curvature energy of the full micromorphic model (or the micro-strain model) it is clear that for $L_c \rightarrow \infty$ the micro-distortion tensor field \mathbf{P} must be constant $\mathbf{P} = \bar{\mathbf{P}}$, provided all curvature coefficients are strictly positive. We calculate this constant in the following. Thus we consider

$$\min_{\mathbf{u}, \bar{\mathbf{P}}} \left[\int_{\Omega} \mu_e \|\text{dev sym}(\mathbf{Du} - \bar{\mathbf{P}})\|^2 + \frac{\kappa_e}{2} \text{tr}^2(\mathbf{Du} - \bar{\mathbf{P}}) + \mu_c \|\text{skew}(\mathbf{Du} - \bar{\mathbf{P}})\|^2 + \mu_{\text{micro}} \|\text{dev sym} \bar{\mathbf{P}}\|^2 + \frac{\kappa_{\text{micro}}}{2} \text{tr}^2(\bar{\mathbf{P}}) dV \right]. \quad (155)$$

The weak form is given by

$$\int_{\Omega} 2\mu_e \langle \text{dev sym}(\mathbf{Du} - \bar{\mathbf{P}}), -\delta \bar{\mathbf{P}} \rangle + \kappa_e \text{tr}(\mathbf{Du} - \bar{\mathbf{P}}) \langle \mathbf{1}, -\delta \bar{\mathbf{P}} \rangle + 2\mu_c \langle \text{skew}(\mathbf{Du} - \bar{\mathbf{P}}), -\delta \bar{\mathbf{P}} \rangle + 2\mu_{\text{micro}} \langle \text{dev sym}(\bar{\mathbf{P}}), \delta \bar{\mathbf{P}} \rangle + \kappa_{\text{micro}} \text{tr}(\bar{\mathbf{P}}) \langle \mathbf{1}, \delta \bar{\mathbf{P}} \rangle dV = 0 \quad \forall \delta \bar{\mathbf{P}}. \quad (156)$$

$$\int_{\Omega} \langle 2\mu_e \text{dev sym}(\mathbf{Du} - \bar{\mathbf{P}}) + \kappa_e \text{tr}(\mathbf{Du} - \bar{\mathbf{P}}) \mathbf{1} + 2\mu_c \text{skew}(\mathbf{Du} - \bar{\mathbf{P}}) - 2\mu_{\text{micro}} \text{dev sym}(\bar{\mathbf{P}}) - \kappa_{\text{micro}} \text{tr}(\bar{\mathbf{P}}) \mathbf{1}, \delta \bar{\mathbf{P}} \rangle dV = 0 \quad \forall \delta \bar{\mathbf{P}}. \quad (157)$$

For constant $\delta \bar{\mathbf{P}}$ this can be rewritten as

$$\left\langle \int_{\Omega} 2\mu_e \text{dev sym}(\mathbf{Du} - \bar{\mathbf{P}}) + \kappa_e \text{tr}(\mathbf{Du} - \bar{\mathbf{P}}) \mathbf{1} + 2\mu_c \text{skew}(\mathbf{Du} - \bar{\mathbf{P}}) - 2\mu_{\text{micro}} \text{dev sym}(\bar{\mathbf{P}}) - \kappa_{\text{micro}} \text{tr}(\bar{\mathbf{P}}) \mathbf{1} dV, \delta \bar{\mathbf{P}} \right\rangle = 0 \quad \forall \delta \bar{\mathbf{P}}. \quad (158)$$

Since $\delta \bar{\mathbf{P}}$ is arbitrary, this implies that

$$\int_{\Omega} 2\mu_e \text{dev sym}(\mathbf{Du} - \bar{\mathbf{P}}) + \kappa_e \text{tr}(\mathbf{Du} - \bar{\mathbf{P}}) \mathbf{1} + 2\mu_c \text{skew}(\mathbf{Du} - \bar{\mathbf{P}}) - 2\mu_{\text{micro}} \text{dev sym}(\bar{\mathbf{P}}) - \kappa_{\text{micro}} \text{tr}(\bar{\mathbf{P}}) \mathbf{1} dV = 0, \quad (159)$$

or

$$\int_{\Omega} 2\mu_e \text{dev sym} \mathbf{Du} + \kappa_e \text{tr}(\mathbf{Du}) \mathbf{1} + 2\mu_c \text{skew} \mathbf{Du} dV = \int_{\Omega} 2\mu_e \text{dev sym} \bar{\mathbf{P}} + \kappa_e \text{tr}(\bar{\mathbf{P}}) \mathbf{1} + 2\mu_c \text{skew} \bar{\mathbf{P}} + 2\mu_{\text{micro}} \text{dev sym} \bar{\mathbf{P}} + \kappa_{\text{micro}} \text{tr}(\bar{\mathbf{P}}) \mathbf{1} dV. \quad (160)$$

Using the orthogonality of $\text{dev sym} \cdot$, $\text{skew} \cdot$ and $\text{tr}(\cdot) \mathbf{1}$ we obtain

$$\int_{\Omega} 2\mu_e \text{dev sym} \mathbf{Du} dV = \int_{\Omega} 2\mu_e \text{dev sym} \bar{\mathbf{P}} + 2\mu_{\text{micro}} \text{dev sym} \bar{\mathbf{P}} dV, \quad (161)$$

$$\int_{\Omega} \kappa_e \operatorname{tr}(\mathbf{D}\mathbf{u}) \, dV = \int_{\Omega} \kappa_e \operatorname{tr}(\overline{\mathbf{P}}) + \kappa_{\text{micro}} \operatorname{tr}(\overline{\mathbf{P}}) \, dV, \quad \int_{\Omega} 2\mu_c \operatorname{skew} \mathbf{D}\mathbf{u} \, dV = \int_{\Omega} 2\mu_c \operatorname{skew} \overline{\mathbf{P}} \, dV,$$

and since $\overline{\mathbf{P}}$ is constant we can write

$$\begin{aligned} \operatorname{dev} \operatorname{sym} \overline{\mathbf{P}} &= \frac{1}{|\Omega|} \int_{\Omega} \frac{\mu_e}{\mu_e + \mu_{\text{micro}}} \operatorname{dev} \operatorname{sym} \mathbf{D}\mathbf{u} \, dV, & \operatorname{tr}(\overline{\mathbf{P}}) &= \frac{1}{|\Omega|} \int_{\Omega} \frac{\kappa_e}{\kappa_e + \kappa_{\text{micro}}} \operatorname{tr}(\mathbf{D}\mathbf{u}) \, dV, \\ \operatorname{skew} \overline{\mathbf{P}} &= \frac{1}{|\Omega|} \int_{\Omega} \operatorname{skew} \mathbf{D}\mathbf{u} \, dV. \end{aligned} \quad (162)$$

Since dev , sym , skew , and tr are linear operators, we obtain equivalently

$$\begin{aligned} \operatorname{dev} \operatorname{sym} \overline{\mathbf{P}} &= \frac{\mu_e}{\mu_e + \mu_{\text{micro}}} \operatorname{dev} \operatorname{sym} \left(\frac{1}{|\Omega|} \int_{\Omega} \mathbf{D}\mathbf{u} \, dV \right), & \operatorname{tr}(\overline{\mathbf{P}}) &= \frac{\kappa_e}{\kappa_e + \kappa_{\text{micro}}} \operatorname{tr} \left(\frac{1}{|\Omega|} \int_{\Omega} \mathbf{D}\mathbf{u} \, dV \right), \\ \operatorname{skew} \overline{\mathbf{P}} &= \operatorname{skew} \left(\frac{1}{|\Omega|} \int_{\Omega} \mathbf{D}\mathbf{u} \, dV \right). \end{aligned} \quad (163)$$

Substituting the ansatz (85) into (163) we obtain $\overline{\mathbf{P}} = \mathbf{0}$. Analogous calculations can be carried out for the micro-strain model for which $\operatorname{skew} \overline{\mathbf{P}} = \mathbf{0}$ and $\mu_c = 0$

$$\operatorname{dev} \overline{\mathbf{S}} = \frac{\mu_e}{\mu_e + \mu_{\text{micro}}} \operatorname{dev} \operatorname{sym} \left(\frac{1}{|\Omega|} \int_{\Omega} \mathbf{D}\mathbf{u} \, dV \right), \quad \operatorname{tr}(\overline{\mathbf{S}}) = \frac{\kappa_e}{\kappa_e + \kappa_{\text{micro}}} \operatorname{tr} \left(\frac{1}{|\Omega|} \int_{\Omega} \mathbf{D}\mathbf{u} \, dV \right). \quad (164)$$

Substituting the ansatz (96) into (164) we obtain $\overline{\mathbf{S}} = \mathbf{0}$.

The integral on the circular cross-section Γ of the gradient of the displacement is

$$\int_{\Gamma} \mathbf{D}\mathbf{u}(x) \, dV = \int_0^{2\pi} \int_0^R \mathbf{D}\mathbf{u}(r, \varphi, z) \, r \, dr \, d\varphi = \begin{pmatrix} 0 & -\pi R^2 \boldsymbol{\vartheta} z & 0 \\ \pi R^2 \boldsymbol{\vartheta} z & 0 & 0 \\ 0 & 0 & 0 \end{pmatrix} = \pi R^2 \boldsymbol{\Theta}(z) \begin{pmatrix} 0 & -1 & 0 \\ 1 & 0 & 0 \\ 0 & 0 & 0 \end{pmatrix}. \quad (165)$$

From (165) it is possible to see that the symmetric part of the integral of $\mathbf{D}\mathbf{u}$ on the circular cross-section is zero, while the skew-symmetric part is zero only if the domain is symmetric with respect z .

For the Cosserat model, letting $L_c \rightarrow \infty$ still implies that $\mathbf{A}(\mathbf{x}) = \overline{\mathbf{A}} = \text{const.}$ must be constant. The same calculations as before yield

$$\overline{\mathbf{A}} = \operatorname{skew} \left(\frac{1}{|\Omega|} \int_{\Omega} \mathbf{D}\mathbf{u} \, dV \right) = \frac{1}{|\Omega|} \int_{\Omega} \mathbf{D}\mathbf{u} \, dV, \quad \text{since } \mathbf{D}\mathbf{u} \in \mathfrak{so}(3). \quad (166)$$

For $\Omega = [0, L] \times \Gamma$ we have

$$\frac{1}{|\Omega|} \int_{\Omega} \mathbf{D}\mathbf{u} \, dV = \frac{1}{L(\pi R^2)} \int_0^L \int_0^{2\pi} \int_0^R \mathbf{D}\mathbf{u}(r, \varphi, z) \, r \, dr \, d\varphi \, dz = \frac{1}{L(\pi R^2)} \left(\boldsymbol{\vartheta} \pi R^2 \frac{z^2}{2} \Big|_0^L \right) = \frac{\boldsymbol{\vartheta}}{2} L = \frac{1}{2} \boldsymbol{\Theta}(L). \quad (167)$$

We remark that the same limit $L_c \rightarrow \infty$ in the relaxed micromorphic model yields a linear elastic response with stiffness $\mathbb{C}_{\text{micro}}$ since $\operatorname{Curl} \mathbf{P} = \mathbf{0}$ does not imply that $\mathbf{P} = \text{const.}$ but $\mathbf{P} = \nabla \boldsymbol{\zeta}$ for some $\boldsymbol{\zeta} : \Omega \in \mathbb{R}^3 \rightarrow \mathbb{R}^3$, see [46].